

**NEUTRONICS CHARACTERISTICS ANALYSIS OF ALFRED WITH  
LFR REFLECTOR COMPARISON AND EVALUATION OF A  
CONCEPTUAL MPRR USING OPENMC**

AQUEEB ANJUM SUNNY (SN. 202128002)  
SAFIUS SAKIB SHUDDHO (SN. 202128028)  
NUSRAT ZAHAN ZARIN (SN. 202128022)

A Thesis Submitted in Partial Fulfillment of the Requirements for the Degree of  
Bachelor of Science in Nuclear Engineering



**DEPARTMENT OF NUCLEAR SCIENCE AND ENGINEERING  
MILITARY INSTITUTE OF SCIENCE AND TECHNOLOGY  
DHAKA, BANGLADESH**

MAY 2025

**Neutronics Characteristics Analysis of ALFRED with LFR Reflector  
Comparison and Evaluation of a Conceptual MPRR using OpenMC**

**B.Sc. Engineering Thesis**

**By**

Aqueeb Anjum Sunny (202128002)  
Safius Sakib Shuddho (202128028)  
Nusrat Zahan Zarin (202128022)

Approved as to style and content by the examiners in May 2025:

Col. Khalid Mahmud  
Head of Department of NSE  
MIST, Dhaka

**President**

---

Dr. Abdus Sattar Mollah  
Professor of NSE  
MIST, Dhaka

**Chairperson (Thesis Supervisor)**

---

Lt. Col. Md. Altab Hossain, PhD EME  
Associate Professor of NSE  
MIST, Dhaka

**Member (Internal)**

---

Jehad Mohammed Haque  
Lecturer of NSE  
MIST, Dhaka

**Member (Internal)**

**Department of Nuclear Science and Engineering, MIST, Dhaka**

**Neutronics Characteristics Analysis of ALFRED with LFR Reflector  
Comparison and Evaluation of a Conceptual MPRR using OpenMC**

**B.Sc. Engineering Thesis**

**By**

Aqueeb Anjum Sunny (202128002)  
Safius Sakib Shuddho (202128028)  
Nusrat Zahan Zarin (202128022)

**Style approved by the Scrutinizers in May 2025:**

---

  
Md Shamim Hassan  
Lecturer of NSE  
MIST, Dhaka

**Member (Internal)**

---

  
Mosharat Belal Tahia  
Lecturer of NSE  
MIST, Dhaka

**Member (Internal)**

**Department of Nuclear Science and Engineering, MIST, Dhaka**

**NEUTRONICS CHARACTERISTICS ANALYSIS OF ALFRED WITH  
LFR REFLECTOR COMPARISON AND EVALUATION OF A  
CONCEPTUAL MPRR USING OPENMC**

**DECLARATION**

We hereby declare that this thesis is our original work, and it has been written by us in its entirety. We have duly acknowledged all the sources of information which have been used in the thesis.

---

Aqueeb Anjum Sunny  
Student No. 202128002

---

Safius Sakib Shuddho  
Student No. 202128028

---

Nusrat Zahan Zarin  
Student No. 202128022

Department of Nuclear Science and Engineering, MIST, Dhaka

## ABSTRACT

### **Neutronics Characteristics Analysis of ALFRED with LFR Reflector Comparison and Evaluation of a Conceptual MPRR using OpenMC**

This thesis conducts a comprehensive neutronics analysis of the Advanced Lead-cooled Fast Reactor European Demonstrator (ALFRED) and a 10 MW Multi-Purpose Research Reactor (MPRR) proposed for Bangladesh, utilizing OpenMC Monte Carlo simulations. For ALFRED, the study validates key neutronics parameters, achieving a  $k_{\text{eff}}$  of 1.07803 (0.054% error from reference 1.07767), a maximum neutron flux of  $2.716 \times 10^{15}$  neutrons/cm $^2$ ·s, a power peaking factor of 1.276, and a control rod worth of -8650 pcm (1.76% error), confirming simulation accuracy and robust reactivity control. Reactivity swing was -2530 pcm (1.94% error from -2580 pcm), reflecting effective feedback modeling. Burnup analysis over 1820 days yields cycle lengths of 1041 days (lead) and 1094 days (LBE), with isotopic depletion showing Pu-241 reduction to 0.70-0.73 of initial mass of Pu-241, and Am-241 production 2.9 times higher in MOX2, posing waste challenges. Coolant activation produces 1 kg of Po-210 in LBE versus 0.089 g in lead, highlighting radiological risks (0.15 MW decay heat). Reflector studies identify BeO as optimal for neutron retention ( $k_{\text{eff}}$  1.11189, leakage 18.512%) and for cycle length (1232.69 days), though BeO increases thermal fission fraction to 1.89% and softens the neutron spectrum. For the MPRR, neutronics evaluation yields a  $k_{\text{eff}}$  of 1.10693 (6 pcm error), an average flux of  $5.8 \times 10^{14}$  neutrons/cm $^2$ ·s (peaking at  $4.8 \times 10^{14}$  neutrons/cm $^2$ ·s, 4% deviation), a power peaking factor of 1.197, and a control rod worth of -2649 pcm, supporting its design for isotope production. The neutron spectrum peaks at 0.1eV, confirming a thermal profile, with fission density reflected in an average power of 0.283 MW per assembly (peak 0.339 MW). Burnup over 90 days reduces  $k_{\text{eff}}$  to 1.003, with U-235 depletion, Xe-135 equilibrium after 40-50 hours, Sm-149 saturation after ~20 days, and Pu-239 increase, yielding an excess reactivity of 1048 pcm (0.86% error from 1039 pcm). The student's t-test was used to conduct the hypothesis test on the multiplication factors ( $k_{\text{eff}}$ ) for both ALFRED and MPRR. This test fails to reject the null hypothesis because it finds no discernible difference between the OpenMC  $k_{\text{eff}}$  value and the

benchmark  $k_{\text{eff}}$  value. Thus, it can be concluded that the OpenMC model in this study is accurate and efficient. This work advances Gen-IV reactor design and nuclear research infrastructure of Bangladesh.

## সারসংক্ষেপ

### Neutronics Characteristics Analysis of ALFRED with LFR Reflector Comparison and Evaluation of a Conceptual MPRR using OpenMC

এই থিসিসটি ওপেনএমসি মন্তে কার্লো সিমুলেশন (OpenMC Monte Carlo Simulation) ব্যবহার করে অ্যাডভান্সড লেড-কুলড ফাস্ট রিঅ্যাস্ট্র ইউরোপিয়ান ডেমনস্ট্রেটর (ALFRED) এবং বাংলাদেশের জন্য প্রস্তুতি ১০ মেগাওয়াট মাল্টি-পারপাস রিসার্চ রিঅ্যাস্ট্র (MPRR)-এর নিউট্রোনিক্স পরিচালনা করে। আলফ্রেড এর জন্য গবেষণাটি মূল নিউট্রোনিক্স পরামিতিগুলিকে যাচাই করে, যেখানে কে-এফেক্টিভ ( $k_{\text{eff}}$ ) ১.০৭৮০৩ (রেফারেন্স ১.০৭৭৬৭ থেকে ০.০৫৪% ত্রুটি), সর্বোচ্চ নিউট্রন ফ্লাক্স  $2.716 \times 10^{15}$  নিউট্রন/সেমি $^2$ -সেকেন্ড (neutrons/cm $^2$ -s), পাওয়ার পিকিং ফ্যাস্ট্র (power peaking factor) ১.২৭৬, এবং কন্ট্রোল রড ওয়ার্থ (control rod worth) -৮৬৫০ পিসিএম (১.৭৬% ত্রুটি) পাওয়া যায়, যা সিমুলেশনের নির্ভুলতা এবং শক্তিশালী প্রতিক্রিয়া নিয়ন্ত্রণ নিশ্চিত করে। রিয়্যাকটিভিটি সুইং (reactivity swing) -২৫৩০ পিসিএম (রেফারেন্স -২৫৮০ পিসিএম থেকে ১.৯৪% ত্রুটি), যা কার্যকর প্রতিক্রিয়া মডেলিং প্রতিফলিত করে। ১৮২০ দিনের বার্নার্প বিশ্লেষণে সাইকেল দৈর্ঘ্য ১০৪১ দিন (লেড) এবং ১০৯৪ দিন (এলবিই) (LBE) পাওয়া যায়, আইসোটোপিক অবক্ষয়ে প্লুটোনিয়াম-২৪১ কমে প্রাথমিক ভরের ০.৭০-০.৭৩ গুণ, এবং মক্স-২ (MOX-2) থেকে অ্যামেরিশিয়াম-২৪১ উৎপাদন ২.৯ গুণ বেশি, যা বর্জ্য চ্যালেঞ্জ (challenge) তৈরি করে। কুল্যান্ট অ্যাস্টিভেশনে (coolant activation) লেড-এ ০.০৮৯ গ্রাম পোলোনিয়াম-২১০ তৈরি হয় যেখানে এলবিই-তে ১ কেজি তৈরি হয়, যা রেডিওলজিকাল বুঁকির (০.১৫ মেগাওয়াট ডিকে (decay) তাপ) নির্দেশক। প্রতিফলক গবেষণা বেরিলিয়াম-অক্সাইডকে নিউট্রন ধারণের জন্য (কে-এফেক্টিভ ১.১১১৮৯, লিকেজ ১৮.৫১২%) এবং সাইকেল দৈর্ঘ্যের জন্য (১২৩২.৬৯ দিন) সর্বোত্তম হিসাবে চিহ্নিত করে, যদিও বেরিলিয়াম-অক্সাইড থার্মাল (thermal) ফিশন ১.৮৯% বাড়ায় এবং নিউট্রন বর্ণালীকে নরম করে। এমপিআরআর-এর জন্য নিউট্রোনিক্স মূল্যায়নে কে-এফেক্টিভ ১.১০৬৯৩ (৬ পিসিএম ত্রুটি), গড় নিউট্রন ফ্লাক্স  $5.8 \times 10^{14}$  নিউট্রন/সেমি $^2$ -সে (শীষে ৪.৮  $\times 10^{14}$  নিউট্রন/সেমি $^2$ -সে, ৪% পার্থক্য), পাওয়ার পিকিং ফ্যাস্ট্র ১.১৯৭, এবং কন্ট্রোল রড ওয়ার্থ -২৬৪৯ পিসিএম পাওয়া যায়, যা আইসোটোপ উৎপাদনের জন্য এর নকশাকে সমর্থন করে। নিউট্রন বর্ণালী ০.১ ইলেক্ট্রন-ভোল্টে সর্বোচ্চ হয়, যা একটি তাপীয় প্রোফাইল নিশ্চিত করে, গড় পাওয়ার (power) প্রতি সমাবেশে ০.২৮৩ মেগাওয়াট (শীষে ০.৩৩৯ মেগাওয়াট) প্রতিফলিত হয়। ৯০ দিনের বার্নার্প কে-

এফেক্টিভ-কে ১.০০৩-এ কমিয়ে দেয়, ইউরেনিয়াম-২৩৫ এর অবক্ষয় ঘটায়, জেনন-১৩৫ কে ৪০-৫০ ঘণ্টার মধ্যে এবং সামারিয়াম-১৪৯ কে প্রায় ২০ দিনে সাম্যাবস্থায় আনে, এবং প্লুটোনিয়াম-২৩৯ কে বৃদ্ধি করে, যা ১০৪৮ পিসিএম (১০৩৯ পিসিএম থেকে ০.৮৬% ত্রুটি) অতিরিক্ত রিয়াকটিভিটি দেয়। হাইপোথিসিস (hypothesis) যাচাই করার জন্যে আলফ্রেড এবং এমপিআরআর এর কে-এফেক্টিভ এর উপর স্টুডেন্ট'স টি-টেস্ট (Students' t-test) করা হয়। এই পরীক্ষাটি নাল (null) হাইপোথিসিসকে প্রত্যাখ্যান করতে ব্যর্থ হয়েছে কারণ এটি ওপেনএমসির কে-এফেক্টিভ মান এবং বেঞ্চমার্ক এর কে-এফেক্টিভ মানের মধ্যে কোনও স্পষ্ট পার্থক্য খুঁজে পায় না। সুতরাং, এই সিদ্ধান্তে পৌঁছানো যেতে পারে যে এই গবেষণায় ব্যবহৃত মডেল দুটি সঠিক এবং দক্ষ। এই কাজটি জেনারেশন-৪ (Gen-IV) রিঅ্যাক্টর নকশা এবং বাংলাদেশের পারমাণবিক গবেষণা অবকাঠামোকে এগিয়ে নিয়ে যাবে।

## ACKNOWLEDGEMENTS

We, Aqueeb Anjum Sunny, Safius Sakib Shuddho, and Nusrat Zahan Zarin, express our heartfelt gratitude to Almighty Allah for His endless mercy and guidance, which have supported us throughout our lives and this thesis journey. His blessings have been our source of strength and motivation.

We are sincerely grateful to our supervisor, Professor Dr. Abdus Sattar Mollah, for his dedicated mentorship and invaluable guidance. His deep knowledge of nuclear science and engineering, combined with his patience and encouragement, helped us tackle the challenges of this project with confidence. His thoughtful feedback greatly improved the quality of our work.

We extend our appreciation to the Department of Nuclear Science and Engineering at the Military Institute of Science and Technology (MIST) for providing a supportive academic environment. The department's resources, facilities, and faculty enabled us to explore nuclear reactor design and neutronics thoroughly and effectively.

A very special heartfelt gratitude is reserved for Mr. ASM Nasim, our former Lecturer, whose role in our academic and research journey significantly affected our background, enthusiasm and efforts.

We owe our parents a particular debt of gratitude who have supported us throughout our lives and helped us get to where we are.

## TABLE OF CONTENTS

<b>ABSTRACT</b>	<b>v</b>
সারসংক্ষেপ	vii
<b>ACKNOWLEDGEMENTS</b>	<b>ix</b>
<b>CHAPTER 1</b>	<b>1</b>
<b>INTRODUCTION</b>	<b>1</b>
1.1    Background of the Thesis	1
1.1.1    Power Reactors	1
1.1.2    Research Reactors	2
1.2    Objectives of the Thesis	2
1.3    Research Motivation	3
1.4    Research Questions	4
1.5    Hypothesis Test	5
1.6    Scope of Research Work	6
1.6.1    Computational Tools and Data Used	6
1.6.2    Simulation Conditions	6
1.6.3    Expected Contributions	6
1.7    Limitations of the Thesis	7
1.8    Structure of the Thesis	8
<b>CHAPTER 2</b>	<b>9</b>
<b>REVIEW OF PREVIOUS STUDIES</b>	<b>9</b>
2.1    ALFRED Neutronics Analysis	9
2.1.1    Introduction	9
2.1.2    Multi-Physics and Safety Studies	11
2.1.3    Research Gaps	13
2.2    ALFRED Reflector Material Selection on Neutronics Properties	14
2.2.1    Introduction	14
2.2.2    SFR	14
2.2.3    GFR	15
2.2.4    LFR	17
2.3    MPRR Neutronics Analysis	18

2.3.1	Introduction	18
2.3.2	VVR-KN Fuel: Characteristics and Rationale	19
2.3.3	Research Gap	20
CHAPTER 3		22
COMPUTATIONAL METHODS AND DESIGN		22
3.1	Overview of OpenMC and Simulation Approach	22
3.1.1	Monte Carlo Method and its Application in OpenMC	22
3.1.2	Limitations of OpenMC	24
3.1.3	Simulation Approach in OpenMC	24
3.1.4	Data Libraries	24
3.1.5	Normalization of Data	25
3.1.5.1	Normalization Factor for Spatial Neutron Flux and Fission Rate	26
3.1.5.2	Normalization Factor for Energy Dependent Neutron Flux	27
3.2	Design of ALFRED Reactor Core	28
3.2.1	ALFRED Core Design	28
3.3	Different Reflector for ALFRED	32
3.4	Design of Multi-Purpose Research Reactor	36
3.4.1	VVR-KN Fuel Design	36
3.4.2	Core Design	38
3.5	Error Calculations	40
3.6	Hypothesis Test	40
CHAPTER 4		41
RESULTS AND DISCUSSIONS		41
4.1	ALFRED Neutronics Analysis	41
4.1.1	Criticality Calculations	41
4.1.2	Neutron Flux	42
4.1.3	Power Distribution	45
4.1.4	Neutron Energy Spectrum	46
4.1.5	Control Rod Worth	48
4.1.6	Fuel Burnup Results	49
4.1.6.1	Effective Multiplication Factor	49

4.1.6.2	Reactivity Swing	51
4.1.6.3	Depletion of Fuel Content	51
4.1.6.4	Normalization of Mass Data	52
4.1.6.5	Detailed Depletion Trends	53
4.1.6.6	Coolant Effects on Depletion	53
4.1.6.7	Implications for Reactor Safety and Sustainability	53
4.1.7	Actinide Production	54
4.1.8	Coolant (Lead and LBE) Activation Comparison	55
4.2	ALFRED Alternative Reflector Material Candidates	58
4.2.1	Effective Multiplication Factor and Leakage	58
4.2.1.1	Boundary Conditions and Their Purpose	59
4.2.1.2	Reflective Boundary Condition Analysis	60
4.2.1.3	Vacuum Boundary Condition Analysis	61
4.2.1.4	Comparative Insights and Conclusion	63
4.2.2	Flux Spectra Comparison	64
4.2.3	Fission Rate Comparison	65
4.2.3.1	Spatial Distribution of Fission Rates	66
4.2.3.2	Contribution of Thermal Fission	68
4.2.3.3	Quantification of Thermal Fission	70
4.2.4	Flux Distribution Comparison at BOC	70
4.2.4.1	Total Neutron Flux Distribution	71
4.2.4.2	Thermal Neutron Flux Distribution	73
4.2.5	Burnup – $k_{\text{eff}}$ and Cycle Length	75
4.2.5.1	Variation of Effective Multiplication Factor with Burnup	75
4.2.6	Burnup - Activation of Reflector Materials	77
4.2.7	Burnup - Isotopic Mass Evolution	79
4.2.7.1	Uranium and Plutonium Isotopes	80
4.2.7.2	Minor Actinides	82
4.3	MPRR Neutronics Analysis	84
4.3.1	Criticality Calculations	85

4.3.2	Neutron Flux	86
4.3.3	Power Distribution	87
4.3.4	Neutron Energy Spectrum	89
4.3.5	Fuel Burnup Results	90
<b>CHAPTER 5</b>		<b>96</b>
<b>CONCLUSION AND FUTURE PERSPECTIVES</b>		<b>96</b>
5.1	Summary of Key Findings	96
5.2	Evaluation	97
5.2.1	Evaluation Against Objectives	97
5.2.2	Assessment of Research Questions and Hypothesis Test	98
5.3	Implications for Reactor Design and Safety	99
5.4	Recommendations for Future Research	100
5.5	Final Remarks	101
<b>REFERENCES</b>		<b>102</b>

# CHAPTER 1

## INTRODUCTION

### 1.1 Background of the Thesis

#### 1.1.1 Power Reactors

In the sectors of power production, research, and medical application, nuclear reactors directly or indirectly play a very important role. For power generation purposes, they can generate a huge amount of energy while releasing very little greenhouse gas. This is an important reason why nuclear reactors are significant in global clean energy solutions. Outside of power generation, reactors are often directly or indirectly used for scientific research, material testing, nuclear agriculture, and medical isotope production.

The Gen-III and Gen-III+ reactors currently available have some common limitations. Addressing to improve these drawbacks, Generation IV (Gen-IV) reactors are being developed to offer:

- Better thermal conversion, providing higher efficiency.
- Improved fuel utilization, including the ability to burn minor actinides.
- Sustainability, through reduced waste production
- Optimized fuel cycle.

Among the various reactor types introduced in Gen-IV, Lead-cooled Fast Reactors (LFRs) are gaining increasing attention due to their advanced safety features, fuel sustainability, and economic potential. Fast reactors (Lead-cooled Fast Reactors, Sodium-cooled Fast Reactors, Gas-Cooled Fast Reactors) operate in the fast neutron spectrum which allows a more efficient utilization of nuclear fuel by utilizing the U-238 nuclides in the fuel. These reactors also enable the transmutation of long-lived minor actinides into shorter-lived isotopes, thus reducing waste. To point out some of the advantages provided by Lead-cooled Fast Reactors (LFRs) are given as following:

- High-temperature operation (above 500 °C), enabling better thermal efficiency.
- Superior neutron economy, allowing the use of a wider range of fuels, including recycled nuclear waste and depleted uranium.

- Inertness of the coolant used, Lead in LFRs, reduces the risk of core damage from coolant interaction.

Advanced Lead-cooled Fast Reactor European Demonstrator (ALFRED) is a small reactor with 300MW thermal power generating capability specifically proposed to test the safety and reliability of European Lead Fast Reactor (ELFR) concept. Currently, this is one of the most promising LFR concepts under development. Its design generally focuses on demonstrating the viability of LFR technologies, ensuring that future reactors can achieve the features they are supposed to. ALFRED serves as a demonstration project to validate LFR feasibility, providing critical data on neutronics behavior, thermal-hydraulics, and materials performance under operational conditions.

### **1.1.2 Research Reactors**

Research Reactors are used in nuclear research, producing medical isotopes, and material testing. For neutron activation analyses, neutron radiography tests, and other fundamental research in nuclear science, an environment with high neutron flux is often needed, which is provided by these reactors.

The Government of Bangladesh has expressed interest in acquiring a 10-20 MW Multi-Purpose Research Reactor (MPRR) to enhance nuclear research capabilities. This would increase the local production of medical isotopes, and support training programs for nuclear researchers as well as nuclear engineers.

However, before commissioning an MPRR, a detailed neutronics and thermal-hydraulic analysis is very important to understand its behavior under different operational conditions ensuring the safety, efficiency, and the compliance with regulatory standards.

## **1.2 Objectives of the Thesis**

The primary objective of this thesis is to conduct a comprehensive neutronics analysis of two distinct reactor systems: ALFRED (a Lead-cooled Fast Reactor) and a Multi-Purpose Research Reactor. The specific objectives for each reactor type are as follows:

**For ALFRED:**

- i. To evaluate key neutronics parameters, including effective multiplication factor ( $k_{\text{eff}}$ ), neutron flux distribution, power peaking factors, and reactivity feedback coefficients, to better understand reactor performance.
- ii. To investigate the burnup characteristics to evaluate long-term core behavior.
- iii. To analyze the neutronics characteristics using different reflector materials ( $\text{Ba}_2\text{Pb}$ ,  $\text{BeO}$ , Graphite, etc.).

**For MPRR:**

- i. To analyze neutronics parameters, such as effective multiplication factor ( $k_{\text{eff}}$ ), neutron flux distribution, power profile, control rod worth etc.
- ii. To investigate burnup characteristics, including the depletion of U-235 and buildup of Pu-239, Xe-135, and Sm-149, to understand the fuel cycle behavior in the reactor.

By achieving these objectives, this study aims to enhance the understanding of neutron transport and core behavior in both fast and thermal reactor systems, providing valuable insights for future reactor design improvements.

### **1.3 Research Motivation**

The global pursuit of sustainable, safe, and efficient nuclear energy systems has driven the development of advanced reactor technologies, particularly Generation IV (Gen-IV) reactors, which promise enhanced safety, improved fuel utilization, and reduced nuclear waste. Among these, Lead-cooled Fast Reactors (LFRs), such as the Advanced Lead-cooled Fast Reactor European Demonstrator (ALFRED), stand out due to their superior neutron economy, high-temperature operation, and ability to transmute long-lived actinides, addressing critical challenges in waste management and fuel sustainability (GIF, 2014). ALFRED, with its  $300 \text{ MW}_{\text{th}}$  capacity, serves as a pivotal demonstrator for validating LFR technology, offering insights into neutronics behavior, material performance, and safety under operational conditions (Alemberti et al., 2013). However, gaps in comprehensive neutronics analysis, particularly regarding long-term core behavior, actinide production,

and reflector material optimization, necessitate further investigation to enhance ALFRED's design and operational efficiency.

Simultaneously, the growing demand for nuclear research infrastructure in developing nations like Bangladesh underscores the need for advanced research reactors. The proposed 10 MW Multi-Purpose Research Reactor (MPRR) aims to bolster Bangladesh's nuclear research capabilities, supporting medical isotope production, neutron scattering, and training for nuclear engineers. The use of VVR-KN low-enriched uranium (LEU) fuel aligns with global non-proliferation standards, but detailed neutronics and burnup analyses are essential to ensure safety, efficiency, and compliance with regulatory standards (Nguyen et al., 2020). The limitations of existing 3 MW TRIGA Mark-II reactor in Bangladesh, particularly its constrained fuel supply, further highlight the urgency of developing a robust MPRR design tailored to national needs (Framatome, 2023).

This thesis is motivated by the need to advance the understanding of neutronics characteristics in both fast (ALFRED) and thermal (MPRR) reactor systems, leveraging the open-source Monte Carlo code OpenMC for high-fidelity simulations. By addressing research gaps in ALFRED's long-term core behavior, reflector material performance, and coolant activation, and by evaluating the MPRR's neutronics for isotope production and research applications, this study contributes to the global development of Gen-IV reactors and Bangladesh's nuclear research ambitions. The integration of detailed burnup analyses, actinide production assessments, and reflector comparisons provides novel insights into reactor design optimization, safety, and sustainability.

## 1.4 Research Questions

To guide this investigation, the following research questions are addressed:

### For ALFRED:

1. What are the key neutronics parameters ( $k_{\text{eff}}$ , flux distribution, power peaking factors etc.) of the ALFRED core, and how do they align with benchmark data?
2. How do burnup characteristics, including isotopic depletion and actinide production, evolve over an extended operational period, and what are the implications for fuel cycle sustainability and waste management?

3. How do different reflector materials influence neutronics performance, including  $k_{\text{eff}}$ , neutron leakage, flux and fission distribution profiles, and cycle length, in the ALFRED core?
4. What are the radiological implications of coolant activation (Lead vs. LBE) in terms of polonium-210 production and decay heat, and how do these affect reactor safety?

**For MPRR:**

1. What are the neutronics parameters (e.g.,  $k_{\text{eff}}$ , neutron flux, power distribution, and control rod worth) of the proposed 10 MW MPRR, and how do they support its design for research and isotope production?
2. How do burnup characteristics, including U-235 depletion and the buildup of neutron poisons (Xe-135, Sm-149) and Pu-239, affect the MPRR's reactivity and operational performance over a 90-day cycle?
3. How does the neutron energy spectrum of the MPRR, particularly its thermal peak, facilitate applications such as isotope production and neutron scattering?

These research questions drive the neutronics analysis, aiming to provide actionable insights for optimizing ALFRED's design as a Gen-IV demonstrator and validating the MPRR's feasibility for Bangladesh's nuclear research infrastructure.

## 1.5 Hypothesis Test

To perform a hypothesis test that confirms whether the OpenMC simulation model for ALFRED's core design and MPRR's core design aligns with benchmark data, the following hypothesis tests have been carried out:

For  $k_{\text{eff}}$ :

- **Null Hypothesis  $H_0$ :** The OpenMC result is statistically equal to the benchmark value (i.e., no significant difference).

$$H_0: k_{\text{eff}}(\text{OpenMC}) = k_{\text{eff}}(\text{Benchmark})$$

- **Alternative Hypothesis H<sub>1</sub>:** The OpenMC result is statistically different from the benchmark value.

$$H_1: k_{\text{eff}}(\text{OpenMC}) \neq k_{\text{eff}}(\text{Benchmark})$$

- **Significance level:**  $\alpha = 0.05$  (standard for 95% confidence).

## 1.6 Scope of Research Work

This study is computational in nature, utilizing advanced Monte Carlo-based neutron transport simulations to analyze reactor behavior under steady-state conditions. It focuses on key reactor physics aspects for the MPRR.

### 1.6.1 Computational Tools and Data Used

1. OpenMC: For neutron transport simulations and reactor physics analysis of ALFRED and MPRR.
2. Nuclear Data Used:
  - a. ENDF/B-VIII.0 and JEFF-3.3 for neutron cross-section data
  - b. PWR and SFR Depletion Chain data for burnup calculations

### 1.6.2 Simulation Conditions

- i. Steady-state operations are assumed, excluding transient and dynamic scenarios.
- ii. Vacuum boundary conditions are applied outside the ALFRED core to isolate reflector effects ( $k_{\text{eff}}$  and leakage) for reflector study of LFR.

### 1.6.3 Expected Contributions

- i. Computational validation against existing benchmark data
- ii. Identification of the most suitable reflector material for ALFRED, based on neutronics performance

- iii. Contribution to reactor safety assessment by evaluating key neutronics parameters and reactivity feedback mechanisms

By focusing on these aspects, this study provides valuable insights into fast reactor technology (LFRs) and research reactor performance (MPRRs), supporting future experimental validation and design improvements.

## 1.7 Limitations of the Thesis

Despite the comprehensive scope, the research has the following limitations:

### **Modeling Approximations:**

1. Simplified core geometry is used.
2. Uniform material properties are assumed, without accounting for microstructural variations that may influence fuel and moderator behavior.
3. Structural and material degradation effects (e.g., radiation damage, material swelling, and long-term mechanical degradation of core components) are not assessed.

### **Computational Constraints:**

1. Thermal-hydraulic feedback is excluded for ALFRED.
2. The study does not model dynamic reactor behavior, including transients, startup/shutdown phases, or accident scenarios.
3. Interpolated temperature-dependent cross-sections are used instead of a fully coupled physics model.
4. Burnup analysis is conducted under fixed power operation, excluding dynamic load-following scenarios.

Finally, all findings are based on Monte Carlo simulations, requiring future experimental comparison for validation.

## **1.8 Structure of the Thesis**

This thesis is organized into five chapters to systematically investigate the neutronics characteristics of the ALFRED core and a conceptual 10 MW MPRR for Bangladesh using OpenMC Monte Carlo simulations:

1. Chapter 1: Introduction establishes the research context by discussing the role of power and research reactors in clean energy and nuclear research. It outlines the thesis objectives, motivation, research questions, and hypotheses, focusing on neutronics analysis and reflector optimization for ALFRED and neutronics evaluation for MPRR. The scope, computational tools, and limitations are also defined to frame the study.
2. Chapter 2: Review of Previous Studies synthesizes existing literature on ALFRED's neutronics, reflector material selection for fast reactors, and neutronics of research reactors like MPRR. It identifies research gaps for ALFRED and the need for detailed MPRR neutronics studies, justifying the contributions of this thesis.
3. Chapter 3: Computational Methods and Design describes the OpenMC Monte Carlo methodology used for neutron transport simulations. It details the design specifications of ALFRED core, reflector configurations, and VVR-KN fuel-based MPRR core, along with simulation conditions, nuclear data libraries, and error calculation approaches.
4. Chapter 4: Results and Discussions presents the simulation outcomes. For ALFRED, it analyzes neutronics parameters (e.g.,  $k_{\text{eff}}$ , neutron flux, power distribution), burnup trends, coolant activation (lead vs. LBE), and the performance of 12 reflector materials. For MPRR, it evaluates neutronics parameters, burnup cycle, and isotopic depletion, confirming its suitability for research.
5. Chapter 5: Conclusion and Future Perspectives summarizes key findings, evaluates them against the research objectives, and discusses implications for reactor design and safety. It provides recommendations for future work to advance ALFRED and MPRR development.

## CHAPTER 2

### REVIEW OF PREVIOUS STUDIES

#### 2.1 ALFRED Neutronics Analysis

##### 2.1.1 Introduction

Studies of various aspects of nuclear reactors consider the safety features of the reactor systems. Thermal hydraulics and neutronics studies of nuclear reactors provide adequate safety margins to adhere to which can significantly reduce the safety concerns as they attempt to find more robust safety features. Nuclear reactors based on the fast neutron spectrum are prominent in their transmutation capability of transuranic actinides. This behavior of the fast reactors helps reduce the amount of nuclear waste thus reducing the long-term radiotoxicity. Fast reactors are designed to burn plutonium generated during their operational lifecycle, a process that enhances their inherent resistance to proliferation by reducing the suitability of the plutonium for weapons-grade material through sustained high burnup, as outlined in the Generation IV International Forum (GIF) Technology Roadmap Update of 2014 (GIF, 2014). This roadmap highlights that the fast reactors produce plutonium-239, a fissile material, utilizing uranium-238 which consists of 99.3% of natural uranium, thereby maximizing the utilization of abundant natural uranium resources and supporting long-term energy sustainability. Among the various fast spectrum nuclear reactor designs, Lead-cooled Fast Reactors (LFRs) have been identified by the GIF as one of the most promising systems for further development and study, owing to their potential to meet the forum's goals of improved safety, economic competitiveness, and minimized nuclear waste, as detailed in the 2014 roadmap provided by the GIF.

LFRs utilize molten lead as their primary coolant, offering a distinct advantage over other fast reactor designs such as Gas-cooled Fast Reactors (GFRs) and Sodium-cooled Fast Reactors (SFRs), which employ helium gas and molten sodium, respectively. LFRs are considered safer than SFRs due to their superior natural circulation capabilities, which enhance heat removal during operational transients, and the significantly higher boiling point of lead (approximately 1749 °C) compared to sodium (883 °C), reducing the risk of coolant boiling under severe accident conditions. Additionally, chemical inertness of lead eliminates the potential for exothermic reactions or fires when exposed to air, water, or

water vapor, a critical safety benefit over sodium, which can ignite spontaneously in such environments, further solidifying the robust safety profile of LFRs. However, this safety advantage is tempered by challenges such as the need for protective oxide layers or coatings on structural materials to mitigate erosion, particularly at elevated temperatures above 870 K, requiring further research into corrosion-resistant materials and their behavior under irradiation (Tuček et al., 2006).

In addition to pure lead, a coolant option for Lead-cooled Fast Reactors (LFRs) is Lead-Bismuth Eutectic (LBE), which offers a significant advantage by lowering the melting point of the coolant to approximately 125 °C, compared to 327 °C for pure lead, thus facilitating easier management of coolant solidification during reactor shutdowns or maintenance. However, the use of LBE as a coolant introduces notable challenges, including increased corrosion within the reactor environment, as the bismuth component accelerates the degradation of structural steels, particularly under long-term exposure, where short-term tests indicate that oxidation kinetics deviate from simple parabolic laws and may follow more complex models like the Tedmon equation or a power law for pure iron, necessitating advanced oxygen control technologies and protective oxide layers to mitigate material degradation. Furthermore, LBE coolant enhances the production of polonium-210, an alpha-emitting toxic radionuclide formed through neutron capture by bismuth-209, posing radiological safety concerns due to its high radiotoxicity, although current research suggests that polonium can be effectively managed with existing control measures, as highlighted in the comprehensive review of LBE coolant properties and challenges (Zhang et al., 2014).

The Advanced Lead-cooled Fast Reactor European Demonstrator (ALFRED), a demonstrator reactor with a nominal thermal power of 300 MW<sub>th</sub>, was proposed by Ansaldo Nucleare under the Lead-cooled European Advanced DEMonstration Reactor (LEADER) project, funded by the European Commission within the 7th Framework Programme, to serve as a scaled prototype for the European Lead Fast Reactor (ELFR) concept, focusing on validating its safety, reliability, and operational feasibility as a lead-cooled fast reactor (LFR) technology. ALFRED's design addresses key challenges identified in prior LFR projects by incorporating specific safety provisions and design options, such as the reactor vessel, steam generators, primary pumps, and decay heat removal system, ensuring alignment with the Generation IV International Forum's goals of enhanced safety, economic competitiveness, and reduced nuclear waste (Alemberti et al., 2013).

### **2.1.2 Multi-Physics and Safety Studies**

Numerous studies have explored ALFRED from various perspectives, with a significant investigation involving the development of a Multiphysics model coupling neutronics and thermal hydraulics to analyze the ALFRED core, utilizing the Monte Carlo-based neutron transport code SERPENT for stochastic neutronics simulations and the computational fluid dynamics (CFD) tool OpenFOAM for thermal hydraulics to compute average temperature distributions of lead coolant, cladding, and fuel within the fuel assemblies. This model enhances neutron physics accuracy by evaluating nuclide cross-sections on-the-fly, accounting for spatially non-uniform temperature distributions, and employs the Temperature Multiplier Scheme (TMS) to reduce computational effort and memory demands, with results consistent with ALFRED's design parameters and existing literature. Future research directions include perturbation analyses to examine nuclear data sensitivities, such as the spatial variation of the effective multiplication factor's sensitivity to lead density and extending the model to simulate transients using SERPENT's dynamic simulation mode for time-dependent Monte Carlo solutions (Di Lecce et al., 2020).

Regarding transient analyses, two critical unprotected transient scenarios specific to Lead-cooled Fast Reactors (LFRs)—namely the Unprotected Loss of Flow (ULOF), where the coolant flow ceases without safety intervention, and the Unprotected Transient OverPower (UTOP), characterized by an unintended increase in reactor power—were meticulously reproduced and subjected to comprehensive safety evaluations through the development of a detailed thermal-hydraulic geometrical scheme encompassing the entire reactor structure. This study utilized the PHISICS/RELAP5-3D coupled approach, where PHISICS, a Parallel and Highly Innovative Simulation for INL Code System developed by Idaho National Laboratory (INL), provides a sophisticated neutron kinetic model capable of handling multi-group energy calculations and angular transport variations, while RELAP5-3D, a validated thermal-hydraulic system code, simulates innovative fluids like lead and lead alloys with a fully integrated multi-dimensional nodalization. The analysis focused on the ALFRED demonstrator, a pool-type LFR with a nominal thermal power of 300 MW<sub>th</sub>, starting from beginning-of-life (BOL) steady-state conditions to assess the reactor's response to these accidental scenarios, ensuring that neutronics and thermal-hydraulics parameters remain within safe limits and demonstrating the robustness of ALFRED's design. The results, consistent with literature data from other independent codes, highlight

the coupled methodology's ability to capture both global system behavior and localized phenomena, such as temperature peaks, paving the way for further evaluations of new ALFRED configurations (Ciurluini et al., 2020).

A comprehensive study on the safety of Lead-cooled Fast Reactors (LFRs), focusing on thermal-hydraulic performance, radiation damage, and primary pool activation in the Advanced Lead-cooled Fast Reactor European Demonstrator (ALFRED) under the LEADER project, utilized neutronics codes (MCNPX, ERANOS), thermal-hydraulic tools (TRACE, ANTEO, CFD), transient simulations (RELAP, CATHARE, SIM-LFR), and lead activation analysis (FISPACT), confirming ALFRED's "robust and forgiving" design, meeting safety standards despite requiring shielding improvements, with ongoing validation efforts (Grasso et al., 2014). The control rod designs for the Advanced Lead-cooled Fast Reactor European Demonstrator (ALFRED) were investigated using various absorber materials, with the conventional boron carbide ( $B_4C$ ) serving as the reference material, while alternative options such as hafnium boride ( $HfB_2$ ), hafnium hydride ( $HfH_{1.18}$ ), and europium oxide ( $Eu_2O_3$ ) were evaluated for their reactivity worth using the Monte Carlo particle transport code OpenMC. This study, aimed at enhancing safety and extending cycle length for next-generation fast reactors, demonstrated that the  $B_4C$ -based reference design effectively meets shutdown and operational requirements, while enriched  $HfB_2$  and  $HfH_{1.18}$  prove viable substitutes for the operational section, with  $HfH_{1.18}$  exhibiting minimal localized impact on core power distribution.  $Eu_2O_3$  showed negligible loss in absorption capacity after multiple irradiation cycles, fulfilling shutdown functions with only partial insertion, though requiring a deeper initial insertion to compensate for reactivity, highlighting its potential as an alternative absorber material. Future assessments are planned to evaluate the safe operating life of these materials, considering irradiation-induced swelling, temperature margins, and gas release effects (Guo et al., 2021).

### 2.1.3 Research Gaps

Despite these advances, several critical gaps remain, particularly in the comprehensive simulation of the ALFRED core with a specific focus on long-term core behavior, actinide production, and fuel burnup characteristics. The purpose of this study is to evaluate the important neutronic parameters such as the axial flux distribution, radial flux distribution, fission rate distribution, power distribution profiles, and burnup characteristics using the open-source Monte Carlo code OpenMC (Romano et al., 2015).

One of the key novel aspects of this work is the use of detailed, time-dependent simulations that account for fuel consumption and actinide production over an extended burnup period of 5 years, which has not been fully explored in the context of ALFRED before. By integrating fuel burnup analysis, actinide generation, and power distribution, this study presents a more comprehensive understanding of the reactor's long-term performance. Another novel aspect is the comparison of different nuclear data libraries, ENDF/B-VIII.0 (Brown et al., 2018) and JEFF-3.3 (Plompen et al., 2020) and their impact on the calculated  $k_{\text{eff}}$  and other neutronic parameters.

Furthermore, the production of long-lived actinides such as Americium-241 (Am-241) and Plutonium-239 (Pu-239) has been a subject of concern in nuclear reactors due to their impact on waste management and radiotoxicity. This study further presents a detailed analysis of actinide production in the ALFRED core using MOX fuels using both coolants lead and lead-bismuth eutectic (LBE), showing the time-dependent evolution of various actinides, such as Np-237, Am-241, Am-243, Cm-244, and Cm-245. The findings indicate significant differences in the actinide production between the MOX1 and MOX2 fuels, the fuel composition used in the inner and outer fuel assemblies in the ALFRED core respectively, a key observation that provides new insight into the fuel composition and its influence on waste management. In LFRs, Polonium production through coolant activation is a point of concern due to its radiotoxicity. Our study also evaluates the concentration buildup of polonium isotopes in ALFRED core in both the cases of Lead and LBE used as coolants.

## 2.2 ALFRED Reflector Material Selection on Neutronics Properties

### 2.2.1 Introduction

Neutron reflectors in fast reactors like ALFRED reduce leakage by reflecting escaping neutrons back into the core, supporting a hard spectrum vital for fuel utilization and actinide transmutation (Lewis, 2008). Effective reflectors require high scattering and low absorption cross-sections, compatibility with lead coolant, and stability under high temperatures and radiation, with minimal moderation. While extensive reflector studies exist for Sodium-cooled Fast Reactors (SFRs) and Gas-cooled Fast Reactors (GFRs), these findings are not directly applicable to Lead-cooled Fast Reactors (LFRs) due to fundamental differences in their design and operational parameters, leaving a gap in detailed analysis for LFRs.

### 2.2.2 SFR

For a compact sodium-cooled breed-and-burn fast reactor (B&BR), a neutronics study employed Monte Carlo simulations to evaluate reflector materials (Pb, LBE, LME, PbO, MgO, Ni, HT-9 steel) for neutron economy, assessing core lifetime, leakage, spectrum, power distribution, CVR, and GEM worth (Hartanto et al., 2015). Lead-based reflectors (Pb, LBE, LME, PbO) surpassed HT-9 by improving reflection and reducing absorption, with PbO matching LBE and LME's neutronic performance and offering better compatibility, despite a slight CVR increase, positioning them as promising alternatives. Another study used OpenMC simulations to evaluate nine reflector materials for the ABR-1000, an SFR, identifying BeO as the optimal axial reflector with minimal neutron leakage (0.0517% at EOL) and uniform flux, and PbO as the best radial reflector with low leakage (0.84335% at EOL) and extended cycle length (Niloy et al., 2025).

While the study's focus on neutronics parameters like leakage, power distribution, and safety, differences in the properties of coolant material used i.e., sodium versus lead coolant, limit direct applicability, underscoring the need for LFR-specific reflector studies. A study on the ASTRID Generation IV sodium-cooled fast reactor (SFR) in France investigated the neutronic performance of magnesium oxide (MgO) as the reference reflector material, comparing it to alternatives like stainless steel, using simplified 1-D and 2-D deterministic models validated by Monte Carlo simulations (Blanchet, 2017). MgO, prized for its

radiation resistance, high-temperature stability, low absorption, and high scattering cross-sections, excelled in reactivity, albedo at core-reflector interfaces, and neutron economy enhancement, though MgAl<sub>2</sub>O<sub>4</sub> and Y<sub>3</sub>Al<sub>5</sub>O<sub>12</sub> showed comparable reactivity, and TiC and ZrC provided slightly better shielding. These results affirm MgO's effectiveness for SFR core performance (Macdonald and Driscoll, 2010).

### 2.2.3 GFR

The neutronic performance of materials for Gas-Cooled Fast Reactor (GFR) applications was extensively evaluated in a study using coupled Monte Carlo (MCNP) and isotopes (ORIGEN) simulations, with CO<sub>2</sub> as the reference coolant (Yu, 2003). The study highlighted that while low macroscopic absorption cross sections ( $\Sigma_a$ ) and slowing-down power ( $\xi\Sigma_s$ ) provide qualitative insights into material suitability, comprehensive calculations are essential for accurate performance assessment. Notably, materials such as Zr<sub>3</sub>Si<sub>2</sub>, ZrC, Ba<sub>2</sub>Pb, and Ni emerged as promising reflector candidates due to their favorable burnup potential and reduced coolant void reactivity, despite trade-offs in reactivity lifetime for some diluents. Plutonium-fueled cores exhibited significantly higher void reactivity compared to U-235-based designs, underscoring fuel choice as a critical design parameter. These findings emphasize the complexity of material selection for GFR service, where neutronic advantages must be balanced against thermal and mechanical considerations.

Further advancing the exploration of reflector materials for fast reactors, another study investigated magnesium oxide (MgO) as a superior alternative to steel in blanket-free designs, leveraging the ERANOS code to model reactivity-limited burnup (Macdonald and Driscoll, 2010). Their findings demonstrated that substituting steel radial and axial reflectors with MgO increased burnup by 30% to 50% in a 2400 MW<sub>th</sub> sodium-cooled fast reactor (SFR) with a unity conversion ratio, a result consistent across both metal and oxide fuel configurations. This enhancement stems from MgO's favorable neutronic properties, including higher albedo compared to steel or depleted uranium blankets, as initially surveyed by Yu, 2003 for GFR reflectors. However, challenges such as interfacial power peaking and a more positive coolant void reactivity late in life were noted, necessitating further design optimization. The study also highlighted MgO's compatibility with sodium and its potential to enable sub-20% U-235 enrichment levels, aligning with safeguards limits and reducing reliance on uranium blankets, a trade-off Yu, 2003 identified with

materials like  $Zr_3Si_2$  and  $Ba_2Pb$ . Together, these works underscore the pivotal role of reflector selection in optimizing fast reactor performance and proliferation resistance.

A neutronics analysis of reflector options for the 75 MW<sub>th</sub> ALLEGRO GFR core evaluated SiC, ZrC,  $Zr_3Si_2$ , and stainless steel (15-15Ti) using Serpent 2.1.32 Monte Carlo simulations (Pónya et al., 2024). Results of this study indicate ZrC as the optimal choice, achieving the highest  $k_{eff}$  of 1.06341 and reserve reactivity of 5962 pcm at beginning of life (BOL). ZrC also provided a more flattened power distribution where peaking factor was found to be 1.179 and reduced fast neutron flux on the reactor pressure vessel (RPV) wall, attributed to its low absorption cross-section and high melting point greater than 3500 K. SiC, while effective in reducing neutron leakage, exhibited excessive thermalization in outer fuel pins, increasing pin-wise power peaking to 1.799 in external assemblies, a concern for core cooling.

In recent developments, another neutronics study of the Allegro-75 MW<sub>th</sub> reactor compared axial, radial, and axial + radial heterogeneous core configurations with UPuC fuel and reflectors like BeO and ZrC, identifying BeO as optimal at a 60 cm axial thickness (Shohanul, 2025). The study identified the axial + radial configuration with UPuC as optimal, achieving a cycle length exceeding ten years, uniform neutron flux, low power peaking factors (PPF), high effective delayed neutron fraction (beta effective), and a negative Doppler constant. Among reflector options, BeO outperformed others at an optimal axial thickness of 60 cm, delivering superior neutronics parameters, though it exhibited a softer neutron spectrum and reduced breeding ratio compared to ZrC. This aligns with earlier findings by Yu, 2003, who evaluated Zr-based compounds like  $Zr_3Si_2$  for GFR reflectors, and Macdonald and Driscoll (2010), who noted BeO's reactivity enhancement in SFRs but flagged its excessive moderation. This work highlights BeO's trade-offs, favoring neutronics stability over transmutation efficiency, underscoring the ongoing challenge of balancing reflector performance with core design objectives in fast reactor systems.

Complementary insights emerge from another detailed neutronics study previously done, where reflector materials for a 250 MW<sub>th</sub> modular GFR were assessed using OpenMC (Raflis et al., 2021). Eight candidates (pure Ni, Mg, Pb, PbO,  $Ba_2Pb$ , BeO, SiC, and  $Zr_3Si_2$ ) were evaluated for neutronics parameters including  $k_{eff}$ , neutron leakage, and core lifetime. BeO emerged as the standout performer, sustaining  $k_{eff}$  greater than 1.0 beyond 20 effective

full power years (EFPY) with a reflector thickness of 60 cm, due to its high albedo (93.5%) and broad scattering cross-section, which minimized leakage to under 3% at a burnup of 250 GWd/MTHM. SiC and  $Zr_3Si_2$  also showed promise, with core lifetimes of 18 and 16 EFPY, respectively, though SiC's softening of the neutron spectrum slightly reduced fast flux efficiency. Lead-based materials (e.g.,  $Ba_2Pb$ ), despite high density, underperformed with higher leakage of about 10% at a burnup of 125 GWd/MTHM and shorter lifetimes of 13-15 EFPY, underscoring the preference for lighter, high-melting-point materials in GFRs.

#### 2.2.4 LFR

A neutronics study of the LOTUS reactor, a 200 MW<sub>th</sub> lead-cooled fast reactor for floating applications, evaluated reflector materials  $Al_2O_3$ , BeO, MgO, PbO,  $SiO_2$ , and  $ZrO_2$  using Serpent Monte Carlo simulations to achieve a 20-year core life (Hong et al., 2023). MgO emerged as the optimal reflector, offering low neutron leakage, a high initial  $k_{eff}$  of 1.16049, a stable reactivity swing of 0.11789, and a uniform power peaking factor of 1.27 at beginning of cycle (BOC), and 1.25 at the end of cycle (EOC), alongside a negative coolant void reactivity of -1862 pcm at BOC, attributed to its high scattering and low absorption properties. BeO, while effective in reflecting neutrons, softened the spectrum, accelerating fuel depletion, making MgO preferable for neutron economy in this lead-cooled design. Another study on the ALMANAR reactor, a 45 MW<sub>th</sub> lead-cooled small modular reactor (SMR), assessed steel, MgO, PbO, and Pb as reflectors using Serpent simulations, selecting 20 cm thick Pb for its compatibility with the lead coolant and contribution to a 22-year core lifetime (Hartanto et al., 2020). The Pb reflector provided a worth of 4000 pcm, reduced core size of radius less than 1m, and ensured a negative coolant void reactivity of -2378 pcm at BOC, enhancing safety by increasing leakage during voiding scenarios. Enrichment zoning further flattened radial power distribution, aligning with compact LFR design goals, though its performance in larger-scale systems like ALFRED requires further exploration.

ALFRED employs Yttria-Stabilized-Zirconia (YSZ) as its reflector material, a choice confirmed by our thesis design. However, its role as a reflector in fast reactors, particularly LFRs, lacks extensive literature support. Unlike SFRs or GFRs, where reflector choices are well-documented, YSZ's neutronics properties in a lead-cooled, fast-spectrum environment remain underexplored, making its evaluation a key contribution of this study.

## **2.3 MPRR Neutronics Analysis**

### **2.3.1 Introduction**

Research reactors serve as essential tools for scientific research, education, and the production of radioisotopes for numerous fields including materials science, medicine, and nuclear physics. Unlike power reactors, these facilities operate at significantly lower power levels (typically below 20 MW) and are designed primarily for neutron generation rather than electricity production, allowing researchers to conduct neutron scattering experiments, neutron activation analysis, and various irradiation services (IAEA, 2022). Their compact design and flexible operating parameters make them particularly valuable for training nuclear engineers, testing new fuel designs, and developing advanced reactor technologies while providing crucial medical isotopes for diagnostic procedures and cancer treatments worldwide.

Bangladesh has been advancing its nuclear research capabilities through the 3 MW TRIGA Mark-II research reactor, operational since 1986 at the Atomic Energy Research Establishment in Savar. This reactor, managed by the Bangladesh Atomic Energy Commission (BAEC), has been instrumental in various applications, including neutron activation analysis, neutron radiography, neutron scattering, radioisotope production (such as Iodine-131 and Technetium-99m), and manpower training (Zulquarnain et al., 2009). However, the sustainability of this facility is challenged by limited availability of its specific fuel type, uranium-zirconium hydride, which, despite resumed production by TRIGA International since 2021, remains constrained by modest global output and Bangladesh's lack of a confirmed fuel supply contract (Framatome, 2023). To address this challenge and enhance its nuclear research infrastructure, Bangladesh is considering the acquisition of a higher-capacity multi-purpose research reactor (MPRR) with a power range of 10-20 MW, utilizing VVR-KN type fuel. This low-enriched uranium fuel, developed by Russia, is used in reactors like the VVR-K in Kazakhstan and aligns with global non-proliferation standards (Arinkin et al., 2017).

A key study supports Bangladesh's nuclear research ambitions by proposing a 10 MW multi-purpose research reactor (MPRR) that aligns with the power range under consideration, utilizing VVR-KN low-enriched uranium fuel to meet advanced research

needs (Nguyen et al., 2020). The research provides valuable insights into the effective use of VVR-KN fuel, demonstrating its suitability for modern research reactors. The study employs neutronics and thermal hydraulics analyses to confirm the reactor's feasibility and safety, ensuring compliance with international non-proliferation standards. This design is particularly relevant for neutronics studies, providing a foundation for analyzing reactor performance and advancing Bangladesh's nuclear science infrastructure.

### **2.3.2 VVR-KN Fuel: Characteristics and Rationale**

The VVR-KN fuel represents a modern evolution within the VVR family of research reactor fuels, primarily developed in Russia, and is distinguished by its use of low-enriched uranium (LEU) with an enrichment level of 19.75% U-235 (Nguyen et al., 2020; Osipovich et al., 2012). This enrichment level is a key advantage, aligning with global efforts to minimize the proliferation risks associated with highly enriched uranium (HEU) used in older VVR fuel types like VVR-S and VVR-C. Compared to other LEU VVR fuels such as VVR-M, the VVR-KN variant is designed to provide a balance of high neutron flux and efficient power output while maintaining this crucial LEU status (Osipovich et al., 2012). The development and adoption of VVR-KN fuel are rooted in the need for a fuel type that not only meets stringent non-proliferation standards but also supports the advanced research and application demands of modern multipurpose research reactors (MPRR) (Nguyen et al., 2020; IAEA Research Reactor Fuel Cycle).

The VVR-KN fuel assembly is characterized by its unique hexagonal plate-type geometry, comprising eight coaxial fuel elements in the standard assembly, with a specific design (five-tube assembly) also available for control rod placement (Nguyen et al., 2020; Hanan and Garner, 2015). The fuel meat consists of Uranium Dioxide ( $\text{UO}_2$ ) dispersed in an Aluminum (Al) matrix, with a uranium density of approximately  $2.8 \text{ gU/cm}^3$  (Arinkin et al., 2017; Nguyen et al., 2020). This composition, combined with the LEU enrichment, allows for a compact core design capable of achieving high neutron fluxes (Nguyen et al., 2020). The fuel elements are typically clad in a SAV-1 aluminum alloy, providing structural integrity and facilitating heat transfer to the coolant (Nguyen et al., 2020). This detailed design, with its coaxial hexagonal tubes, presents unique challenges for neutronic and thermal-hydraulic modeling, requiring sophisticated computational tools for accurate analysis (Zavala et al., 2025; Nguyen et al., 2020).

The rationale for utilizing VVR-KN fuel in MPRRs is diverse. Its LEU composition inherently reduces nuclear proliferation risks, a paramount consideration in contemporary reactor design and operation (Osipovich et al., 2012). Furthermore, VVR-KN fuel has demonstrated its capability to achieve high thermal neutron fluxes, a critical requirement for the diverse applications of MPRRs, including radioisotope production, neutron activation analysis, and material testing (Nguyen et al., 2020; Osipovich et al., 2012). The successful conversion of the WWR-K research reactor in Kazakhstan from HEU to VVR-KN fuel serves as a significant case study, validating the fuel's performance and reliability in a real-world application and even showing potential improvements in neutron-physical characteristics (Arinkin et al., 2017; Nguyen et al., 2020; Hanan and Garner, 2015).

### **2.3.3 Research Gap**

The neutronics performance of VVR-KN fuel, a low-enriched uranium (LEU) option for multi-purpose research reactors (MPRRs), is critical for advancing Bangladesh's nuclear research infrastructure, yet it remains underexplored due to the fuel's relatively recent development (Nguyen et al., 2020; Arinkin et al., 2017). While studies have demonstrated VVR-KN's suitability for achieving high neutron fluxes in reactors like the 10 MW conceptual MPRR, comprehensive analyses of long-term core behavior, including fuel burnup, neutron poison accumulation, and actinide production, are limited. These parameters are essential for ensuring reactor safety, efficiency, and operational longevity, particularly for a country like Bangladesh planning a 10-20 MW MPRR. Furthermore, neutronics simulations for VVR-KN fuel rely on specific computational tools, necessitating validation studies using multiple codes and tools to ensure accurate results.

The 10 MW MPRR conceptual design serves as a valuable basis for neutronics research, providing a foundation for evaluating VVR-KN fuel performance in Bangladesh's planned research reactor (Nguyen et al., 2020). However, the hexagonal geometry of VVR-KN fuel assemblies presents challenges for accurate neutron transport modeling, requiring high-fidelity simulations to capture neutron flux distributions, power profiles, and depletion characteristics. Validation studies using multiple computational codes are essential, especially if Bangladesh considers scaling the 10 MW design to a 10-20 MW MPRR, which may introduce additional uncertainties in neutronics behavior. Such studies are vital for

optimizing reactor performance for applications like radioisotope production and neutron scattering while meeting international safety standards.

This part of the thesis contributes to addressing these gaps by developing a preliminary neutronics model for an MPRR, based on the 10 MW conceptual design, using OpenMC with the ENDF/B-VIII.0 nuclear data library (OpenMC and ENDF reference). The study explores critical neutronics parameters, including effective multiplication factor ( $k_{\text{eff}}$ ), neutron flux, and power distribution, while placing particular emphasis on extended analyses such as fuel depletion, neutron poison buildup, and actinide generation. These investigations provide deeper insights into core behavior over time, supporting the development of effective MPRR designs for Bangladesh. By leveraging advanced computational tools and cross-validating results, this research aims to enhance the understanding of VVR-KN fuel performance, paving the way for a safe and efficient nuclear research infrastructure in Bangladesh.

## CHAPTER 3

### COMPUTATIONAL METHODS AND DESIGN

#### 3.1 Overview of OpenMC and Simulation Approach

OpenMC is an open-source neutron photon transport simulation code based on the Monte Carlo Method. OpenMC can track how these particles move and interact within a defined geometry and with different materials. It is widely used in designing and analysis of nuclear reactors. OpenMC uses a stochastic approach, instead of solving the complex neutron transport equation directly it simulates the behavior of each particle by tracking the random interactions like scattering, absorption, fission. By simulating a large number of particles, it can statistically estimate the desired quantities such as  $k_{\text{eff}}$ , neutron flux, reaction rates. OpenMC primarily operates in the continuous-energy mode, where it runs the transport simulations using continuous energy cross section data.

The stochastic neutron-photon transportation code OpenMC uses the Monte Carlo method for the use of neutronics analysis of a reactor core (Romano et al., 2015). It was first developed in 2011 by MIT's Computational Reactor Physics Group, but community development is still ongoing today. It can compute fixed source,  $k$ -eigenvalue, and subcritical multiplication on models constructed using CAD representation or with constructive solid geometry. It supports both continuous- energy and multigroup transport. It has built-in Python and C/C++ APIs that makes data preprocessing, post processing, visualization and depletion calculations much more comfortable.

##### 3.1.1 Monte Carlo Method and its Application in OpenMC

The Monte Carlo method is a stochastic computational technique that uses random sampling to solve deterministic problems. Instead of solving neutron transport equations analytically or using deterministic discretization methods, it tracks individual neutron histories by probabilistically modeling their interactions within the reactor environment. One of its key strengths is its ability to accurately represent complex reactor geometries without the need for excessive simplifications, unlike deterministic methods, which often require spatial meshing and approximations. Additionally, it incorporates continuous energy interactions, meaning that neutron interactions are modeled across a wide spectrum of energies rather than being restricted to predefined energy groups. This enhances the

accuracy of cross-section evaluations, allowing for more realistic neutron behavior modeling in fast and thermal reactor systems.

The method also accounts for probabilistic neutron behaviors, including:

- **Scattering:** Neutrons change direction and energy upon colliding with atomic nuclei, affecting neutron flux distributions.
- **Absorption:** Some neutrons are captured by fuel or structural materials, leading to nuclear reactions or decay.
- **Fission:** When neutrons interact with fissile materials (e.g., U-235, Pu-239), they may induce fission, releasing energy and secondary neutrons that sustain the chain reaction.

By tracking millions of neutron histories, the Monte Carlo method provides high-fidelity simulations of neutron transport, making it an essential tool for reactor physics, shielding analysis, and criticality safety assessments.

When applied in OpenMC, the Monte Carlo method enables high-precision simulations of neutron transport, allowing for the detailed calculation of key reactor physics parameters such as neutron flux, effective multiplication factor ( $k_{\text{eff}}$ ), and power distribution in both ALFRED and MPRR.

- **Neutron Flux Calculation:** OpenMC tracks neutron trajectories and interactions, providing a spatial and energy-dependent distribution of neutron flux. This helps analyze neutron economy, fuel utilization, and core performance.
- **Effective Multiplication Factor ( $k_{\text{eff}}$ ):** By simulating neutron population behavior over multiple generations, OpenMC determines  $k_{\text{eff}}$ , which indicates whether the reactor is critical, subcritical, or supercritical. This is crucial for reactor startup, shutdown, and safety assessments.
- **Power Distribution:** OpenMC models fission reaction rates across different reactor regions, helping evaluate energy deposition, heat generation, and core thermal performance. This information is vital for designing efficient cooling and fuel management strategies.

### 3.1.2 Limitations of OpenMC

Despite its high accuracy and flexibility, the Monte Carlo method in OpenMC comes with significant computational demands due to its statistical approach:

- **Large Number of Simulated Histories:** To reduce statistical uncertainties, OpenMC must simulate millions or even billions of neutron histories, which requires high-performance computing resources.
- **Slow Convergence for Rare Events:** In systems with low neutron flux regions (e.g., reflectors or shields), achieving statistically significant results takes longer compared to deterministic methods.
- **Parallel Computing Needs:** Large-scale Monte Carlo simulations often require multi-core processing and cluster computing to improve efficiency and reduce computational time.

Regardless of these challenges, OpenMC's scalability and accuracy make it a powerful tool for reactor analysis, enabling detailed neutronics evaluations of ALFRED and MPRR to optimize their design and performance.

### 3.1.3 Simulation Approach in OpenMC

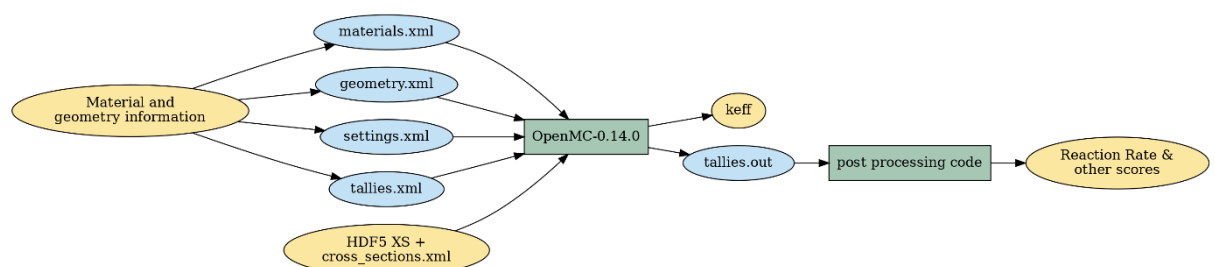


Fig. 3.1: Workflow chart of OpenMC.

### 3.1.4 Data Libraries

In OpenMC simulations, selecting appropriate nuclear data libraries is crucial for accurate modeling of neutron interactions. This study utilized two prominent cross-section libraries: ENDF/B-VIII.0 and JEFF-3.3.

**ENDF/B-VIII.0:** This library encompasses comprehensive incident neutron data, photoatomic data, atomic relaxation data, and thermal scattering data. The incident neutron data is processed at six distinct temperatures: 250 K, 293.6 K, 600 K, 900 K, 1200 K, and 2500 K, facilitating simulations across a range of thermal conditions. All ACE files for this library were generated using NJOY 2016.68 (Brown et al., 2018).

**JEFF-3.3:** This library provides incident neutron and thermal scattering data. Similar to ENDF/B-VIII.0, the incident neutron data is available at six temperatures: 250 K, 293.6 K, 600 K, 900 K, 1200 K, and 2500 K. Notably, JEFF-3.3 does not include its own photoatomic or atomic relaxation sub-libraries; hence, data from ENDF/B-VIII.0 is incorporated to supplement these aspects. The ACE files were also produced using NJOY 2016.68 (Plompen et al., 2020).

For depletion analyses, OpenMC requires a depletion chain file in XML format, detailing decay data, fission product yields, and transmutation pathways. In this study, the PWR depletion chain was employed for the Multi-Purpose Research Reactor (MPRR), while the SFR depletion chain was utilized for the ALFRED core. These chain files are accessible on OpenMC's official website. Pre-generated HDF5-formatted nuclear cross-section data libraries, including ENDF/B-VIII.0 and JEFF-3.3, are available for download from OpenMC's data library repository. Utilizing these libraries ensures consistency and reliability in simulation results.

By integrating these data libraries and depletion chains, the study ensures robust and precise modeling of neutron behavior and material transmutation within the reactor systems under investigation.

### 3.1.5 Normalization of Data

OpenMC outputs the fission rate in units of [fissions/src] and neutron flux in [neutrons-cm/src], where "src" denotes the source neutron population used in the simulation. To express these quantities in conventional or physical units (fissions/s and neutrons/cm<sup>2</sup>-s), a normalization procedure was applied using the reactor's thermal power.

### 3.1.5.1 Normalization Factor for Spatial Neutron Flux and Fission Rate

The total recoverable heating energy from fission events, recorded in eV per source neutron (eV/src), was used to derive a scaling factor.

$$f_{\text{fission}} = \frac{P}{qH} \quad (3.1)$$

where,

P = Thermal Power (W),

H = heating tally (eV/src),

q =  $1.602 * 10^{-19}$  (J/eV), and

$f_{\text{fission}}$  = fission normalization factor (src/s).

### Fission Rate Conversion

The tallied fission rate (fissions/src) was scaled to physical units (fissions/s) by multiplying by  $f_{\text{fission}}$ :

$$\text{Normalized Fission Rate (fissions/s)} = \text{Fission Rate (fissions/src)} \cdot f_{\text{fission}} (\text{src/s})$$

### Neutron Flux Conversion

The neutron flux tally (neutrons-cm/src) was normalized to [neutrons/cm<sup>2</sup>·s] by accounting for the spatial mesh volume V(cm<sup>3</sup>):

$$f = \frac{f_{\text{fission}}}{V} \quad (3.2)$$

Then the tallied neutron flux (neutrons-cm/src) was scaled to physical units (neutrons/cm<sup>2</sup>·s) by multiplying by f:

$$\text{Normalized Neutron Flux (neutrons/cm}^2\text{-s)} = f \cdot \text{Neutron Flux (neutrons-cm/src)}$$

This approach aligns with standard Monte Carlo normalization techniques, where absolute reaction rates are derived from a known power or source strength.

### 3.1.5.2 Normalization Factor for Energy Dependent Neutron Flux

The energy-dependent neutron flux was tallied in units of [neutrons/cm-src] across a logarithmically spaced energy grid from  $1 \times 10^{-5}$  eV to 20 MeV, comprising 501 energy bins. To convert this to physical units [neutrons/cm<sup>2</sup>-s], a comprehensive normalization procedure was developed.

Additional tallies were implemented for:

- i. Total fission reaction rate [fissions/source]
- ii. Neutron production rate from fission [neutrons/source]

### Fuel-Specific Energy Release Parameters

The normalization requires the energy released per fission (Q-value), which varies by isotope. The effective Q-value for MOX fuel was calculated as a volume-weighted average of-

1. MOX1 (21.7% PuO<sub>2</sub> + 78.3% UO<sub>2</sub>)
2. MOX2 (27.8% PuO<sub>2</sub> + 72.2% UO<sub>2</sub>)

### Normalization Calculation

The conversion from [neutrons-cm/src] to [neutrons/cm<sup>2</sup>-s] was done using-

$$\phi_{normalized}(E) = \phi(E) \cdot \frac{P\vartheta}{VQ\kappa} \quad (3.3)$$

where,

$P$  = reactor thermal power (300 MW =  $3 \times 10^8$  J/s)

$\vartheta$  = neutrons produced per fission [neutrons/fission]

$V$  = total fuel volume [cm<sup>3</sup>]

$Q$  = effective energy release per fission [J/fission]

$\kappa$  = neutron production rate [neutrons/src]

A dimensional analysis provides the unit of the right-hand side to be equal to-

$$\frac{\left(\frac{\text{neutrons} \cdot \text{cm}}{\text{src}}\right)\left(\frac{\text{J}}{\text{s}}\right)\left(\frac{\text{neutrons}}{\text{fission}}\right)}{\left(\text{cm}^3\right)\left(\frac{\text{J}}{\text{fission}}\right)\left(\frac{\text{neutrons}}{\text{src}}\right)} = \frac{\left(\frac{\text{neutrons} \cdot \text{cm}}{1}\right)\left(\frac{1}{\text{s}}\right)\left(\frac{1}{1}\right)}{\left(\text{cm}^3\right)\left(\frac{1}{1}\right)\left(\frac{1}{1}\right)} = \frac{\text{neutrons}}{\text{cm}^2 \cdot \text{s}}$$

The previous spatial normalization method was not used for energy-dependent flux because of the following two reasons-

1. Spectrum Destruction: The heating tally collapses all energies into a single value, erasing critical spectral details needed for energy-resolved analysis.
2. Neutron Balance: Energy-dependent reactions (e.g., resonances, thresholds) require preserving the flux-energy shape, which the heating tally cannot provide.

The energy-structured method explicitly tracks spectral effects and neutron production, making it mandatory for spectral quantities. The spatial method remains valid only for integrated (energy-averaged) values like total power or core-wide flux.

## 3.2 Design of ALFRED Reactor Core

### 3.2.1 ALFRED Core Design

The ALFRED conceptual design is a 300MWth pool system created to demonstrate the feasibility of European LFR (ELFR) technology for potential future commercial use. ALFRED is a small-sized pool-type reactor that has a core with 171 hexagonal fuel assemblies (FAs). Additionally, there are twelve (12) control rod (CR) positions and four (4) positions for safety rods (SRs). There are two rows with a total of 108 dummy elements surrounding the core that serve as a reflector, Yttria-Zirconia is used as the material inside these dummy assemblies. The 171 FAs are radially divided into two zones- an inner zone with 57 FAs and an outer zone with the other 114 FAs. The fuel consists of MOX pellets with two different plutonium enrichments in the inner (21.7% named MOX1 fuel here) and outer zones (27.8% named MOX2 fuel here). Each FA consists of 127 fuel pins and is cooled by pure molten lead. Fig. 3.2 illustrates the primary system and core layout of ALFRED (Luzzi et al., 2014). The important parameters of the ALFRED core in this study are summarized in Table 3.1 (Grasso et al, 2014; Ibrahim et al., 2021; El. Alem et al, 2024). Table 3.2 contains the details of all of the materials used in modeling the ALFRED core (Ibrahim et al., 2021; El. Alem et al, 2024; Sobolev et al., 2009).

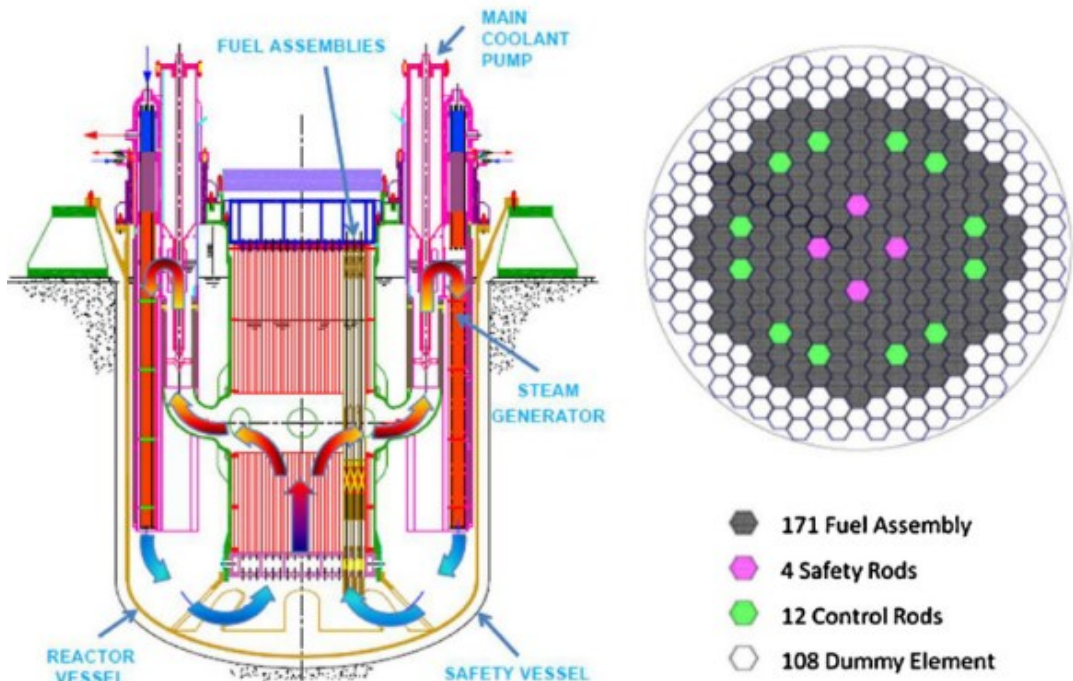


Fig. 3.2: Primary system of ALFRED and core layout.

Table 3.1: Essential parameters for ALFRED core

Main Parameters	Value
Core Thermal Power	300MW <sub>th</sub>
Electric Power	~125MWe
Cladding Material	Austenitic Steel (15–15Ti)
Coolant Material	Lead (Pb)
Inlet temperature of coolant	400 °C
Outlet temperature of coolant	480 °C
Fill gas	He
FA concept	Closed Hexagonal
Number of Control Rod Assembly	12
Number of inner/outer zone fuel sub-assemblies (FAs)	57/114
Number of Safety Rods	4
Number of pins/FA	127
Dummy Elements	108

Table 3.2: Material composition for ALFRED core

Parameters	Value
Type of fuel	MOX
U isotopic composition (wt.%)	$^{234}\text{U} = 0.003$ $^{235}\text{U} = 0.404$ $^{236}\text{U} = 0.010$ $^{238}\text{U} = 99.583$
Pu isotopic composition (wt.%)	$^{238}\text{Pu} = 2.332$ $^{239}\text{Pu} = 56.873$ $^{240}\text{Pu} = 26.997$ $^{241}\text{Pu} = 6.105$ $^{242}\text{Pu} = 7.693$
Absorber Material	Boron Carbide [ $\text{B}_4\text{C}$ (90% $^{10}\text{B}$ )]
Dummy Element Material	Yttria-Zirconia ( $\text{ZrO}_2\text{-Y}_2\text{O}_3$ )

Table 3.3: Geometric specifications of ALFRED core

Specifications	Values (mm)
Length of Fuel Pin	600
Inner Diameter of Fuel Pellet	2.0
Outer Diameter of Fuel Pellet	9.0
Inner Diameter of Cladding	9.3
Outer Diameter of Cladding	10.5
Length of Active Zone	600
Length of Upper Plenum	120
Length of Lower Plenum	550

A pin cell of ALFRED core was designed using the values in Table 3.3 (Luzzi et al., 2014), which is shown in Fig. 3.3 with its dimensions.

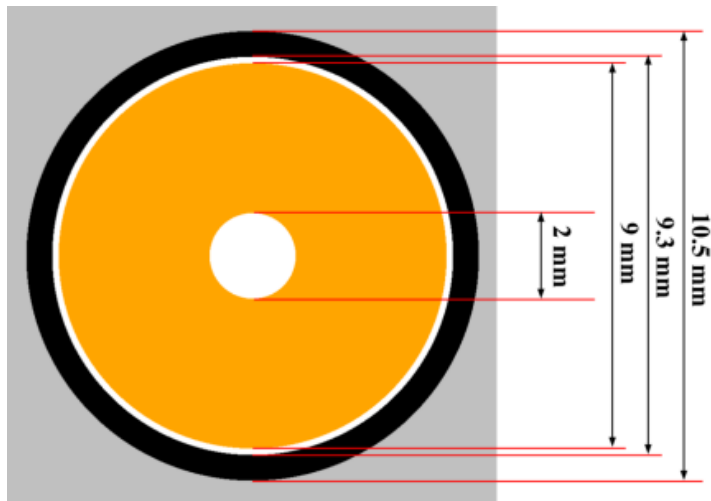


Fig. 3.3: Fuel pincell cross-section of ALFRED.

Fig. 3.4 shows the cross-sectional view of the whole ALFRED reactor core where the inner FAs are colored red, outer FAs are colored yellow, dummy assemblies are colored purple, and control rod assemblies are black. As no behavioral change due to shutdown assemblies was studied, the shutdown assemblies are four empty spaces identified in Fig. 3.4.

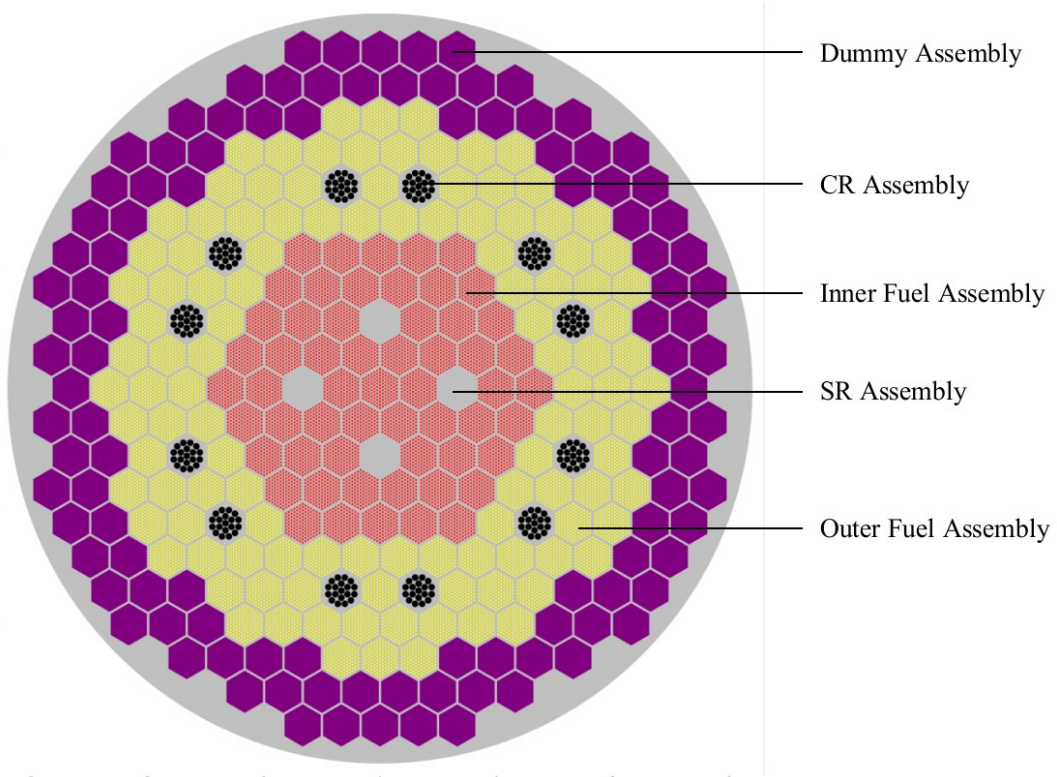


Fig. 3.4: Cross-sectional view (radial) of the ALFRED core.

### 3.3 Different Reflector for ALFRED

During the neutronics analysis of ALFRED, a degree of unexpected neutron thermalization was observed, as shown in Fig. 4.5, Chapter 4.1. Given that lead is used as the primary coolant, the reactor is expected to maintain a hard neutron spectrum. However, deviations from this expectation led to further investigation into potential sources of moderation. The study revealed that the reflector material significantly influenced neutron energy distribution, leading to thermalization effects, shown in Fig. 4.6, Chapter 4.1.

In the ALFRED model reference to LFRs, the reflector or dummy assemblies were composed of Yttria-Zirconia. To assess the impact of different materials on core neutronics, a systematic comparative study was conducted. The selected reflector candidates include:

$\text{Ba}_2\text{Pb}$ ,  $\text{BeO}$ , Graphite, Lead, Magnesium,  $\text{MgO}$ ,  $\text{PbO}$ ,  $\text{PbS}$ ,  $\text{SiC}$ ,  $\text{Zr}_3\text{Si}_2$ , and  $\text{ZrC}$ .

The effectiveness of each reflector material was evaluated based on the following key neutronics parameters:

- i. Effective multiplication factor ( $k_{\text{eff}}$ ) and neutron leakage
- ii. Thermal fission fraction
- iii. Neutron energy spectrum
- iv. Thermal neutron flux in the reflector
- v. Total neutron flux distributions at BOL
- vi. Fission rate distributions and power peaking
- vii. Variation of  $k_{\text{eff}}$  with burnup
- viii. Activation of reflector materials

To isolate the direct influence of reflector materials, a reflective boundary condition was applied outside the active core region on the top and bottom of the core, ensuring that axial leakage effects did not interfere with the results. This allowed for a precise evaluation of how different materials impact neutron reflection and moderation. Again, for understanding the effect after utilizing each material in reflector assemblies, simulating the operational scenario,  $k_{\text{eff}}$  and leakage were calculated.

Fig. 3.5 illustrates the ALFRED core configuration, where the reflector assemblies are distinguished by their brown color.

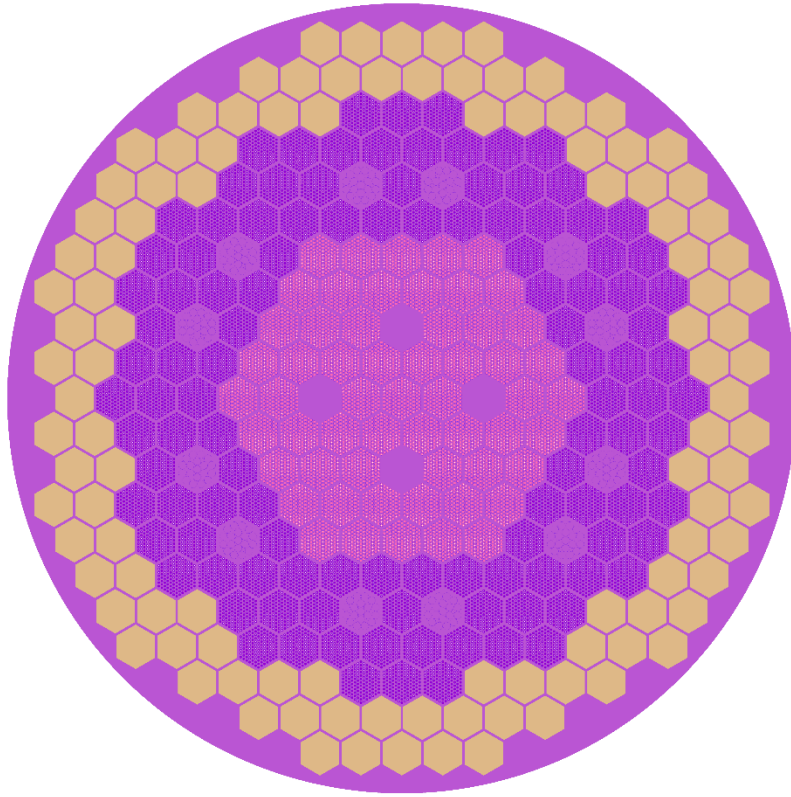


Fig. 3.5: ALFRED core configuration.

Table 3.4: Properties of reflector materials

<b>Materials</b>	<b>Nuclides</b>	<b>Atomic Percentage (ao)</b>	<b>Density (g/cm<sup>3</sup>)</b>
	Zr90	$1.636657 \times 10^{-1}$	
	Zr91	$3.569153 \times 10^{-2}$	
	Zr92	$5.455524 \times 10^{-2}$	
	Zr94	$5.528688 \times 10^{-2}$	
Yttria-Zirconia	Zr96	$8.906977 \times 10^{-3}$	6.08
	O16	$6.620422 \times 10^{-1}$	
	O17	$2.515125 \times 10^{-4}$	
	O18	$1.327508 \times 10^{-3}$	
	Y89	$1.827240 \times 10^{-2}$	

Table 3.4: Properties of reflector materials (continued)

<b>Materials</b>	<b>Nuclides</b>	<b>Atomic Percentage (ao)</b>	<b>Density (g/cm<sup>3</sup>)</b>
Ba <sub>2</sub> Pb	Ba130	$7.333333 \times 10^{-4}$	
	Ba132	$6.666667 \times 10^{-4}$	
	Ba134	$1.613333 \times 10^{-2}$	
	Ba135	$4.393333 \times 10^{-2}$	
	Ba136	$5.233333 \times 10^{-2}$	
	Ba137	$7.486667 \times 10^{-2}$	5.82
	Ba138	$4.780000 \times 10^{-1}$	
	Pb204	$4.666667 \times 10^{-3}$	
	Pb206	$8.033333 \times 10^{-2}$	
	Pb207	$7.366667 \times 10^{-2}$	
BeO	Pb208	$1.746667 \times 10^{-1}$	
	Be9	$5.000000 \times 10^{-1}$	
	O16	$4.988103 \times 10^{-1}$	
	O17	$1.895000 \times 10^{-4}$	3.02
C	O18	$1.000200 \times 10^{-3}$	
	C12	$9.889220 \times 10^{-1}$	
	C13	$1.107800 \times 10^{-2}$	1.75
Pb	Pb204	$1.400000 \times 10^{-2}$	
	Pb206	$2.410000 \times 10^{-1}$	
	Pb207	$2.210000 \times 10^{-1}$	11.34
	Pb208	$5.240000 \times 10^{-1}$	
Mg	Mg24	$7.895100 \times 10^{-1}$	
	Mg25	$1.002000 \times 10^{-1}$	1.738
	Mg26	$1.102900 \times 10^{-1}$	

Table 3.4: Properties of reflector materials (continued)

<b>Materials</b>	<b>Nuclides</b>	<b>Atomic Percentage (ao)</b>	<b>Density (g/cm<sup>3</sup>)</b>
MgO	Mg24	$3.947550 \times 10^{-1}$	3.58
	Mg25	$5.010000 \times 10^{-2}$	
	Mg26	$5.514500 \times 10^{-2}$	
	O16	$4.988103 \times 10^{-1}$	
	O17	$1.895000 \times 10^{-4}$	
	O18	$1.000200 \times 10^{-3}$	
PbO	Pb204	$7.000000 \times 10^{-3}$	9.53
	Pb206	$1.205000 \times 10^{-1}$	
	Pb207	$1.105000 \times 10^{-1}$	
	Pb208	$2.620000 \times 10^{-1}$	
	O16	$4.988103 \times 10^{-1}$	
	O17	$1.895000 \times 10^{-4}$	
PbS	O18	$1.000200 \times 10^{-3}$	7.6
	Pb204	$7.000000 \times 10^{-3}$	
	Pb206	$1.205000 \times 10^{-1}$	
	Pb207	$1.105000 \times 10^{-1}$	
	Pb208	$2.620000 \times 10^{-1}$	
	S32	$4.752037 \times 10^{-1}$	
SiC	S33	$3.743450 \times 10^{-3}$	3.21
	S34	$2.097995 \times 10^{-2}$	
	S36	$7.290000 \times 10^{-5}$	
	Si28	$4.611484 \times 10^{-1}$	
	Si29	$2.341580 \times 10^{-2}$	
	Si30	$1.543580 \times 10^{-2}$	
C12	C12	$4.944610 \times 10^{-1}$	3.21
	C13	$5.539000 \times 10^{-3}$	

Table 3.4: Properties of reflector materials (continued)

<b>Materials</b>	<b>Nuclides</b>	<b>Atomic Percentage (ao)</b>	<b>Density (g/cm<sup>3</sup>)</b>
$\text{Zr}_3\text{Si}_2$	Zr90	$3.087000 \times 10^{-1}$	4.89
	Zr91	$6.732000 \times 10^{-2}$	
	Zr92	$1.029000 \times 10^{-1}$	
	Zr94	$1.042800 \times 10^{-1}$	
	Zr96	$1.680000 \times 10^{-2}$	
	Si28	$3.689187 \times 10^{-1}$	
	Si29	$1.873264 \times 10^{-2}$	
$\text{ZrC}$	Si30	$1.234864 \times 10^{-2}$	6.73
	Zr90	$2.572500 \times 10^{-1}$	
	Zr91	$5.610000 \times 10^{-2}$	
	Zr92	$8.575000 \times 10^{-2}$	
	Zr94	$8.690000 \times 10^{-2}$	
	Zr96	$1.400000 \times 10^{-2}$	
	C12	$5.000000 \times 10^{-1}$	

### 3.4 Design of Multi-Purpose Research Reactor

#### 3.4.1 VVR-KN Fuel Design

The multipurpose research reactor features an open pool-type configuration with a central core and a reflector surrounding the core (with reasonable amount of free space available in the reflector to position facilities/devices) (Teruel and Rizwan-uddin, 2009). It uses light water as both moderator and coolant, while beryllium rods serve as the neutron reflector to enhance neutron economy. The reactor core is compact and consists of 36 fuel assemblies arranged in 61 hexagonal cells. These assemblies include 27 standard fuel assemblies (FA-1) and 9 control fuel assemblies (FA-2). The FA-1 contains eight fuel elements where seven are outer hexagonal tubes and one is a central cylindrical tube and the FA-2 consists of five fuel elements, and it includes a central guide tube designed for control rod insertion. This concentric tube configuration increases surface area for better heat transfer and allows

compact packing in the reactor core. The fuel used is VVR-KN, a Russian tube-type fuel that contains Low-Enriched Uranium (LEU) at 19.75% enrichment, embedded in an aluminum matrix. The specifications of the fuel element are given in Table 3.5 (N. D. Nguyen et al., 2014; Nguyen et al., 2020).

Table 3.5: Specifications of fuel element

Parameters	Values
Fuel Type	VVR-KN
Fuel Content	UO <sub>2</sub> -Al
U-235 Enrichment (wt.%)	19.75%
Fuel Length (mm)	600 ± 2
Fuel Diameter (mm) in each FE	0.7
Fuel Density (g/cm <sup>3</sup> )	2.8
Cladding Material	Aluminum Alloy SAV-1
Cladding Thickness (mm) in each FE	0.45x2
Ribs Length (mm)	1.5
Number of Ribs per Element	Hexagonal 06, Cylindrical 03

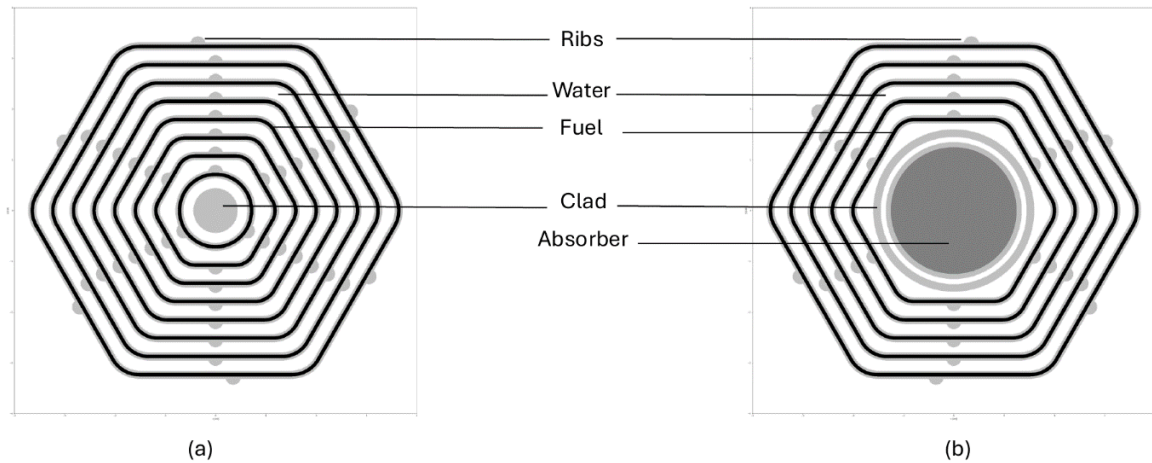


Fig. 3.6: Design of FA-1 (a) and FA-2 (b).

### 3.4.2 Core Design

The core design of the 10 MW MPRR is carefully optimized for high performance, flexibility, and safety. The specifications of the core are given in Table 3.6 (N. D. Nguyen et al., 2014; Nguyen et al., 2020). It supports long fuel cycles, high neutron flux, and a wide range of irradiation options. The compact hexagonal configuration with VVR-KN fuel and beryllium reflectors makes it suitable for both current research demands and future expansion in nuclear science and technology.

Table 3.6: Specifications of fuel assembly and reactor core

Parameters	Values
Shape	Hexagonal
Number of Fuel Assemblies	36: FA-1 (27), FA-2 (09)
Reactor Type	Open Pool
Thermal power	10 MW
Number of Control Rods	09
Number of Shim Rods, B4C	06
Number of Safety Rods, B4C	02
Number of Automatic Regulating Rod, SS	01
Core Height	180 cm
Core Radius	113.5 cm

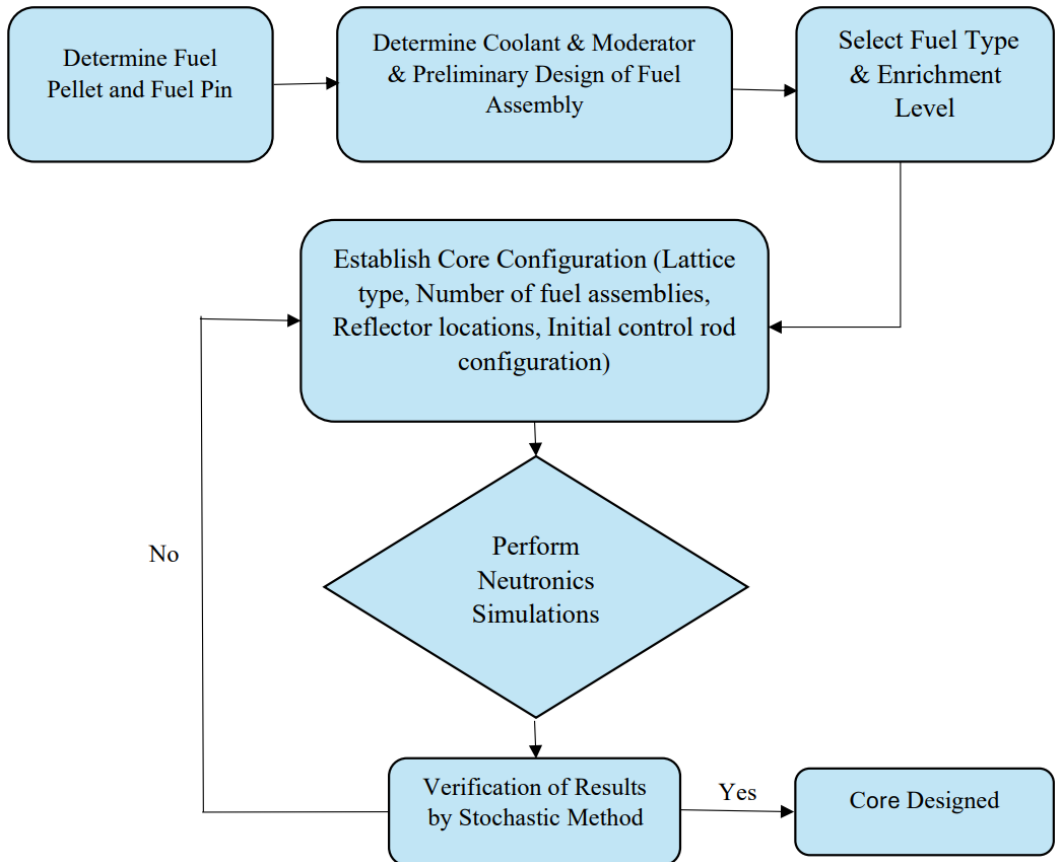


Fig. 3.7: Core design steps.

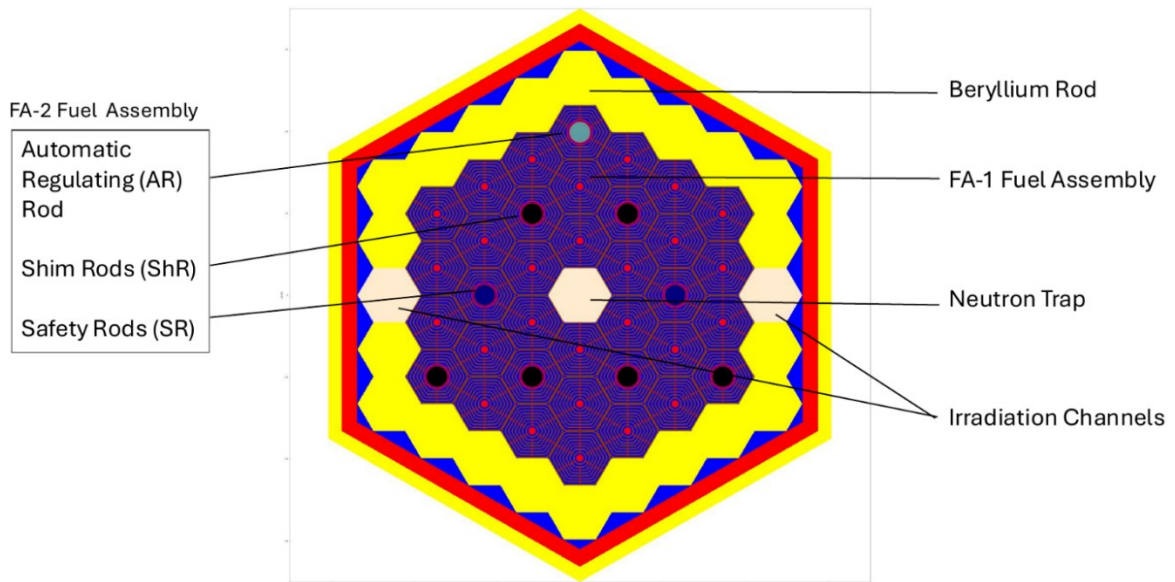


Fig. 3.8: Configuration of the MPRR core.

### 3.5 Error Calculations

To ensure the reliability and accuracy of the computational results presented in this thesis, error calculations are performed to compare the calculated values with established standard values from the literature. This validation step is critical for assessing the precision of the simulation models and methodologies employed. Errors are quantified using two distinct equations throughout the thesis: Equation 3.4 for percentage error and Equation 3.5 for error in pcm (per cent mile), a unit commonly used in nuclear engineering to express reactivity deviations. The pcm unit represents parts per hundred thousand, and this metric is particularly useful in reactor physics to quantify small reactivity changes.

$$\text{error} = \frac{|\text{calculated value} - \text{standard value}|}{\text{standard value}} \times 100 \quad (3.4)$$

$$\text{error (pcm)} = \frac{|\text{calculated value} - \text{standard value}|}{\text{standard value}} \times 10^5 \quad (3.5)$$

These error calculations are applied consistently across the thesis to validate key results against benchmark data or experimental references. By presenting errors, the analysis offers a comprehensive view of the simulation accuracy, facilitating comparisons with literature values and supporting the credibility of the findings.

### 3.6 Hypothesis Test

The t-test statistic is calculated with the Equation 3.6.

$$t = \frac{\bar{x} - \mu_0}{s/\sqrt{n}} \quad (3.6)$$

where,

$\bar{x}$  is the OpenMC  $k_{\text{eff}}$ ,

$\mu_0$  is the benchmark  $k_{\text{eff}}$ ,

$s$  is the sample standard deviation, and

$n$  is the number of simulations run.

## CHAPTER 4

### RESULTS AND DISCUSSIONS

#### 4.1 ALFRED Neutronics Analysis

After completion of the model, simulations were run, and different data from the neutronic perspective were collected, such as the effective multiplication factor ( $k_{\text{eff}}$ ), axial and radial neutron flux, power generation in each fuel assembly, etc. This data is tabulated and compared in the following sections.

##### 4.1.1 Criticality Calculations

The Effective Multiplication Factor ( $k_{\text{eff}}$ ) was calculated at the Beginning of Cycle (BOC) using both the ENDF/B-VIII.0 and JEFF-3.3 data libraries to compare the differences between the obtained results. Table 4.1 contains these data as well as the reference values taken from literature (Lodi et al., 2015) that used these specific data libraries.

Table 4.1: Effective multiplication factor (At BOC) - data library comparison:

Calculated Values	Reference Values	Error in pcm
1.07803 (ENDF/B-VIII.0)	1.07767 (ENDF/B-7.1b)	33
1.08611 (JEFF-3.3)	1.08367 (JEFF3.1.2)	225

The findings indicate that the effective multiplication factor ( $k_{\text{eff}}$ ) calculated using the ENDF/B-VIII.0 version is in agreement with the reference values from the ENDF/B-7.1b library, with only a 33 pcm difference (Lodi et al., 2015). Similarly, the JEFF-3.3 data library aligns strongly with the JEFF-3.1.2 reference values, showing a difference of 225 pcm (Lodi et al., 2015).

When comparing the two reference values, the ENDF/B-7.1b gives a  $k_{\text{eff}}$  value of 1.07767, while the JEFF-3.1.2 gives a value of 1.08367. This comparison shows that the JEFF reference value is higher by approximately 0.006, which might suggest differences in the nuclear data or methodologies used between the JEFF and ENDF libraries. Looking at the calculated values, the ENDF/B-VIII.0 produces a  $k_{\text{eff}}$  of 1.07803, while the JEFF-3.3 library

gives a value of 1.08611. Here, the calculated value from the JEFF library is about 0.008 higher, aligning with the trend in the reference values. This suggests that, while both libraries offer reliable predictions of the effective multiplication factor, the JEFF library may provide more conservative estimates in certain situations (Plompen et al., 2020). Recognizing these differences is essential for accurate neutronic analysis and choosing the right data libraries for specific applications. The value 1.08611 acquired using JEFF library also agrees with a value of 1.08621 from another similar study (Ganjaroodi et al., 2023), with an acceptable error of 9.21 pcm.

#### **T-Test:**

$$t = \frac{1.07803 - 1.07767}{0.00235/\sqrt{100}} = 1.53$$

Degrees of freedom = 99, critical t-value  $\approx 1.984$ . Since  $|t| = 1.53 < 1.984$ , failed to reject  $H_0$ .

No significant difference was found between OpenMC  $k_{\text{eff}}$  value and benchmark  $k_{\text{eff}}$  value.

#### **4.1.2 Neutron Flux**

Fig. 4.1 visualizes the axial flux profile which is important because it has a direct impact on the reactor's heat distribution and neutron economy. As the core gets closer to the top, the neutron flux tends to drop. This phenomenon occurs due to the geometrical buckling in a reactor core.

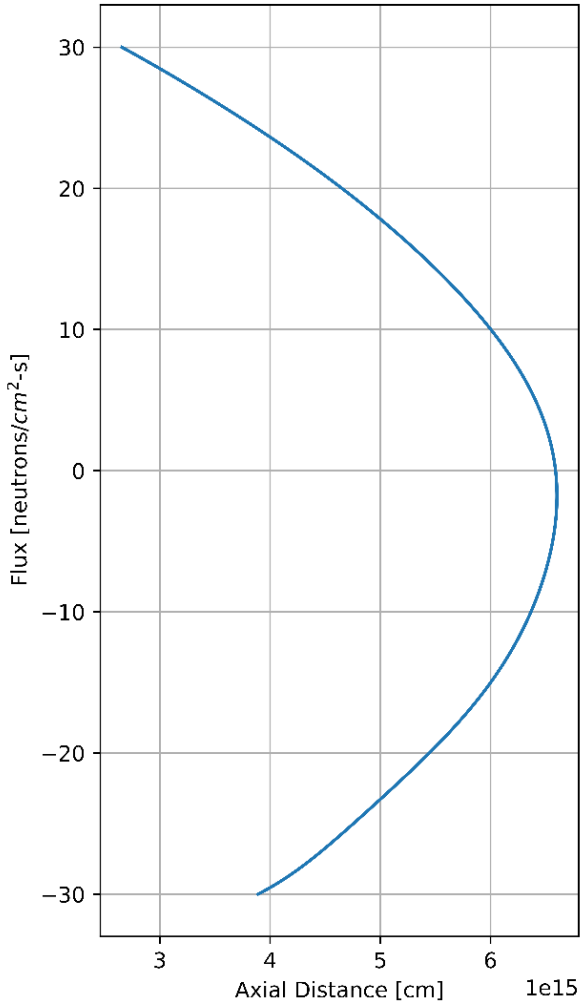


Fig. 4.1: Axial flux distribution profile.

The neutron flux changes from the reactor core's center to its outside edge in a radial direction, which is described by the radial flux distribution shown in Fig. 4.2, where it is visualized for the whole energy spectrum. Because the neutrons in fast reactors have high energy hence controlling their radial behavior is essential to maximizing fuel burnup and coolant usage, this is particularly important. The neutron flow typically peaks close to the core's center and then progressively declines as it moves outside. The results show that the mean neutron flux is in practical units,  $1.066 \times 10^{15}$  neutrons/cm<sup>2</sup>-s. The maximum neutron flux found and normalized after the simulation was  $2.716 \times 10^{15}$  neutrons/cm<sup>2</sup>-s near the center of the core, which agrees with the reference value of  $2.56 \times 10^{15}$  neutrons/cm<sup>2</sup>-s from the literature with an error of 6.09% (Ciurluini et al., 2020).

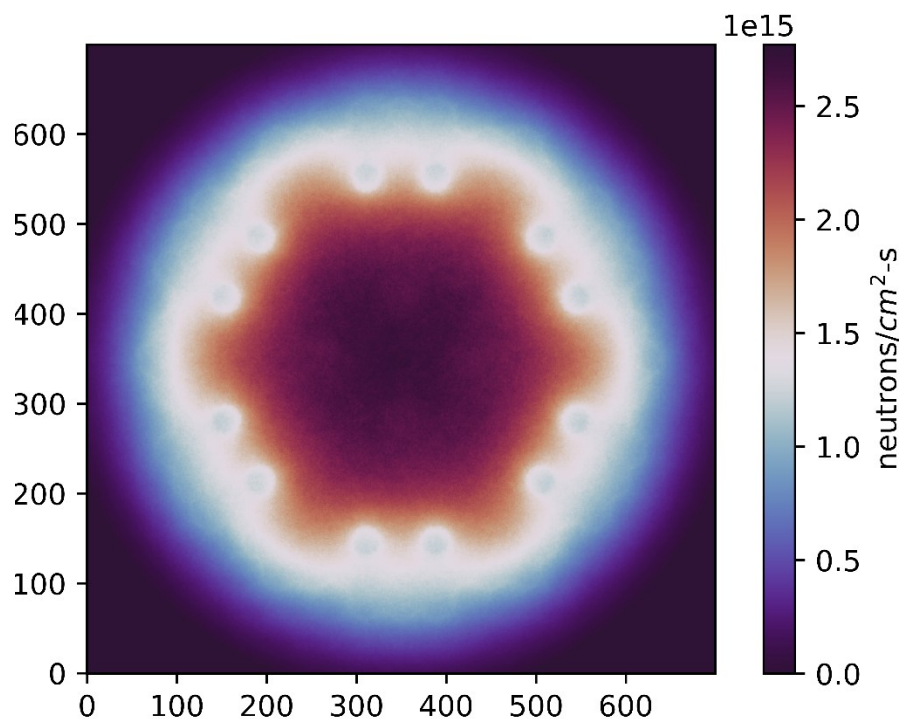


Fig. 4.2: Graph of radial flux distribution.

A Three-Dimensional (3D) plot of the radially distributed neutron flux is shown in Fig. 4.3 which is useful for comprehending and visualizing the variations in neutron flux throughout the reactor core. The fuel and neutron interactions are stronger near the center, where the fissile material is concentrated, hence this central peaking is normal. It is also noticeable that in the positions of the control rods and the shutdown rods, there is a drop in the neutron flux, this is because there is no fissile material in the mentioned positions.

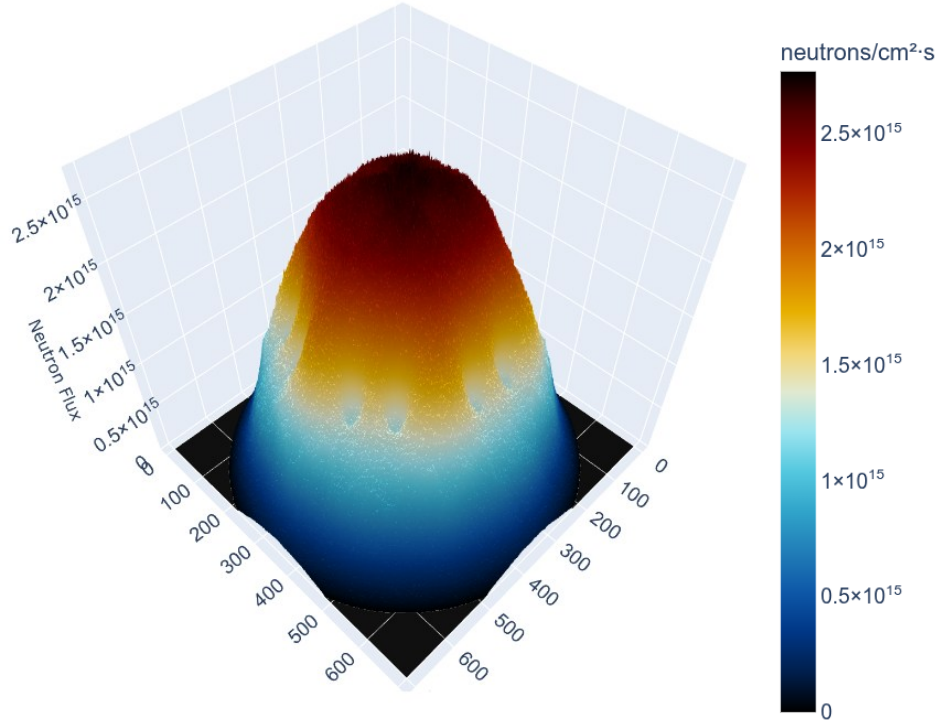


Fig. 4.3: 3D distribution of neutron flux (plotted using plotly).

#### 4.1.3 Power Distribution

The way power is distributed across the various fuel assemblies reveals information about the reactor's local and global operations. Typically, the core power distribution plot displays power output as a 2D grid that varies with the location of each fuel assembly within the core. This enables us to determine if power generation is consistent or if there are regions with underperformance or flux peaking. Using OpenMC's DistribCell feature, it was possible to calculate the value of generated power in each fuel assembly using the heating values in each of the cases. The results, shown in Fig. 4.4, show the spatial distribution of power generation across the core. From this, the maximum power was found to be 2.209 MW, tabulated in Table 4.2 which is in agreement with previous studies providing the value of 2.34 MW (Grasso et al., 2014) with a margin of 5.59% error. In this study, the average power value was calculated as 1.732 MW. The power peaking factor (PPF) is known to be the ratio of maximum and average power values. From the results, the ratio of these two parameters is calculated to be 1.276.

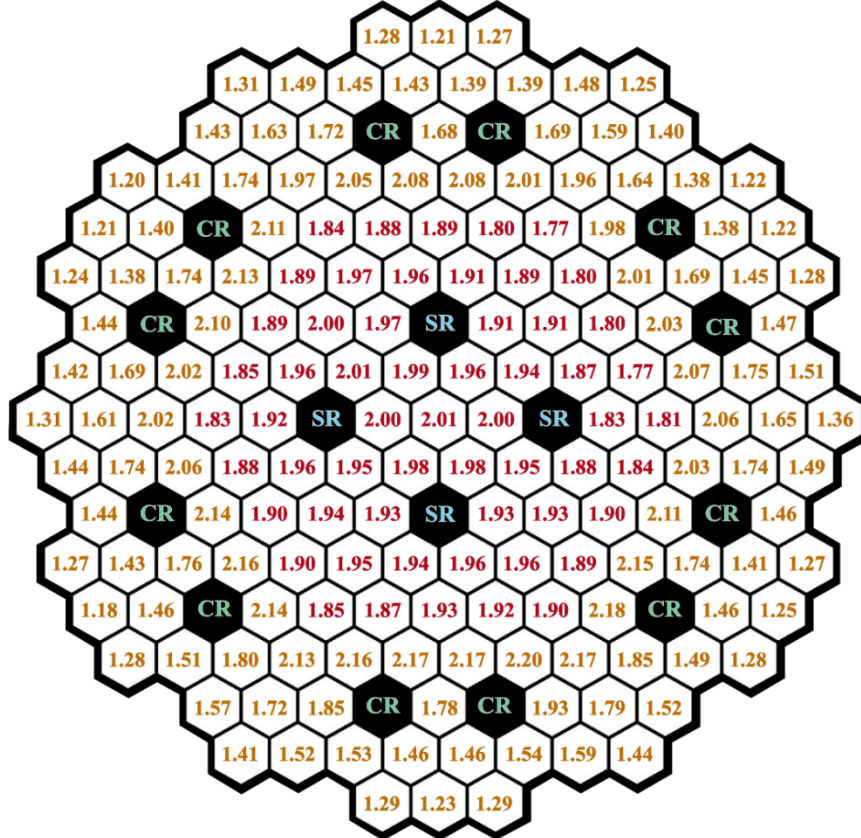


Fig. 4.4: Power (MW) for each fuel assembly.

#### 4.1.4 Neutron Energy Spectrum

The neutron energy spectrum is an essential characteristic in understanding the behavior of neutrons in the core of a nuclear reactor, as it influences reactivity and fuel utilization. In the ALFRED reactor, the coolant is lead. The neutronic behavior of lead in the fast energy range is characterized by low neutron absorption and moderation, which typically results in a harder neutron spectrum.

As illustrated in Fig. 4.5, the energy-dependent neutron flux spectrum shows the distribution of neutron energies across various energy groups. The fast neutron spectrum dominates, given that the lead coolant does not significantly moderate the neutrons. This results in a significant portion of the neutron flux being concentrated in the fast neutron energy range (typically in the order of MeV), characteristic of fast reactors. However, in the Fig. shown, a pure hard neutron spectrum is not found, rather some thermalization does occur, and thermal flux is found to be about  $10^{12}$  neutrons per cross-sectional area per second.

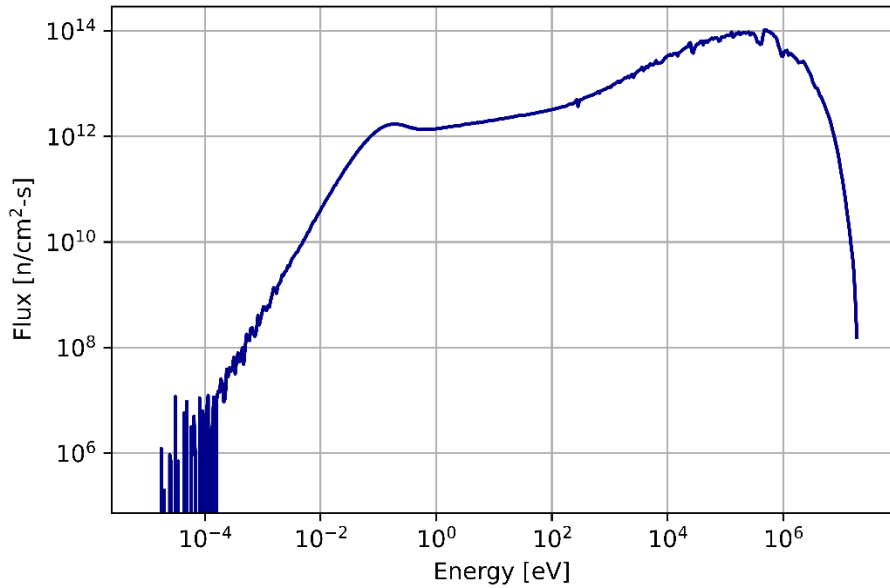


Fig. 4.5: Energy dependent neutron flux spectrum.

From Fig. 4.6, which shows the neutron flux distribution of only the energies between 0-0.025 eV (thermal neutron energy range), it is clearly observable that the thermalization occurs due to the interaction of neutrons with only the reflector material, in this case Yttria-Zirconia.

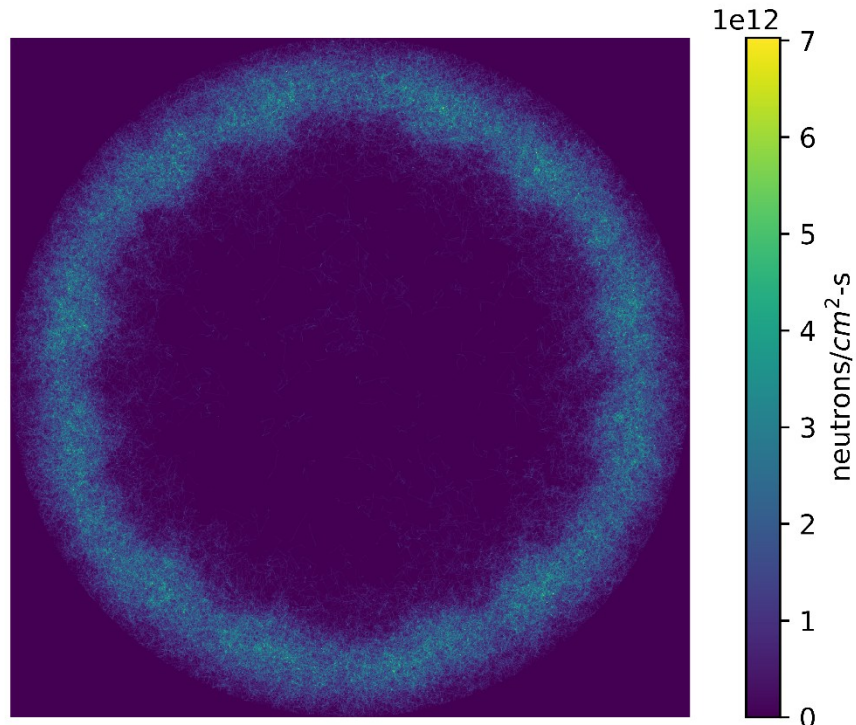


Fig. 4.6: Thermal neutron flux distribution over the whole core.

#### 4.1.5 Control Rod Worth

The Integral Control Rod Worth (CRW) represents how reactivity changes with control rod insertion or removal in the core, typically forming a sigmoidal (S-shaped) curve. Fig. 4.7 shows that as control rods are withdrawn, the negative reactivity inserted by the control rods decreases, with maximum negative reactivity induced when fully inserted. This behavior is essential for safely shutting down or stabilizing the reactor during operational transients.

The calculated control rod worth in this study was -8650 pcm, which aligns well with the value of -8500 pcm reported in previous studies (Grasso et al., 2014), with an error of only 1.76%. This strong agreement demonstrates the reliability of the model in accurately simulating the reactivity control mechanisms in the ALFRED core. The relatively large negative value of the control rod worth indicates that the ALFRED reactor design is highly responsive to control rod insertion, meaning that even small adjustments can have a significant impact on the reactor's reactivity. Also, the sharp flux gradients around the control rod position seen in Fig. 4.2 can cause sudden changes in neutron absorption when the control rod moves through these regions, delivering a sawtooth trend seen in Fig. 4.7.

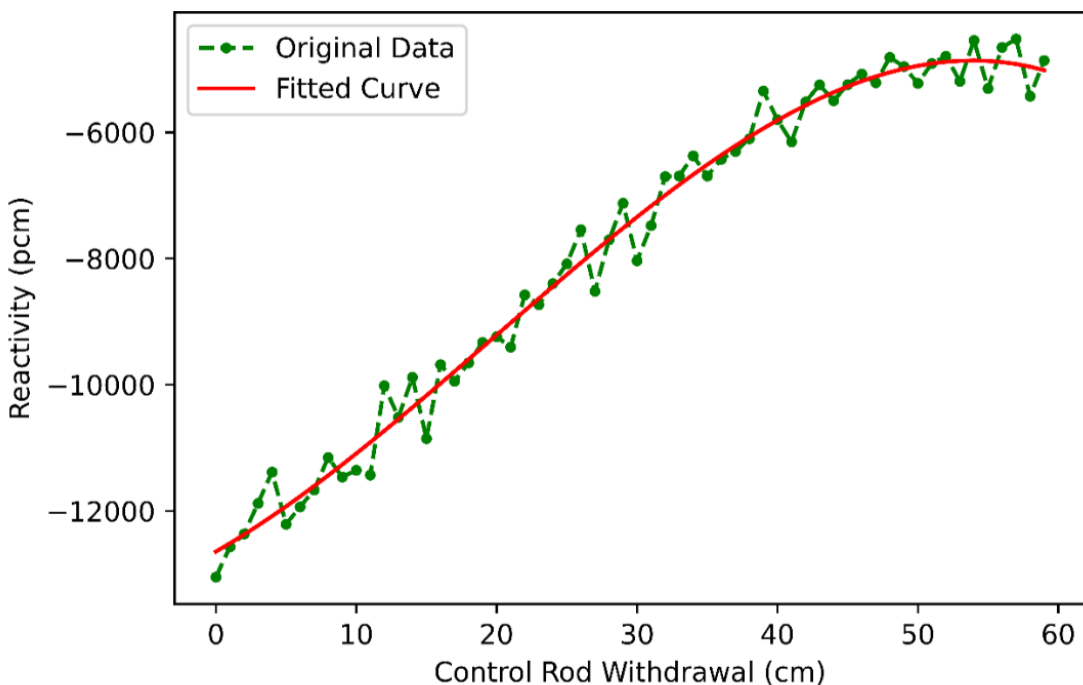


Fig. 4.7: Integral control rod worth graph.

Table 4.2: Neutronic parameters of the modeled ALFRED core

Parameter	Calculated Values	Reference Values	Error (%)
$k_{\text{eff}}$	1.07803	1.07767	0.054
Reactivity Swing in 1 year averaged (pcm)	-2530	-2580	1.94
Maximum Neutron Flux (n/cm <sup>2</sup> -s)	2.716x10 <sup>15</sup>	2.56x10 <sup>15</sup>	6.09
Average Neutron Flux (n/cm <sup>2</sup> -s)	1.066x10 <sup>15</sup>	—	—
Maximum Thermal Neutron Flux (n/cm <sup>2</sup> -s)	7.028x10 <sup>12</sup>	—	—
Max Power (MW)	2.209	2.34	5.59
Mean Power (MW)	1.732	—	—
Power Peaking Factor	1.276	—	—
Control Rod Worth (pcm)	-8650	-8500	1.76

The control rod worth of -8650 pcm in Table-4.2 is in well agreement with the value -8650 pcm with an error of 1.76% established in literature (Grasso et al., 2014).

#### 4.1.6 Fuel Burnup Results

Though the choice of coolant in the ALFRED reactor is pure lead, for burnup simulations done in this study, both lead and LBE were considered and compared.

##### 4.1.6.1 Effective Multiplication Factor

A 5-year burnup cycle was simulated using half-year steps, corresponding to a total of 1820 days, with the effective multiplication factor ( $k_{\text{eff}}$ ) tracked to assess the reactor's criticality over time. The decrease in  $k_{\text{eff}}$  is illustrated in Fig. 4.8, which presents the evolution of  $k_{\text{eff}}$  as a function of burnup time for both lead and LBE coolants, derived from detailed computational simulations. Through linear interpolation of the  $k_{\text{eff}}$  data, the time at which  $k_{\text{eff}}$  crosses the criticality threshold of 1 was determined to be approximately 1041 days for lead and 1094 days for LBE, reflecting the slight influence of coolant type on the neutron

economy and burnup progression. Though both values are slightly different, they align with the previously established value shown in Fig. 4.9, with variations attributed to the interpolation method and specific data resolution (Lodi et al., 2015). These findings provide valuable insights into the reactor's operational lifetime and fuel management strategies, highlighting the need for further analysis to optimize coolant selection and extend cycle efficiency.

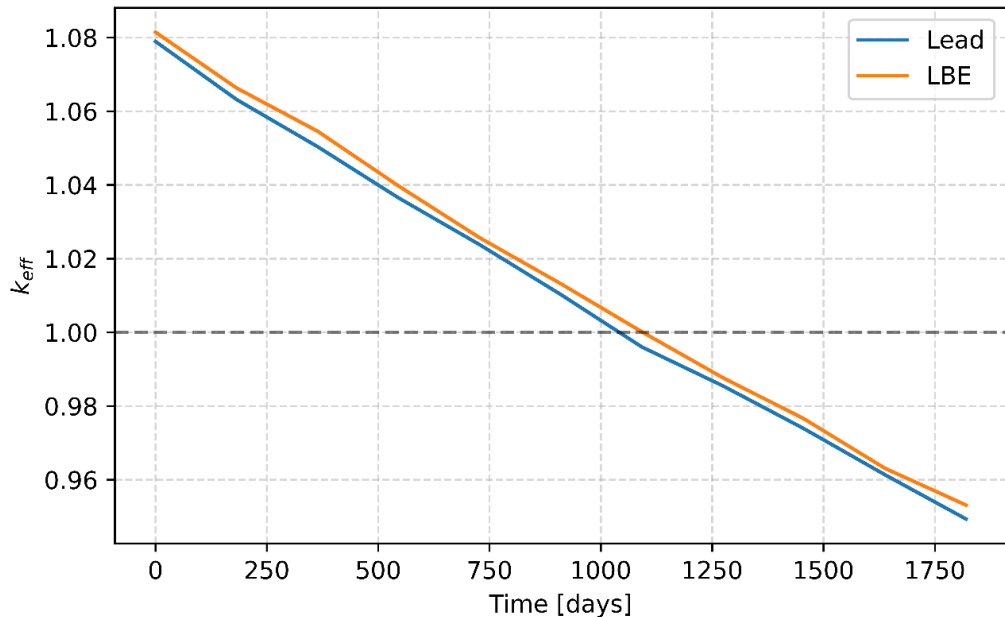


Fig. 4.8:  $k_{\text{eff}}$  as a function of burnup time.

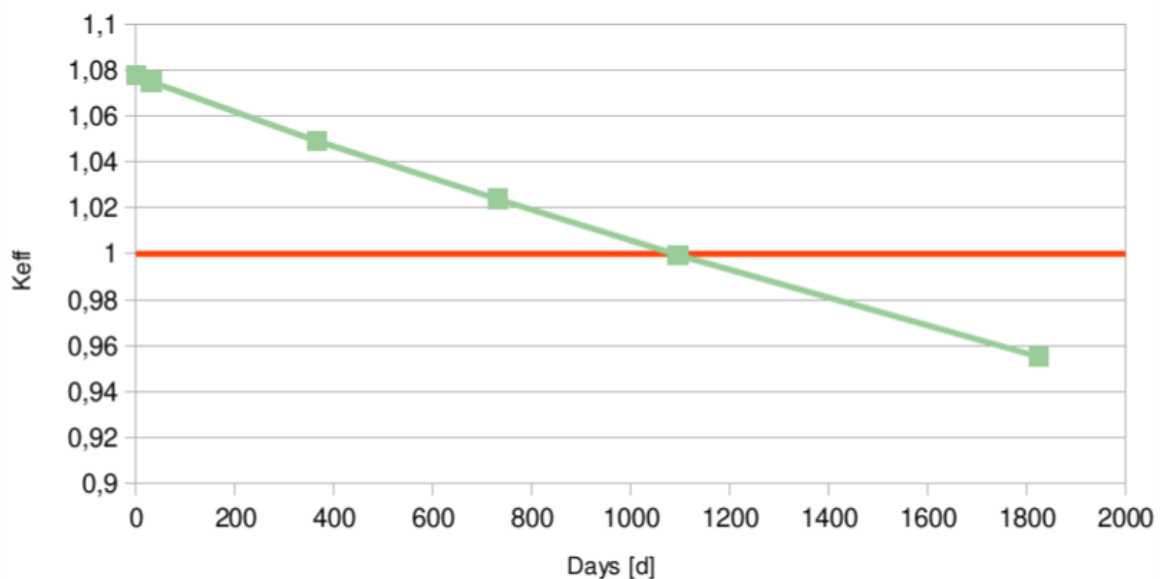


Fig. 4.9:  $k_{\text{eff}}$  as a function of burnup time.

#### **4.1.6.2 Reactivity Swing**

The reactivity swing, which quantifies the change in reactivity due to fuel burnup and isotopic depletion, is a critical parameter for evaluating the reactor's control requirements and safety margins throughout its operational lifecycle. The calculated reactivity swing value of -2530 pcm, as presented in Table 4.2, closely aligns with the reference value of -2580 pcm reported in the literature (Grasso et al., 2014), with a minimal difference of 50 pcm between the two figures. This small variation reflects a high degree of consistency between the computational outcomes of this study and the established reference data, reflecting the reliability of the simulation methodology employed to assess the reactor's operational stability over the one-year cycle. The observed alignment suggests that the model accurately captures the dynamic evolution of neutronics parameters, including the depletion of fissile materials and the buildup of neutron absorbers, over the specified period.

#### **4.1.6.3 Depletion of Fuel Content**

The depletion behavior of key fuel isotopes i.e., uranium-238, plutonium-239, plutonium-240, and plutonium-241 in both MOX1 and MOX2, was analyzed over an 1820-day operational cycle in ALFRED. Fig. 4.10 presents a consolidated view of the relative mass reduction of these isotopes under two coolant types: pure lead (usually used in ALFRED) and a lead-bismuth eutectic (LBE). The results highlight distinct depletion patterns, with Pu-241 exhibiting the most significant reduction in both MOX1 and MOX2, followed by Pu-239, while U-238 and Pu-240 display more gradual declines, reflecting their respective roles in the neutron economy of the reactor.

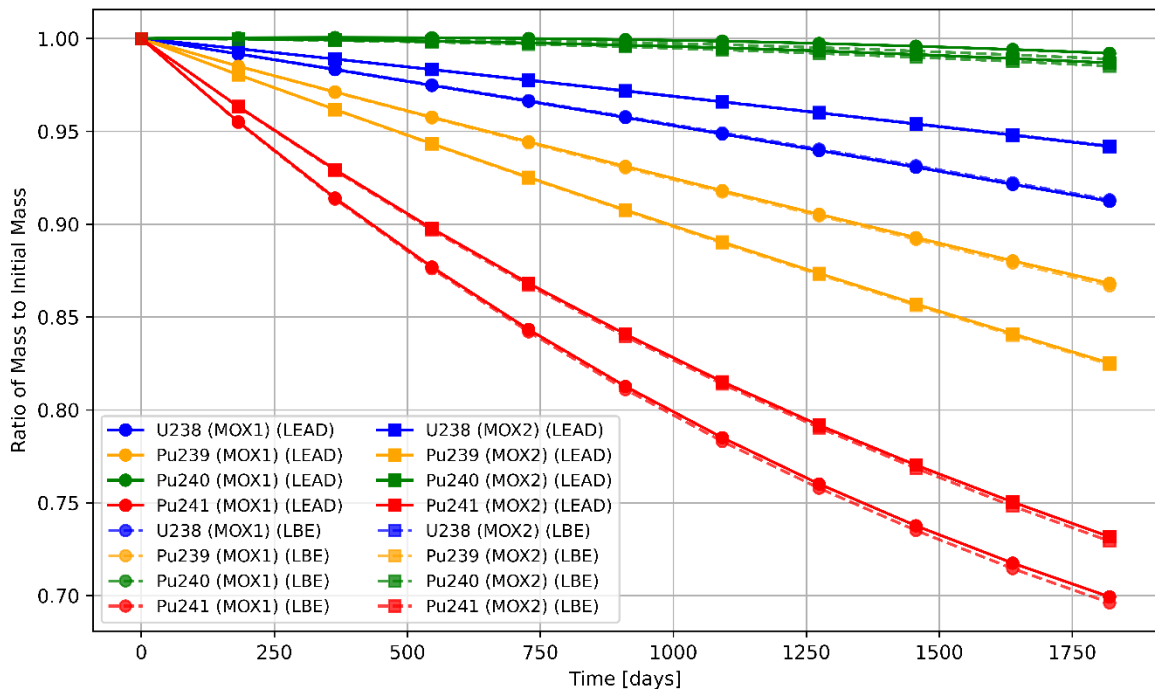


Fig. 4.10: Reduction in relative mass of fuel isotopes for both coolants.

#### 4.1.6.4 Normalization of Mass Data

To enable a fair comparison across isotopes with varying initial compositions, the mass of each isotope was normalized by dividing its mass at each timestep by its initial mass at the start of the cycle. This process was applied uniformly to all isotopes in both MOX1 and MOX2 fuels under lead and LBE coolants. For example, the mass of U-238 in the MOX1 assembly with lead coolant was scaled relative to its initial value, ensuring that all normalized mass ratios begin at 1.0. This normalization is reflected in the y-axis of Fig. 4.10, labeled "Ratio of Mass to Initial Mass," which provides a clear metric for tracking relative depletion over time. Normalization is crucial for this analysis as it standardizes the depletion trends, allowing for a direct comparison of relative mass changes despite differences in the initial isotopic compositions of MOX1 and MOX2 fuels. By establishing a common baseline, this method emphasizes proportional changes, making it easier to distinguish the depletion rates. For instance, the normalized data reveals that Pu-241 depletes at a faster rate than Pu-239.

#### **4.1.6.5 Detailed Depletion Trends**

In Fig. 4.10, Pu-241 shows the most pronounced depletion, decreasing to approximately 0.70 of its initial mass in MOX1 and 0.73 in MOX2 under lead coolant by the end of the cycle. Pu-239 follows with a reduction to 0.87 in MOX1 and 0.82 in MOX2. In contrast, U-238 depletes more slowly, reaching 0.91 in MOX1 and 0.94 in MOX2, while Pu-240 remains nearly stable, fluctuating around 0.99 due to its production from Pu-239 via neutron capture and its slower depletion rate in the fast neutron spectrum.

#### **4.1.6.6 Coolant Effects on Depletion**

The influence of coolant type on depletion rates is subtle but observable. For instance, Pu-241 in MOX2 depletes to 0.729 with LBE coolant compared to 0.732 with lead coolant, suggesting a slightly slower depletion rate with LBE. This difference may stem from variations in neutron moderation and absorption properties between lead and LBE, as LBE's bismuth content can alter the neutron spectrum and interaction probabilities. However, the overall impact of coolant type remains minor, indicating that both lead and LBE are viable for maintaining consistent depletion behavior in the ALFRED reactor.

#### **4.1.6.7 Implications for Reactor Safety and Sustainability**

The observed isotopic depletion patterns have significant implications for the safety and sustainability of fast reactors like ALFRED. The substantial reduction in Pu-241, a highly fissile isotope, reduces its contribution to reactivity over time, while the slower depletion of Pu-239, another key fissile isotope, ensures sustained criticality, supported by U-238's gradual conversion to Pu-239 through neutron capture. The near-stability of Pu-240 aids in maintaining a balanced neutron economy. These trends collectively reduce the accumulation of long-lived actinides, lowering the long-term radiotoxicity of spent fuel, a key consideration for waste management. Furthermore, the consistent depletion behavior across coolants enhances the reactor's sustainability by optimizing fuel utilization and minimizing high-radiotoxicity waste, aligning with the broader objectives of advanced nuclear energy systems to improve efficiency and reduce environmental impact.

#### 4.1.7 Actinide Production

The production of minor actinides i.e., neptunium-237, americium-241, americium-243, curium-244, and curium-245 was assessed over a 5-year burnup cycle (1820 days) using half-year steps for MOX1 and MOX2 fuels with lead and LBE coolants.

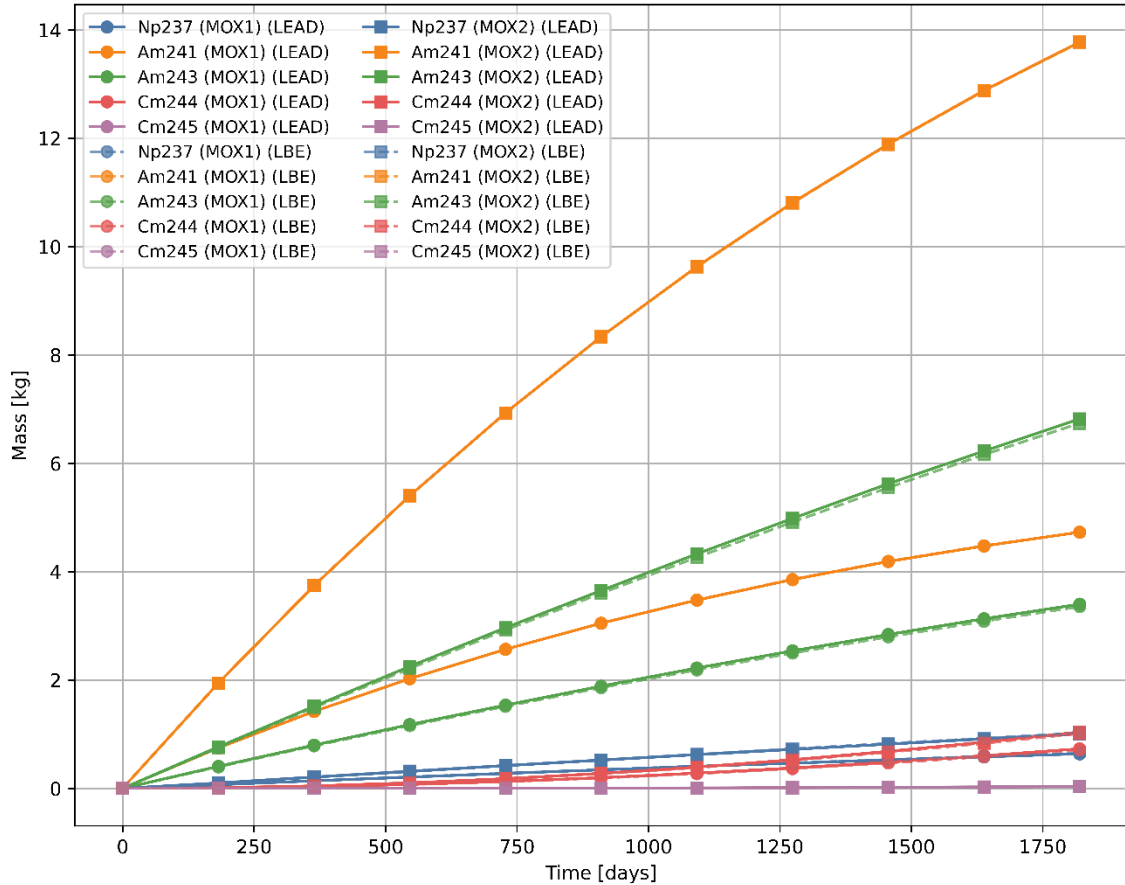


Fig. 4.11: Evolution of minor actinides from MOX1 and MOX2 using both coolants.

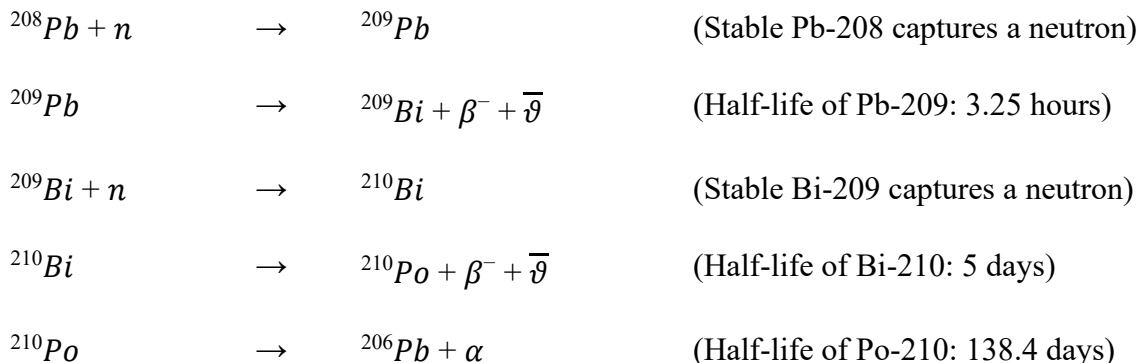
Fig. 4.11 plots the absolute masses (in kilograms) against time which shows a steady increase in actinide production due to neutron capture and decay, with MOX2 exhibiting higher yields than MOX1, due to its greater plutonium content and neutron flux. At 1500 days, the figure indicates that Am-241 production from MOX2 is approximately 2.9 times that of MOX1, while Np-237, Am-243, and Cm-244 are approximately 2.0 times higher; Cm-245 remains negligible.

These findings are critical for waste management, as long-lived Am-241 (470 years) and Cm-244 (18.1 years) increase spent fuel radiotoxicity, while negligible Cm-245 (8250 years) is a positive outcome. Future research should explore core design optimization or

transmutation to reduce long-lived actinide production, enhancing the ALFRED fuel cycle's sustainability.

#### 4.1.8 Coolant (Lead and LBE) Activation Comparison

The choice of coolant in the ALFRED reactor is pure lead. Although pure lead is chemically inert and has stable isotopes ( $\text{Pb-208}$ ,  $\text{Pb-207}$ ,  $\text{Pb-206}$ , and  $\text{Pb-204}$ ) in a fast reactor, different isotopes of lead can absorb neutrons and convert to certain radioactive isotopes. One of the isotopes of concern is Po-210, which is a highly radiotoxic alpha-emitting isotope. During normal operation, Po-210 does not pose any health risks while it remains in the coolant, but small amounts may collect in the cover gas which could evaporate outside the primary system (Mao et al., 2014). The production process of Po-210 in an LFR is described below:



In this study, we have also switched out the coolant of the ALFRED reactor with Lead-Bismuth Eutectic (LBE) to find out if there is any characteristic difference. LBE is usually chosen to be used in an LFR because of the lower melting point (123.5 °C for LBE rather than 327.5 °C for Lead). The activation products and their activities in Lead and LBE coolants are analyzed and compared using OpenMC depletion simulations. The results are presented in Fig. 4.12, which focuses on the most significant activation products at the End of Life (EOL) for both coolants.

To identify the most significant activation products, a filtering threshold of 200,000 Bq (0.2 MBq) was applied to the per-nuclide activities at EOL. This threshold is derived from the IAEA Safety Standards Series No. GSG-17, "Application of the Concept of Exemption" (IAEA, 2023), which provides generic exemption levels for radionuclides in bulk materials.

According to Section 4.16–4.22 of GSG-17, the exemption level for most radionuclides is set at an activity concentration of 1 Bq/g, ensuring that the annual effective dose to individuals does not exceed 10  $\mu$ Sv (0.01 mSv), the criterion for exemption in planned exposure situations. For the coolant materials, in our case Lead (Pb) and Lead-Bismuth Eutectic (LBE), this activity concentration must be converted to a total activity threshold using the material's density and volume.

The density of Lead is approximately 11.34 g/cm<sup>3</sup> (at room temperature, a standard value for solid lead, though molten lead in the reactor will have a lower density), and the density of LBE is approximately 10.5 g/cm<sup>3</sup> (typical for LBE at reactor operating temperatures). The coolant volume, as defined in the OpenMC simulation, is 4,940,843.15 cm<sup>3</sup>.

First, the activity concentration of 1 Bq/g is converted to Bq/cm<sup>3</sup>:

$$\text{For Lead: } 1 \text{ Bq/g} \times 11.34 \text{ g/cm}^3 = 11.34 \text{ Bq/cm}^3$$

$$\text{For LBE: } 1 \text{ Bq/g} \times 10.5 \text{ g/cm}^3 = 10.5 \text{ Bq/cm}^3$$

Next, the total activity threshold for the entire material (summing the contributions of all nuclides) is calculated by multiplying the activity concentration by the volume:

$$\text{For Lead: } 11.34 \text{ Bq/cm}^3 \times 4,940,843.15 \text{ cm}^3 = 56,029,161.32 \text{ Bq} \approx 56.03 \text{ MBq}$$

$$\text{For LBE: } 10.5 \text{ Bq/cm}^3 \times 4,940,843.15 \text{ cm}^3 = 51,878,853.08 \text{ Bq} \approx 51.88 \text{ MBq}$$

This total activity threshold represents the maximum allowable activity in the entire material to meet the 10  $\mu$ Sv dose criterion, assuming all nuclides contribute equally. Since the analysis focuses on per-nuclide activities, a per-nuclide threshold is derived by dividing the total activity threshold by the number of nuclides present in each material. For Lead, 260 nuclides were identified in the final time step, and for LBE, 157 nuclides were identified:

$$\text{Per-nuclide threshold for Lead: } 56.03 \text{ MBq} / 260 = 0.2155 \text{ MBq} = 215,500 \text{ Bq}$$

$$\text{Per-nuclide threshold for LBE: } 51.88 \text{ MBq} / 157 = 0.3304 \text{ MBq} = 330,400 \text{ Bq}$$

The chosen threshold of 200,000 Bq (0.2 MBq) is slightly more conservative than the calculated value for Lead and LBE, ensuring that nuclides contributing significantly to the total activity are captured. This threshold aligns with the radiological safety criteria outlined in GSG-17 while focusing on nuclides that exceed the exemption level in the context of the ALFRED reactor coolant.

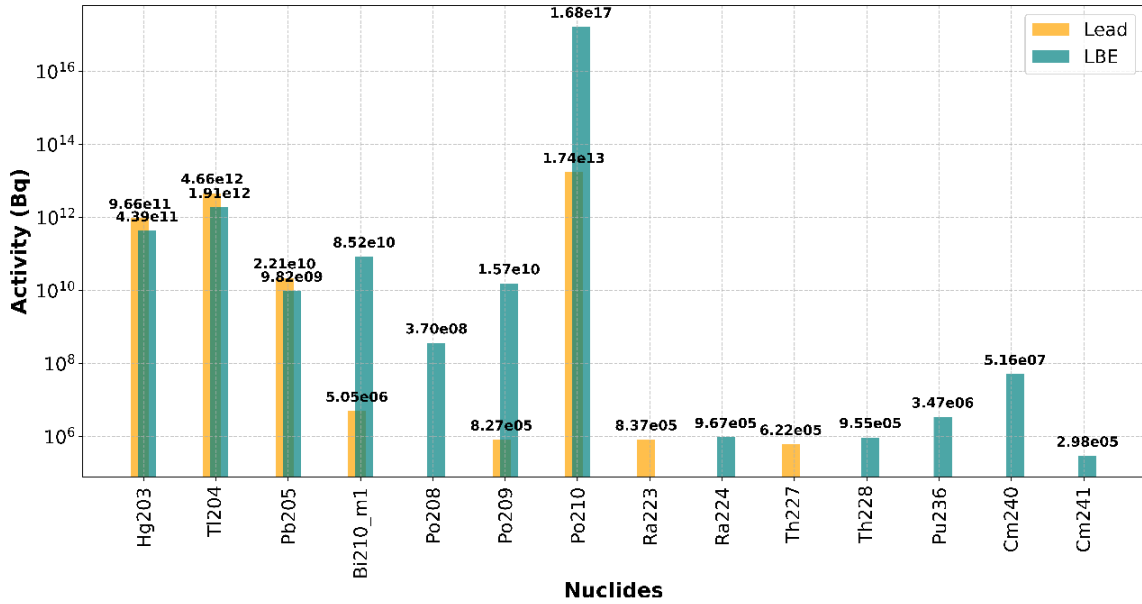


Fig. 4.12: Activity of activation products at the EOL for Lead and LBE coolants in the ALFRED core.

Significant differences are observed between the two coolants, shown in Fig. 4.12. For Lead, the dominant nuclides include Po-210 with an activity of  $1.74 \times 10^{13}$  Bq, followed by Tl-204 at  $4.66 \times 10^{12}$  Bq and Hg-203 at  $9.66 \times 10^{11}$  Bq. Other notable nuclides in Lead include Pb-205 ( $2.21 \times 10^{10}$  Bq), Ra-223 ( $8.37 \times 10^5$  Bq), and Th-227 ( $6.22 \times 10^5$  Bq), all above the 200,000 Bq threshold. In LBE, Po-210 exhibits a dramatically higher activity of  $1.68 \times 10^{17}$  Bq, reflecting the presence of bismuth, which enhances polonium production through neutron capture and decay chains. Other notable nuclides in LBE include Bi-210m ( $8.52 \times 10^{10}$  Bq), Po-209 ( $1.57 \times 10^{10}$  Bq), Po-208 ( $3.70 \times 10^8$  Bq), Tl-204 ( $1.91 \times 10^{12}$  Bq), Hg-203 ( $4.39 \times 10^{11}$  Bq), Pb-205 ( $9.82 \times 10^9$  Bq), Ra-224 ( $9.67 \times 10^5$  Bq), Th-228 ( $9.55 \times 10^5$  Bq), Pu-236 ( $3.47 \times 10^6$  Bq), Cm-240 ( $5.16 \times 10^7$  Bq), and Cm-241 ( $2.98 \times 10^5$  Bq). The higher activity of Po-210 in LBE underscores the increased radiological hazard associated with bismuth-containing coolants, highlighting a key trade-off in the choice of coolant for LFRs.

Pb-209 is produced from neutron absorption in the core and reaches an equilibrium concentration in about 200 days. In the case of pure lead, the concentration of stable Pb-206 decreases continuously. For LBE, the concentration of Pb-206 decreases initially but starts to increase after 200 days, as it is produced from the decay of Po-210, which is more abundant in LBE due to the presence of bismuth. In the pure lead model, after 1825 Effective Full Power Days (EFPD), approximately 0.089 g of Po-210 is produced, whereas in the LBE model, the amount is approximately 1 kg. This amount of Po-210 in the LBE

model will produce a decay heat of about 150 kW in the core, contributing to the thermal load that must be managed during reactor operation and shutdown. Also, it is crucial to develop efficient filtration systems for minimizing the associated risks, particularly the potential release of Po-210 into the cover gas and beyond the primary system. The higher production of Po-210 from LBE, amplifies the need for robust mitigation strategies. Further studies can be conducted on these filtration systems to ensure the overall safety of LFRs, addressing both the radiological hazards and the thermal management challenges posed by Po-210 decay heat.

## 4.2 ALFRED Alternative Reflector Material Candidates

The selection of reflector materials in the Advanced Lead-cooled Fast Reactor European Demonstrator (ALFRED) significantly influences its neutronics performance. Reflectors are critical in fast reactors like ALFRED, as they reduce neutron leakage and help maintain a hard neutron spectrum, which is essential for efficient fuel utilization and actinide transmutation. This section presents the results of a comparative neutronics analysis using various reflector materials, as outlined in Section 3.3, to identify their impact on key parameters such as the  $k_{\text{eff}}$ , neutron leakage, thermalization effects, and power distribution.

### 4.2.1 Effective Multiplication Factor and Leakage

The effective multiplication factor ( $k_{\text{eff}}$ ) and neutron leakage percentage were calculated for each reflector material at the Beginning of Cycle (BOC) using OpenMC with the ENDF/B-VIII.0 nuclear data library. To evaluate the reflective properties of various materials and their impact on the neutronics of the ALFRED core, two distinct boundary conditions: reflective and vacuum, were chosen to isolate and compare the effects of neutron leakage under different scenarios. These parameters provide insight into the reflector's ability to retain neutrons within the core and sustain criticality. Table 4.3 summarizes the results, while Fig. 4.26 and Fig. 4.27 visualize the  $k_{\text{eff}}$  and leakage trends, respectively. By comparing the  $k_{\text{eff}}$  and leakage values under these two conditions, we can discern the reflective capabilities of each material in an idealized context (reflective condition) versus their resilience in a practical, leakage-prone environment (vacuum condition).

#### 4.2.1.1 Boundary Conditions and Their Purpose

**Reflective Boundary Condition:** This condition applies reflective boundaries to the top and bottom planes of the core, effectively eliminating axial leakage. By preventing neutron loss in the axial direction, this setup isolates the radial leakage influenced by the reflector material surrounding the core, allowing a focused assessment of each material's radial reflection efficiency. Essentially, how well it reflects neutrons back into the core from the sides.

**Vacuum Boundary Condition:** In contrast, the vacuum condition applies vacuum boundaries to the top and bottom planes of the core, permitting leakage in both radial and axial directions. This setup mimics a more realistic operational scenario where neutrons can escape through all boundaries, as might occur during actual reactor operation. It provides a comprehensive view of how reflector materials perform under conditions where both radial and axial losses challenge neutron retention and criticality.

Table 4.3:  $k_{\text{eff}}$  and leakage in ALFRED core for different reflector materials

Materials	Reflective Boundary Condition		Vacuum Boundary Condition		Axial Leakage (%)
	$k_{\text{eff}}$	Leakage (%)	$k_{\text{eff}}$	Leakage (%)	
Yttria-Zirconia	1.22542	4.556	1.07884	20.17834	15.62234
Ba <sub>2</sub> Pb	1.20846	9.578	1.06134	24.88696	15.30896
BeO	1.25955	4.029	1.11189	18.51193	14.48293
Graphite	1.23900	6.769	1.08682	21.73615	14.96715
Lead	1.22600	9.074	1.07456	24.30084	15.22684
Magnesium	1.21746	9.559	1.06739	24.56023	15.00123
MgO	1.24195	5.704	1.08635	21.17209	15.46809
PbO	1.23037	7.649	1.07754	23.32001	15.67101
PbS	1.22269	9.168	1.06752	24.37779	15.20979
SiC	1.22870	6.217	1.07809	21.65363	15.43663
ZrC	1.22300	4.119	1.07795	19.90363	15.78463
Zr <sub>3</sub> Si <sub>2</sub>	1.22190	7.782	1.07037	23.44241	15.66041

The analysis below evaluates their performance in the ALFRED core, focusing on radial reflection efficiency under reflective conditions and overall neutron retention under vacuum conditions.

#### 4.2.1.2 Reflective Boundary Condition Analysis

Under reflective conditions, axial leakage is eliminated, isolating radial reflection efficiency. As depicted in Fig. 4.26 and Fig. 4.27, BeO achieves the highest  $k_{eff}$  of 1.25955 and the lowest leakage of 4.029%, demonstrating superior radial neutron reflection and minimal absorption. MgO follows with a  $k_{eff}$  of 1.24195 and 5.704% leakage, indicating strong radial performance. Graphite records a  $k_{eff}$  of 1.23900 and 6.769% leakage, also reflecting neutrons effectively. Yttria-Zirconia, the baseline material, yields a  $k_{eff}$  of 1.22542 and 4.556% leakage, performing moderately. In contrast, Ba<sub>2</sub>Pb exhibits the lowest  $k_{eff}$  of 1.20846 and the highest leakage of 9.578%, indicating poor radial reflection efficiency.

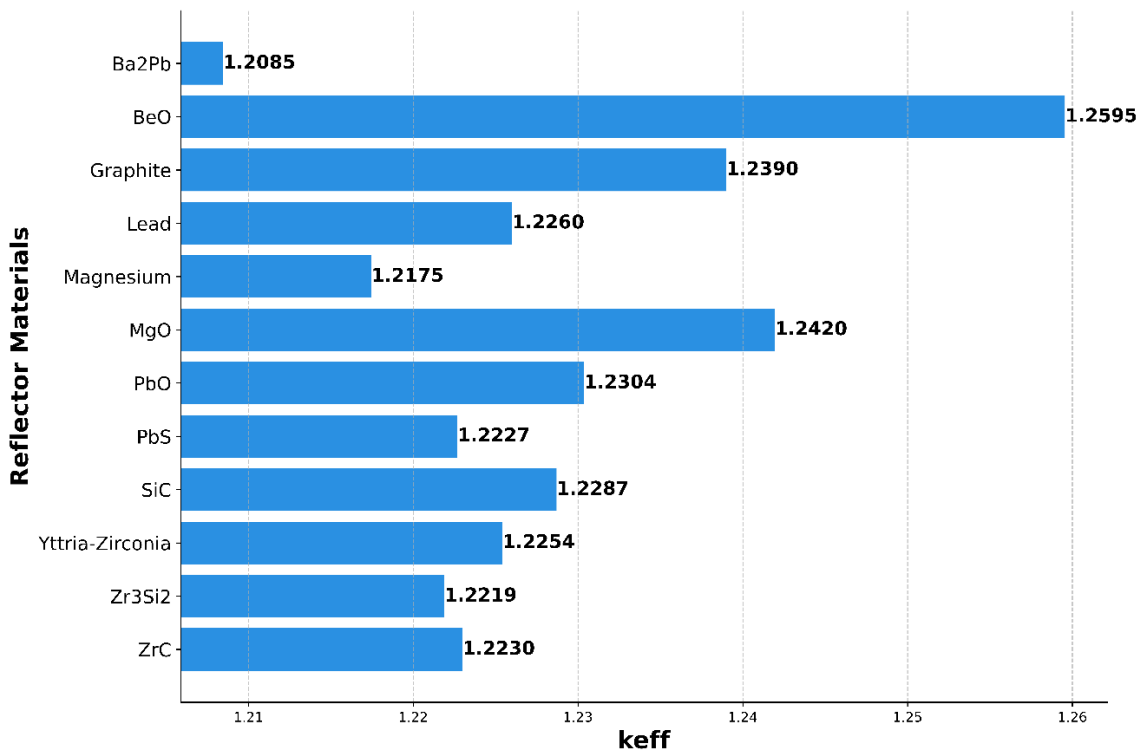


Fig. 4.26:  $k_{eff}$  for different reflector materials (only radial leakage).

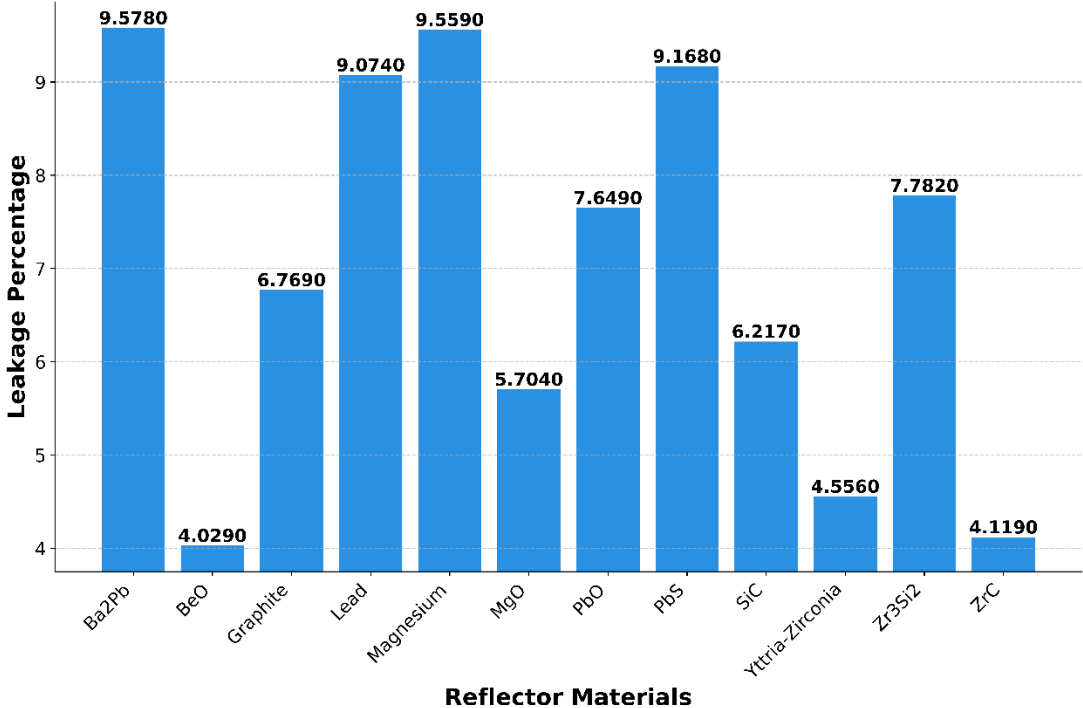


Fig. 4.27: Leakage percentage of different reflector materials (only radial leakage).

#### 4.2.1.3 Vacuum Boundary Condition Analysis

In an operating reactor, reflector materials must minimize neutron losses to sustain a fission chain reaction. Vacuum boundary conditions, simulating a realistic environment with both radial and axial leakage, test the materials' ability to return neutrons to the core, enhancing  $k_{\text{eff}}$  while reducing leakage.

As depicted in Fig. 4.28 and Fig. 4.29, BeO excels under vacuum conditions, achieving the highest  $k_{\text{eff}}$  of 1.11189 and the lowest leakage of 18.512%. This performance ensures criticality with minimal neutron loss, making it the top performer. ZrC and Yttria-Zirconia also perform well, with  $k_{\text{eff}}$  values of 1.07795 and 1.07884, and leakage rates of 19.904% and 20.178%, respectively, offering stable neutron retention despite slightly lower  $k_{\text{eff}}$  compared to BeO.

MgO and Graphite maintain high  $k_{\text{eff}}$  values (1.08682 and 1.08635, respectively), indicating strong criticality support. However, their leakage rates of 21.736% and 21.172% suggest less effectiveness in minimizing neutron loss compared to the top performers. SiC ( $k_{\text{eff}}$  1.07809, leakage 21.654%) shows similar moderate performance.

PbO and Zr<sub>3</sub>Si<sub>2</sub> exhibit balanced but unremarkable performance, with  $k_{\text{eff}}$  values of 1.07754 and 1.07037, and leakage rates of 23.32% and 23.442%, respectively. Lead, Magnesium, PbS, and Ba<sub>2</sub>Pb perform poorly, with  $k_{\text{eff}}$  values ranging from 1.06134 to 1.07456 and high leakage rates exceeding 24% (24.301%, 24.56%, 24.378%, and 24.887%). Their limited ability to reflect neutrons back to the core results in significant neutron economy losses, rendering them less suitable for the ALFRED core.

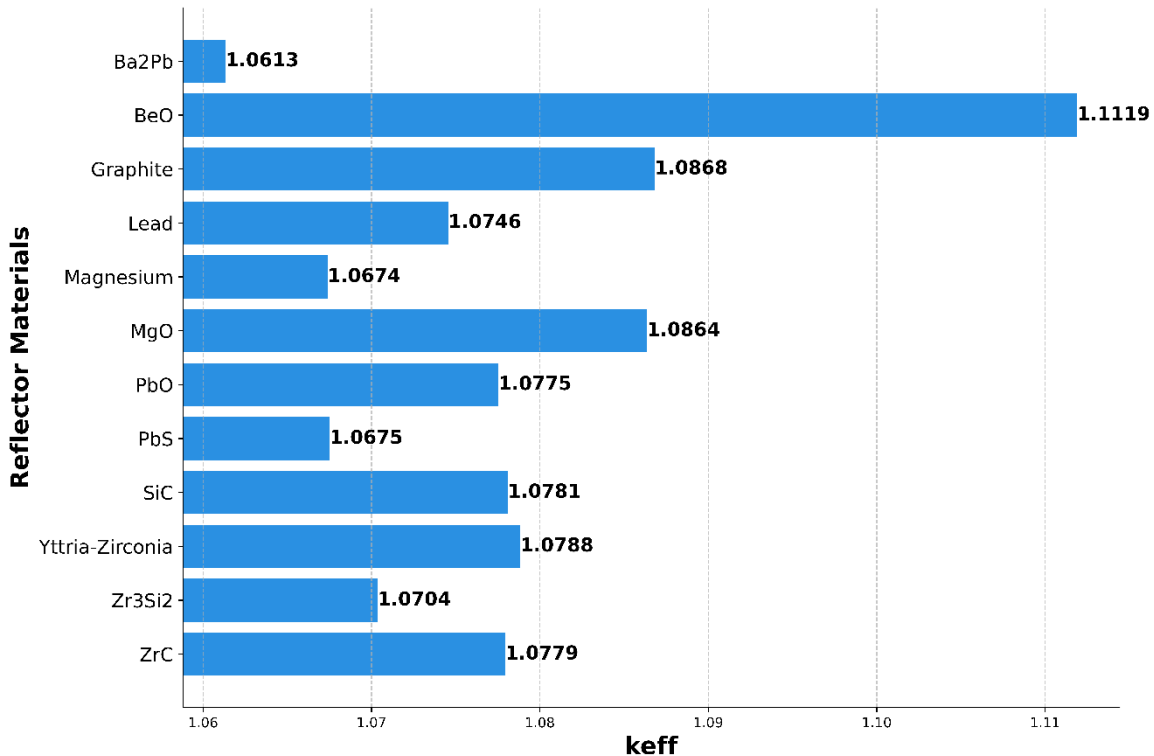


Fig. 4.28:  $k_{\text{eff}}$  for different reflector materials (axial and radial leakage).

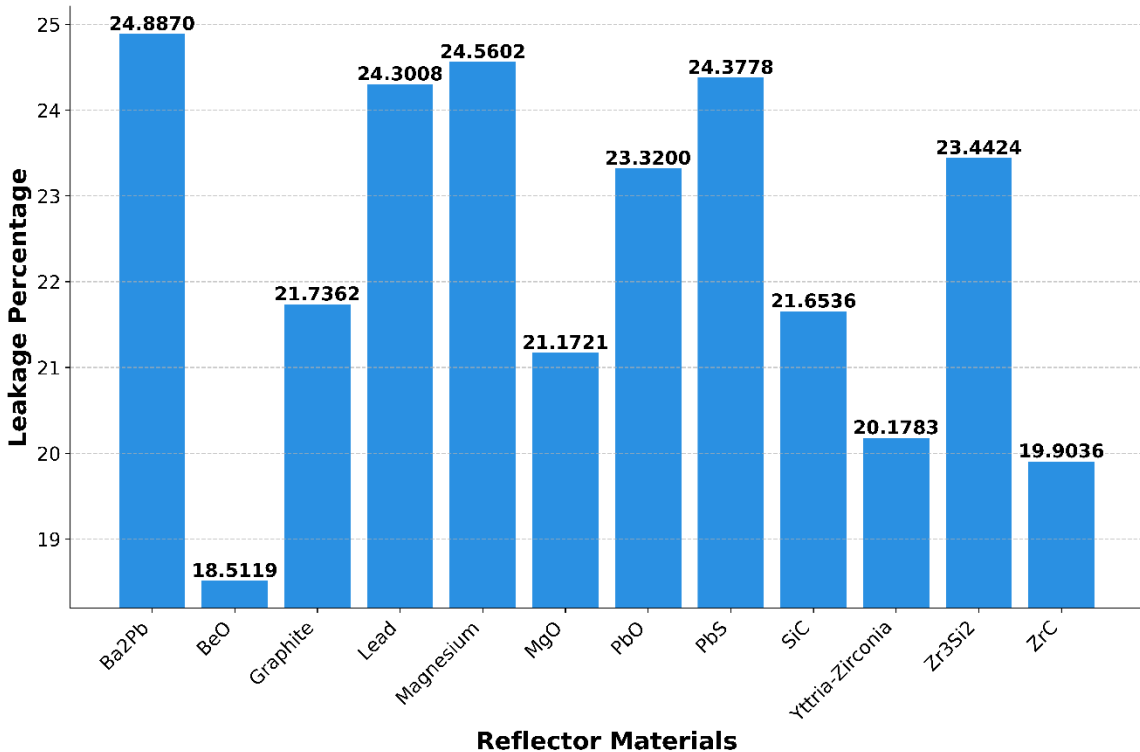


Fig. 4.29: Leakage percentage of different reflector materials (axial and radial leakage).

#### 4.2.1.4 Comparative Insights and Conclusion

The transition from reflective to vacuum conditions highlights significant shifts in material performance due to axial leakage. BeO, which excels radially under reflective conditions ( $k_{\text{eff}}$  1.25955, leakage 4.029%), maintains its strong performance under vacuum conditions with a  $k_{\text{eff}}$  of 1.11189 and leakage of 18.512%. Its ability to minimize total leakage makes it the most effective for neutron retention in a realistic reactor scenario.

Conversely, Ba<sub>2</sub>Pb, despite its modest radial performance under reflective conditions ( $k_{\text{eff}}$  1.20846, leakage 9.578%), performs poorly under vacuum conditions ( $k_{\text{eff}}$  1.06134, leakage 24.887%). This suggests that its radial reflection capabilities are insufficient against axial losses. Similarly, Yttria-Zirconia, with moderate radial performance ( $k_{\text{eff}}$  1.22542, leakage 4.556%), performs better under vacuum conditions ( $k_{\text{eff}}$  1.07884, leakage 20.178%) than expected, showing improved resilience to axial leakage.

Materials like ZrC and SiC offer a balanced compromise, maintaining reasonable  $k_{\text{eff}}$  and low leakage under vacuum conditions (ZrC:  $k_{\text{eff}}$  1.077948, leakage 19.903628%; SiC:  $k_{\text{eff}}$  1.078091, leakage 21.653634%), making them viable alternatives to BeO. In conclusion,

the vacuum boundary condition, which accounts for both radial and axial leakage, reorders material effectiveness, with BeO as the most promising reflector for optimizing neutron economy in the ALFRED core, followed by ZrC and Yttria-Zirconia. However, further analysis of additional neutronics parameters is necessary to determine the optimal alternative reflector material conclusively.

#### 4.2.2 Flux Spectra Comparison

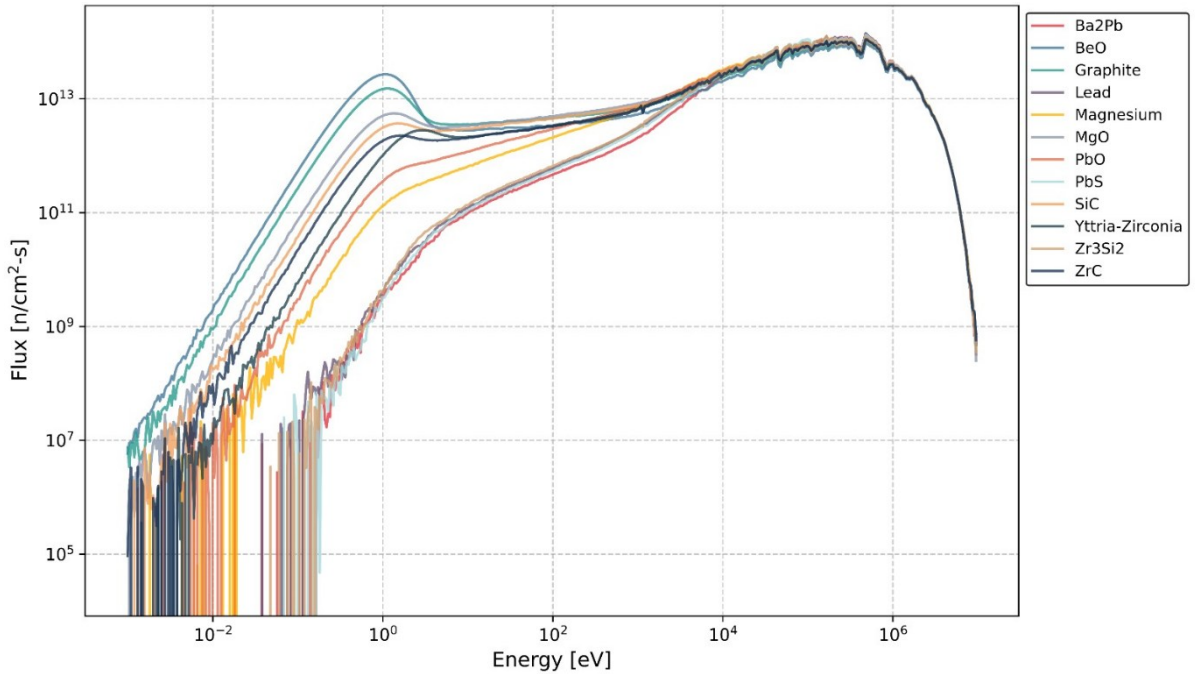


Fig. 4.30: Energy dependent flux distribution for different reflector materials.

Fig. 4.30 and Fig. 4.31 compare the neutron flux spectrums of the ALFRED model for different reflector materials. The reflectors Ba<sub>2</sub>Pb, PbS, Lead, Zr<sub>3</sub>Si<sub>2</sub> show a typical hardened spectrum with an energy peak in the 1 MeV region as such in fast reactors. The other reflectors show a moderate to high peak in the thermal energy region. The reflectors with the highest neutron thermalization are BeO, Graphite, MgO and SiC in that order. This is likely due to the inelastic scattering in light elements for those reflectors.

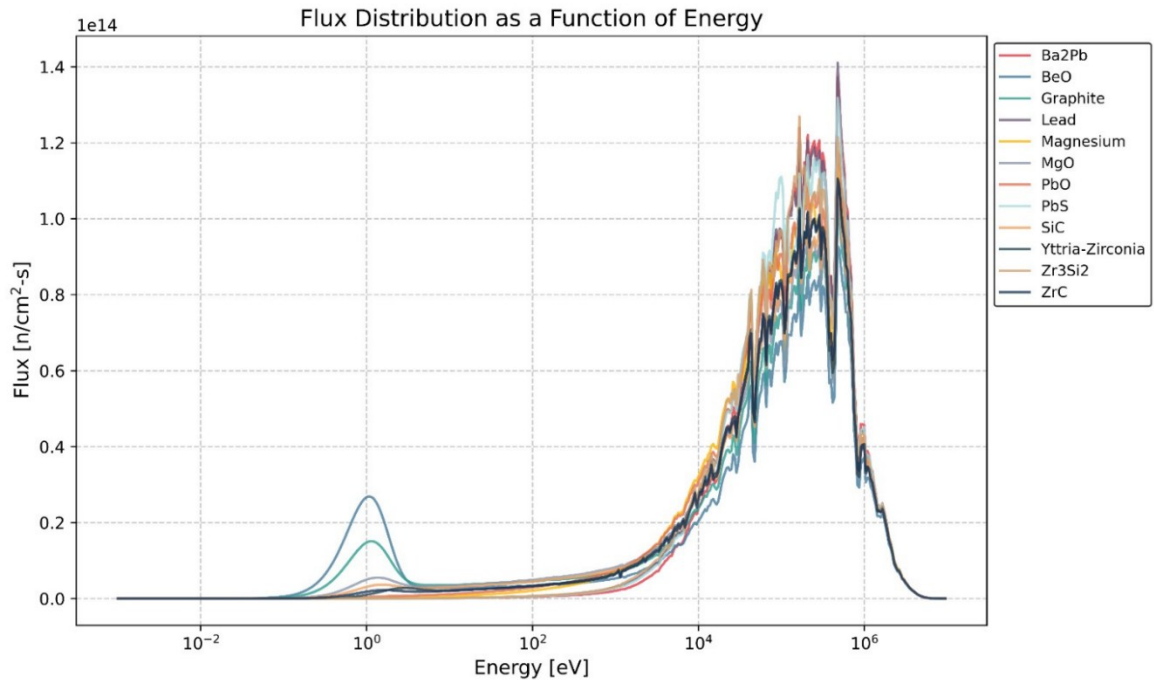


Fig. 4.31: Energy dependent flux distribution for different reflector materials.

Fig. 4.30 has logarithmic scales taken on both axes to properly distinguish between the thermalization effect while Fig. 4.31 has only the energy axis in logarithmic scale to clearly see the relative neutron energy peaks.

#### 4.2.3 Fission Rate Comparison

This subsection examines the fission rate distributions in the ALFRED core for 12 reflector materials i.e., Yttria-Zirconia, Ba<sub>2</sub>Pb, BeO, Graphite, Lead, Magnesium, MgO, PbO, PbS, SiC, ZrC, and Zr<sub>3</sub>Si<sub>2</sub>, focusing on spatial variations, thermal fission contributions, and their implications for the reactor's neutronic performance.

#### 4.2.3.1 Spatial Distribution of Fission Rates

Fission rate distributions were analyzed across the ALFRED core, which consists of inner and outer fuel zones containing mixed oxide (MOX) fuel. In the inner fuel zone, fission rates were highly uniform across all reflectors, with minimal variations. This consistency reflects the dominance of the fast neutron flux in the inner zone, which is less influenced by the reflector due to its distance from the core-reflector interface.

At the outer fuel periphery, adjacent to the reflector, fission rates varied noticeably depending on the reflector material. The total fission rate distribution, shown in Fig. 4.32, reveals that BeO, Graphite, MgO, and SiC induced a pronounced fission rate peak at the periphery, with BeO exhibiting the most significant increase, followed by Graphite, MgO, and SiC. Magnesium and Zr<sub>3</sub>Si<sub>2</sub> showed a moderate increase in fission rates at the periphery, while Yttria-Zirconia, Ba<sub>2</sub>Pb, Lead, PbO, PbS, and ZrC displayed minimal variation compared to the inner zone. The elevated fission rates for BeO, Graphite, MgO, and SiC are attributed to enhanced neutron reflection and moderation, which increases the neutron flux in the peripheral region. Fig. 4.30 illustrates the neutron flux spectrum, revealing a softer spectrum for these four reflectors, with increased thermal neutron populations compared to the other reflectors. This softening is likely driven by high neutron scattering cross-sections (e.g., in Graphite and MgO) and (n, 2n) reactions (e.g., in BeO), which generate additional low-energy neutrons.

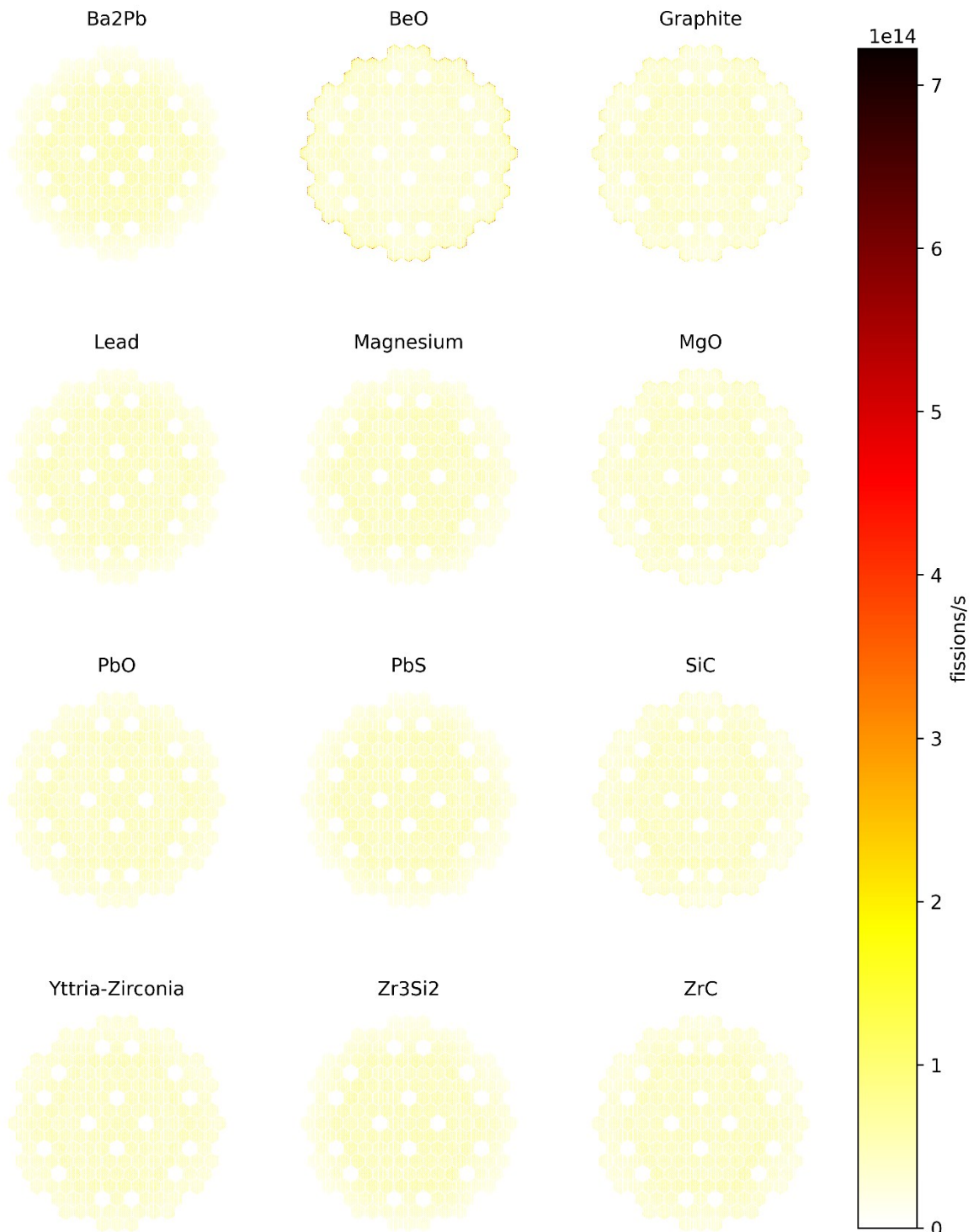


Fig. 4.32: Fission rate distribution over the whole core for different reflectors.

#### 4.2.3.2 Contribution of Thermal Fission

To investigate the cause of the fission rate peak at the outer periphery, a fission rate tally for thermal neutrons (0–0.025 eV), where fission is most probable, was analyzed. Fig. 4.33 depicts the thermal fission rate distribution across the core, showing that BeO, Graphite, MgO, and SiC exhibit significant thermal fission at the outer fuel periphery, with rates reaching up to  $10^{13}$  fissions/s near the core-reflector interface. Magnesium and Zr<sub>3</sub>Si<sub>2</sub> displayed lower but noticeable thermal fission in this region, while Yttria-Zirconia, Ba<sub>2</sub>Pb, Lead, PbO, PbS, and ZrC showed minimal thermal fission activity. The concentration of thermal fission at the periphery for BeO, Graphite, MgO, and SiC directly corresponds to their observed fission rate peaks, confirming that thermal fission is a primary driver of the elevated rates in these cases. This thermal fission activity arises because these reflectors moderate fast neutrons into the thermal energy range, enhancing fission in the peripheral fuel assemblies. This observation is consistent with the softer flux spectrum in Fig. 4.30, highlighting the interplay between reflector material properties and neutron energy distribution in the ALFRED core.

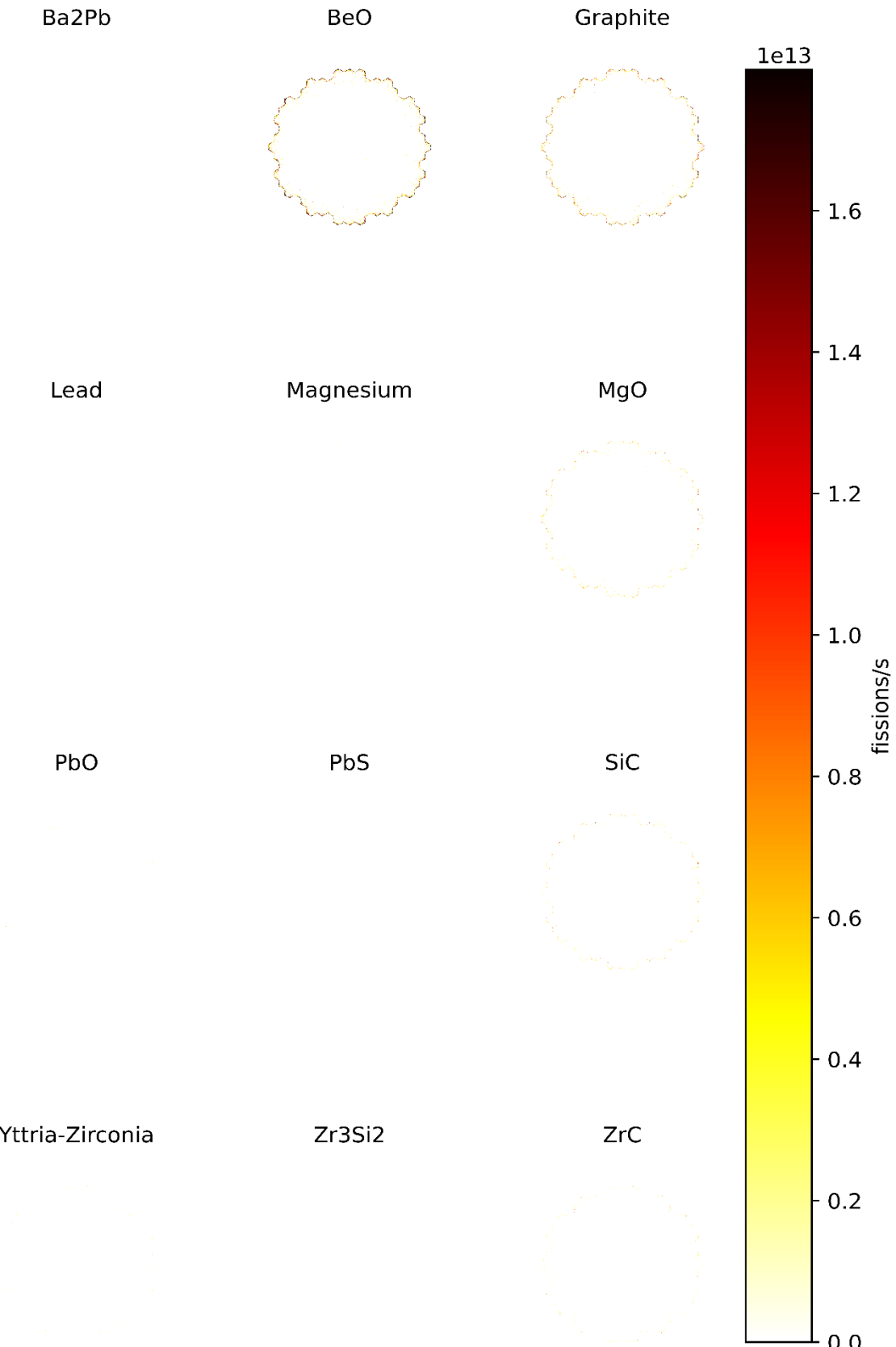


Fig. 4.33: Thermal fission rate distribution over the whole core for different reflectors.

#### 4.2.3.3 Quantification of Thermal Fission

The contribution of thermal fission was quantified by calculating the thermal fission fraction, defined as the ratio of thermal fission (0–0.025 eV) to total fission across all neutron energies. Fig. 4.34 presents these fractions, with BeO exhibiting the highest fraction at 1.89%, followed by Graphite at 0.95%, MgO at 0.26%, and SiC at 0.16%. ZrC (0.07%), Zr<sub>3</sub>Si<sub>2</sub> (0.03%), and PbO (0.01%) showed minimal contributions, while Yttria-Zirconia, Ba<sub>2</sub>Pb, Lead, Magnesium, and PbS had negligible fractions at 0.00%

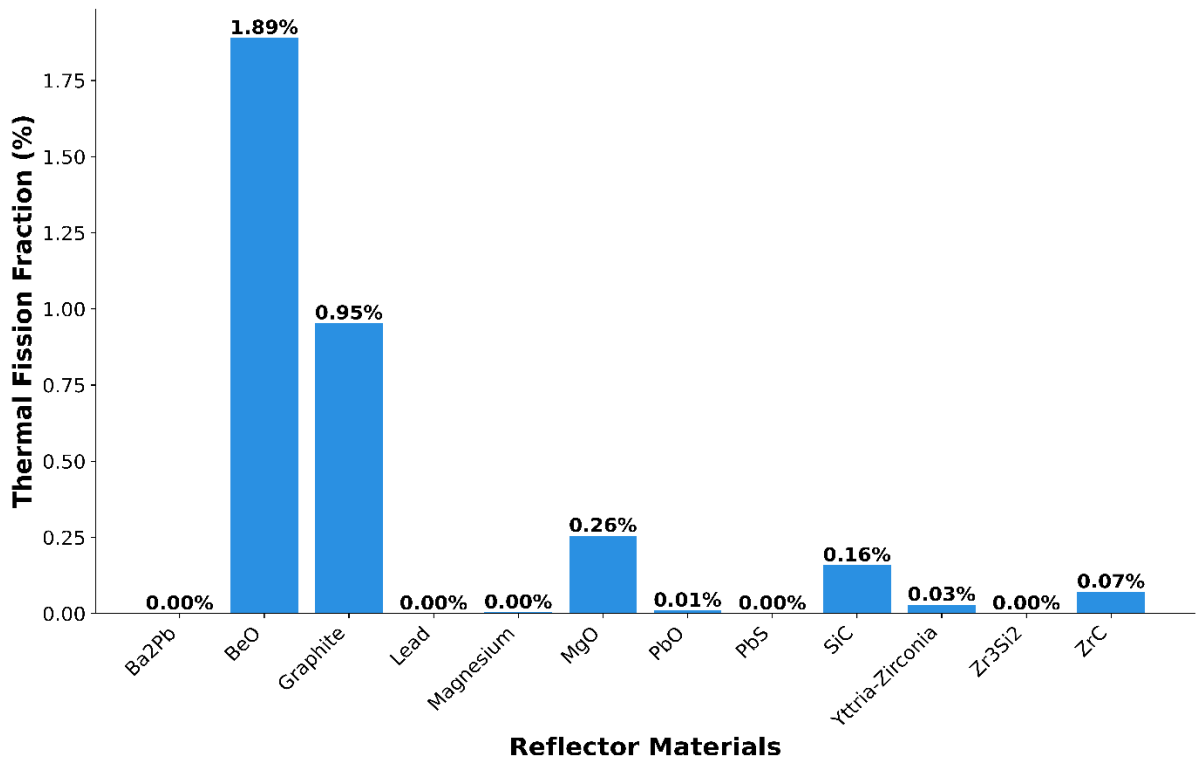


Fig. 4.34: Thermal fission percentages of different reflector materials.

#### 4.2.4 Flux Distribution Comparison at BOC

This subsection analyzes the neutron flux distributions in the ALFRED core at the beginning of cycle (BOC) for the 12 reflector materials, examining both the total neutron flux across all energies and the thermal neutron flux in the 0–0.025 eV range. The neutron flux distribution directly influences the fission rates discussed in the previous subsection, as it determines the availability of neutrons for inducing fission in the MOX fuel. Understanding the spatial variation of the flux, particularly the thermal component,

provides insight into how reflector materials affect neutron moderation and reflection, impacting the overall neutronic performance of the 300 MW<sub>th</sub> ALFRED reactor.

#### 4.2.4.1 Total Neutron Flux Distribution

The total neutron flux distribution across all energies was analyzed to assess the overall neutron behavior in the ALFRED core. Fig. 4.35 illustrates this distribution, showing that Ba<sub>2</sub>Pb, Magnesium, PbS, and Zr<sub>3</sub>Si<sub>2</sub> exhibit a high neutron flux, particularly in the inner fuel zone, with fluxes reaching up to  $3.5 \times 10^{15}$  neutrons/cm<sup>2</sup>·s. This high flux in the inner zone suggests that these reflectors are effective at reflecting fast neutrons back into the core, enhancing the neutron population in the central region where fast fission dominates. In contrast, BeO, Graphite, and MgO display a more uniform neutron flux distribution across the core, with fluxes ranging from  $1.5 \times 10^{15}$  to  $2.5 \times 10^{15}$  neutrons/cm<sup>2</sup>·s and minimal variation between the inner and outer fuel zones. This uniformity indicates that these reflectors moderate neutrons more effectively, reducing the fast flux gradient across the core. Notably, BeO shows a slight peak at the edge of the outer fuel zone, with a higher flux (up to  $2.5 \times 10^{15}$  neutrons/cm<sup>2</sup>·s) near the core-reflector interface, likely due to enhanced neutron reflection and moderation in this region. The uniform flux distribution for BeO, Graphite, and MgO aligns with their pronounced fission rate peaks at the periphery (Section 4.1.1), as a more balanced flux distribution supports consistent fission across the core, with a slight enhancement at the edges

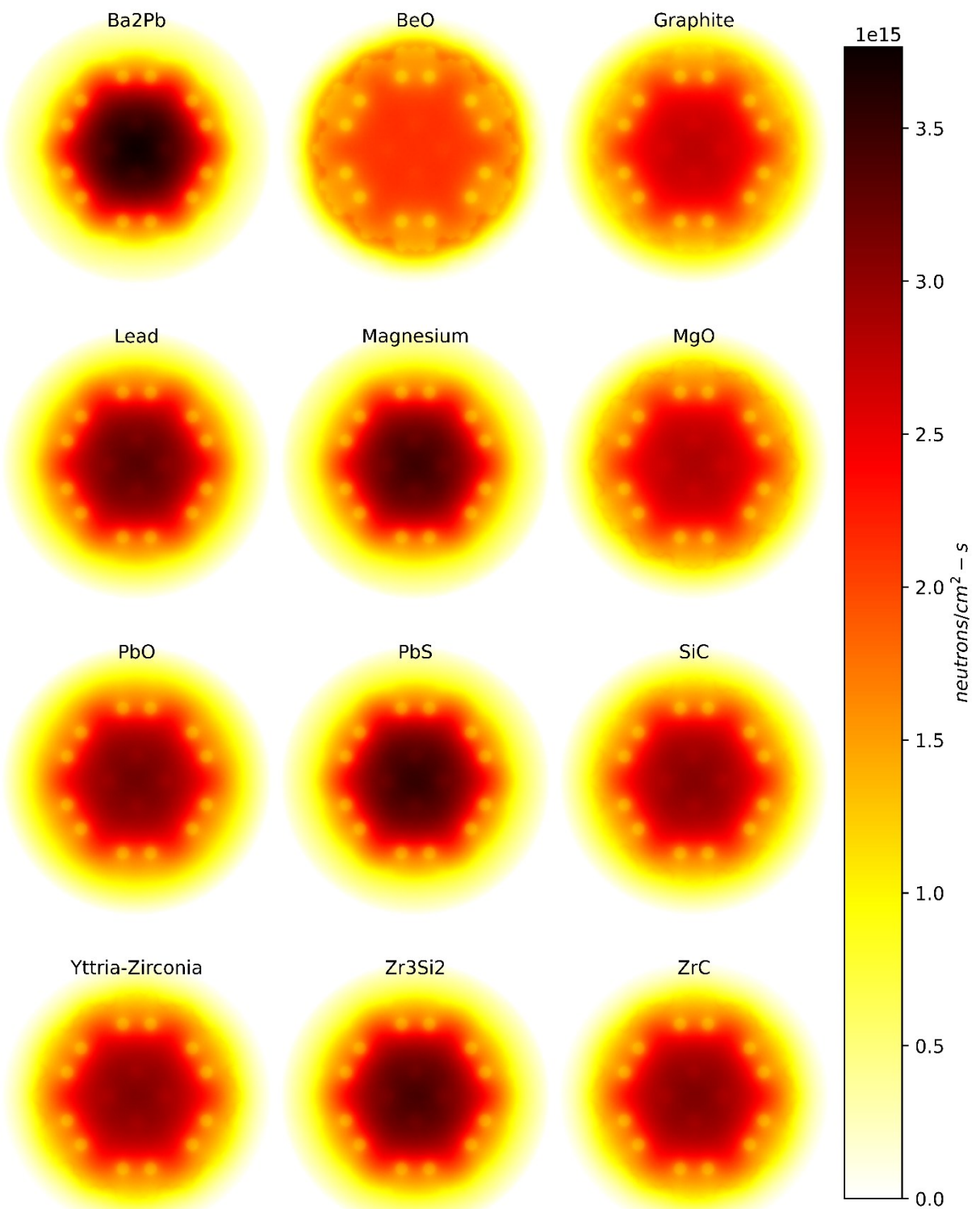


Fig. 4.35: Flux distribution over the whole core for different reflector materials.

#### 4.2.4.2 Thermal Neutron Flux Distribution

A separate flux tally was calculated for thermal neutrons (0–0.025 eV) to evaluate the extent of neutron thermalization in the core, which is critical for understanding the thermal fission contributions observed in Section 4.2.3.2. Fig. 4.36 reveals the thermal neutron flux distribution, showing that BeO, Graphite, and MgO exhibit the highest concentration of thermal neutrons, with fluxes up to  $1.2 \times 10^{13}$  neutrons/cm<sup>2</sup>·s in the reflector region, spreading inward to the outer fuel zone. This high thermal flux is consistent with their ability to moderate fast neutrons, as evidenced by the softer flux spectrum in Fig. 4.30 and their high thermal fission fractions. SiC, ZrC, Yttria-Zirconia, and PbO show moderate to low thermal neutron flux, with SiC having the highest among them (up to  $0.6 \times 10^{13}$  neutrons/cm<sup>2</sup>·s), followed by ZrC, Yttria-Zirconia, and PbO, indicating some degree of moderation but less pronounced than BeO, Graphite, and MgO. The remaining reflectors—Ba<sub>2</sub>Pb, Lead, Magnesium, PbS, and Zr<sub>3</sub>Si<sub>2</sub>—depict negligible thermal neutron flux (near 0 neutrons/cm<sup>2</sup>·s), suggesting minimal moderation and aligning with their low thermal fission fractions. The concentration of thermal flux in the reflector region for BeO, Graphite, and MgO explains their elevated thermal fission rates at the outer fuel periphery (Fig. 4.33), as thermal neutrons in this region enhance fission in the peripheral fuel assemblies.

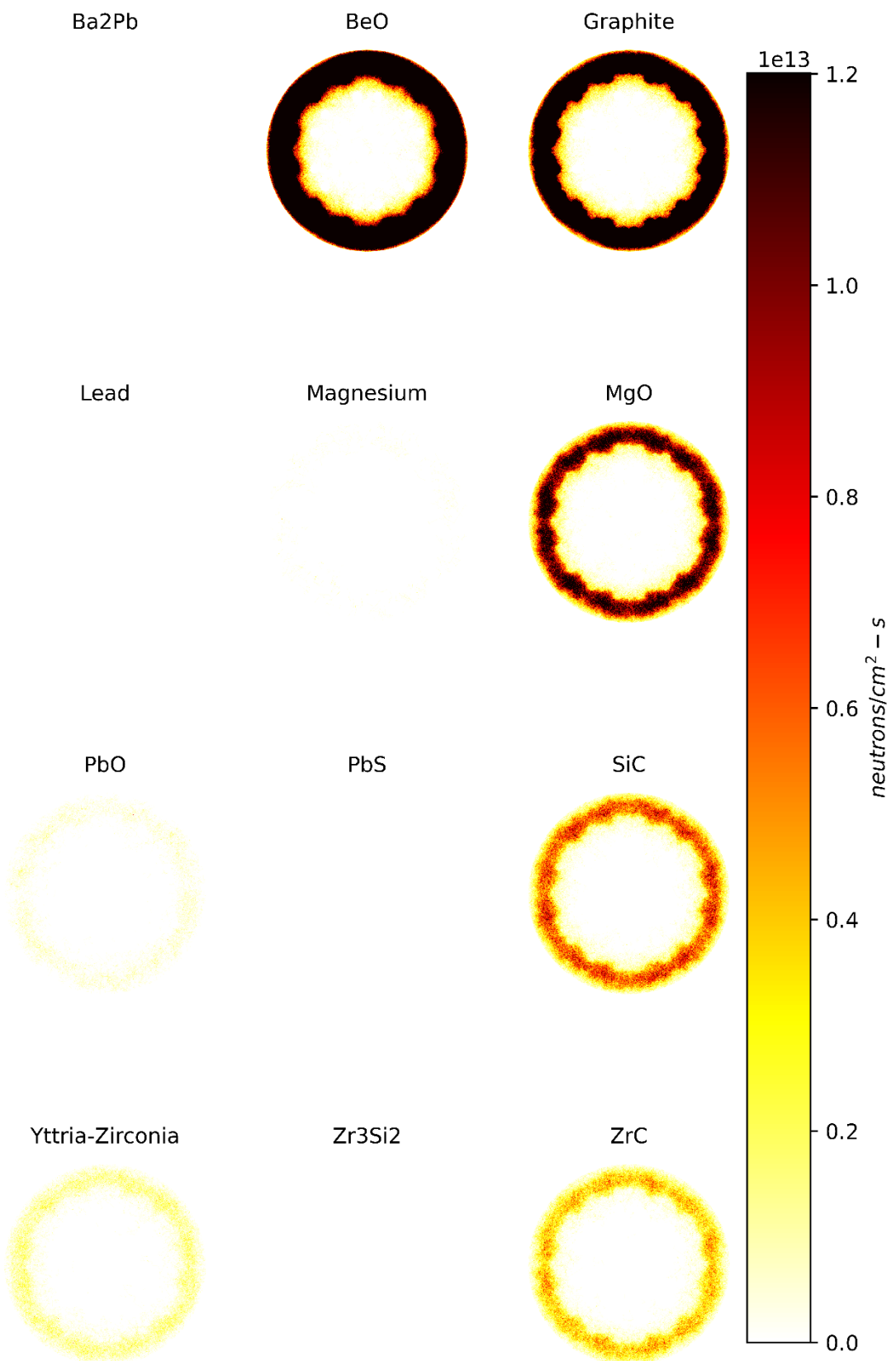


Fig. 4.36: Thermal flux observed for different reflectors.

#### 4.2.5 Burnup – $k_{\text{eff}}$ and Cycle Length

This subsection evaluates the burnup characteristics of the ALFRED core for the 12 reflector materials, focusing on the effective multiplication factor ( $k_{\text{eff}}$ ) over time and the resulting fuel cycle length. Burnup analysis provides insights into the reactivity behavior of the core as fuel is depleted, which is critical for determining the operational duration of the reactor before refueling. By examining  $k_{\text{eff}}$  trends and the time to reach criticality, this analysis highlights how reflector materials influence the reactor's reactivity and cycle length, complementing the fission rate and flux distribution findings in previous subsections.

##### 4.2.5.1 Variation of Effective Multiplication Factor with Burnup

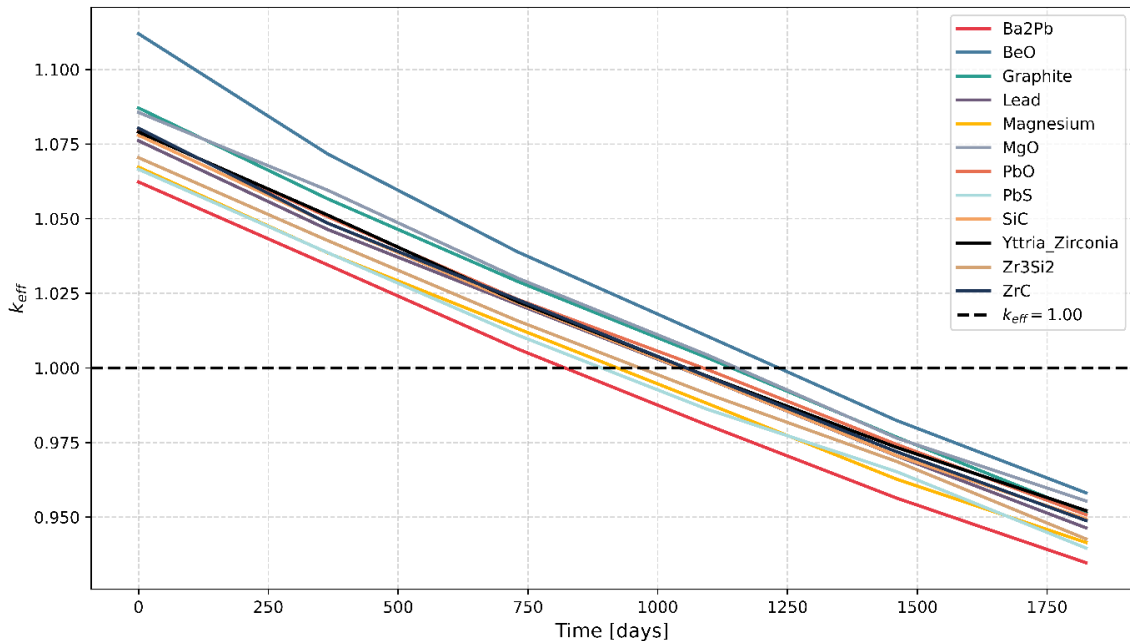


Fig. 4.37: Effective multiplication factor ( $k_{\text{eff}}$ ) vs burnup time for different reflectors.

A burnup analysis was conducted to assess the reactivity characteristics of the ALFRED core with each reflector. Fig. 4.37 depicts the gradual decrease in the effective multiplication factor ( $k_{\text{eff}}$ ) for the 12 reflectors over a burnup period of 1750 days. The horizontal dotted line at  $k_{\text{eff}}=1.0$  represents the criticality threshold, below which the reactor can no longer sustain a chain reaction without refueling. All reflectors start with  $k_{\text{eff}}$  values between 1.075 and 1.10, indicating excess reactivity at the beginning of cycle (BOC). Over time,  $k_{\text{eff}}$  decreases due to fuel depletion and the buildup of fission products, which act as

neutron poisons. BeO, MgO, and Graphite exhibit the slowest decline in  $k_{\text{eff}}$ , maintaining higher reactivity for a longer period, with BeO showing a particularly steep initial slope in the first 365 days, suggesting significant excess reactivity during this timeframe. In contrast, reflectors like Ba<sub>2</sub>Pb, Yttria-Zirconia, and Lead show a faster decline, crossing the criticality threshold earlier, indicating shorter cycle lengths. The slower decline for BeO, MgO, and Graphite aligns with their enhanced neutron economy, as seen in their high thermal flux (Section 4.2.4.2) and thermal fission fractions (Section 4.2.3.3), which help sustain reactivity over time.

#### 4.2.5.2 Fuel Cycle Length

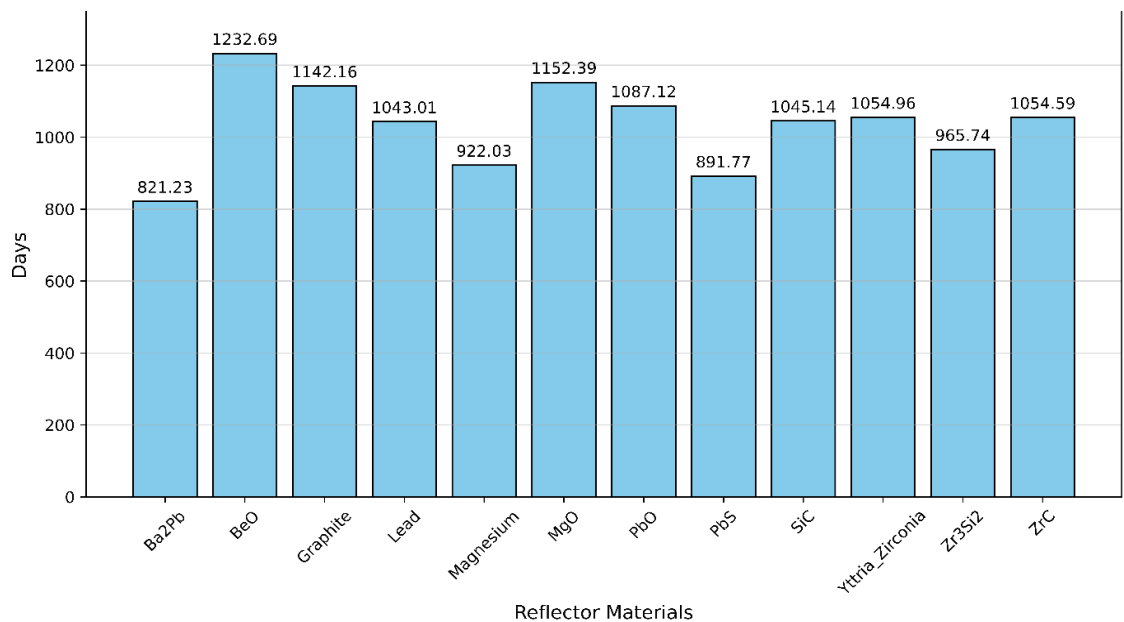


Fig. 4.38: Time to reach criticality for different reflector materials.

The time to reach criticality, effectively the fuel cycle length, was calculated for each reflector using the  $k_{\text{eff}}$  trends from Fig. 4.37. Fig. 4.38 shows that BeO, MgO, and Graphite take the longest to reach criticality, with cycle lengths of 1232.69 days, 1142.16 days, and 1152.39 days, respectively. BeO's exceptionally long cycle length is attributed to its high neutron moderation and reflection capabilities, which enhance neutron economy and sustain reactivity over time, consistent with its uniform flux distribution (Section 4.2.4.1) and high thermal fission fraction (Section 4.2.3.). MgO and Graphite follow closely, benefiting from similar neutronic properties, including significant thermal flux in the reflector region (Section 4.2.2). Conversely, Ba<sub>2</sub>Pb has the shortest cycle length at 821.23 days, followed by Yttria-Zirconia at 965.74 days and Lead at 1043.01 days, reflecting their

limited moderation and lower neutron economy, as evidenced by their negligible thermal flux (Section 4.2.2). Other reflectors, such as SiC (1045.14 days) and ZrC (1054.59 days), fall in the middle, balancing moderate neutron reflection with limited thermalization.

#### **4.2.6 Burnup - Activation of Reflector Materials**

Throughout the reactor core's operational lifespan, as the fuel materials undergo compositional changes, the structural materials also transform due to activation caused by the intense neutron flux. This phenomenon extends to the reflector materials, which are similarly subjected to high neutron irradiation, leading to the formation of activation products. To investigate this, the composition of various reflector materials after burnup within the core model, excluding the original elements present in the reflectors, were isolated and analyzed to reveal the activation products formed during operation.

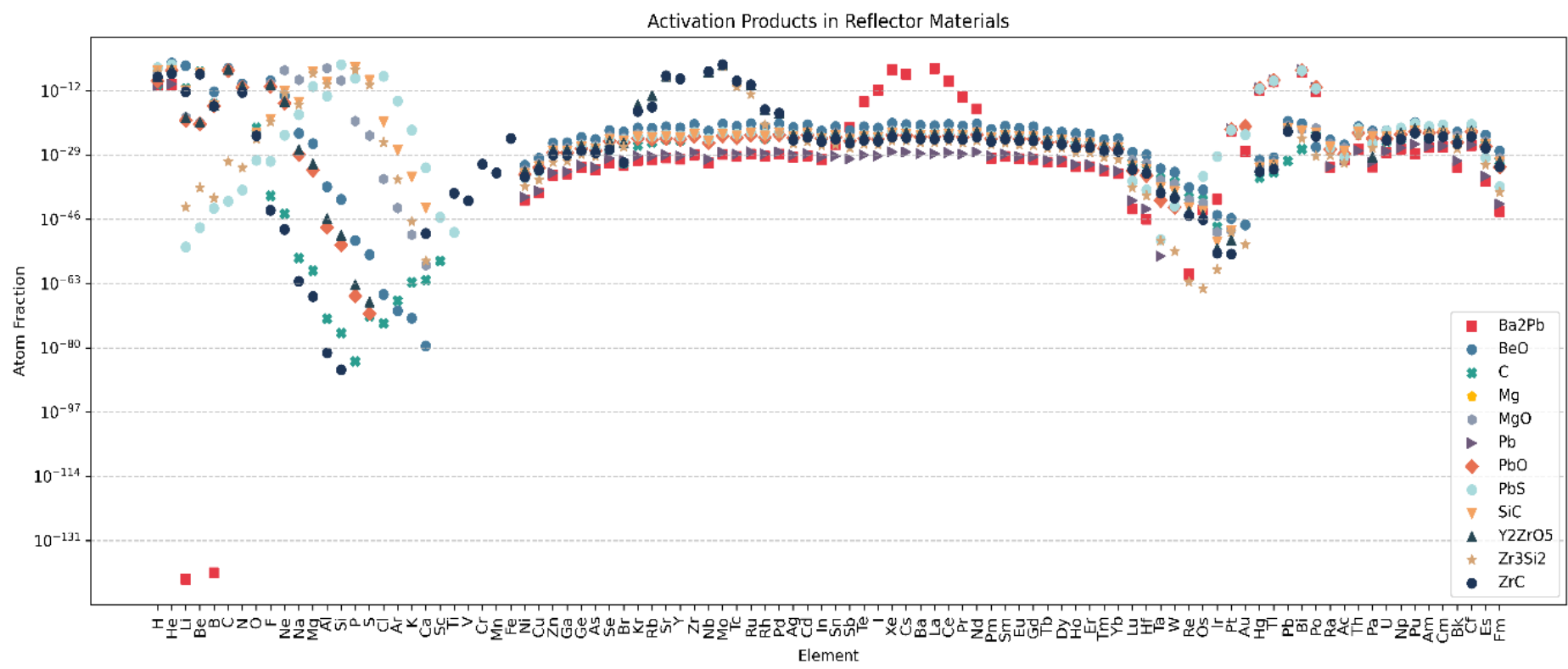


Fig. 4.39: Activation product comparison for the reflector materials.

Fig. 4.39 presents a dot plot illustrating the distribution of activation product elements across all simulated reflectors. The x-axis lists the elements identified as activation products, while the y-axis represents the atom fraction of these elements on a logarithmic scale. Each dot represents the presence of a specific activation product in a given reflector, with different colors and shapes corresponding to distinct reflector materials, as indicated in the legend (e.g., Ba<sub>2</sub>Pb, BeO, C, Mg, etc.). The plot reveals a wide range of activation products, with atom fractions varying significantly across elements and reflector types. Notably, certain elements, such as those around the middle of the x-axis, exhibit higher atom fractions and appear consistently across multiple reflectors, indicating more significant activation. In contrast, other elements show much lower atom fractions and are less prevalent, suggesting minimal activation in specific reflectors. This variability highlights the influence of reflector material composition on the type and quantity of activation products formed under neutron irradiation. The clustering of data points for some elements also suggests that certain activation products are more likely to form in specific reflector materials, providing insight into the neutron-induced transmutation processes occurring within the core.

#### 4.2.7 Burnup - Isotopic Mass Evolution

This subsection analyzes the mass evolution trends of key isotopes in the ALFRED core's MOX fuel (combined inner and outer fuel regions) over a 1750-day burnup period, focusing on the qualitative impact of the 12 reflector materials on neutronic behavior. The analysis is divided into two parts: transuranic elements (U-238, Pu-239, Pu-240, Pu-241), which drive fission and fuel cycle dynamics, and minor actinides (Np-237, Am-241, Am-243, Cm-244), which affect waste and safety considerations. By emphasizing trends rather than specific masses, this qualitative evaluation complements the burnup characteristics in Section 4.2.5, providing insights into the neutronic performance of the LFR model.

#### 4.2.7.1 Uranium and Plutonium Isotopes

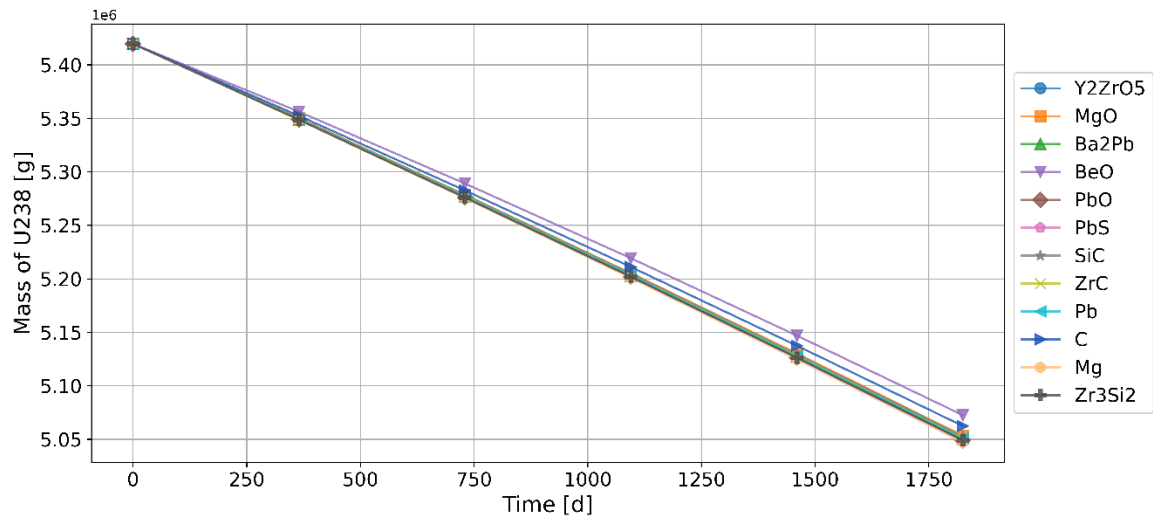


Fig. 4.40: Variation of U-238 across burnup time.

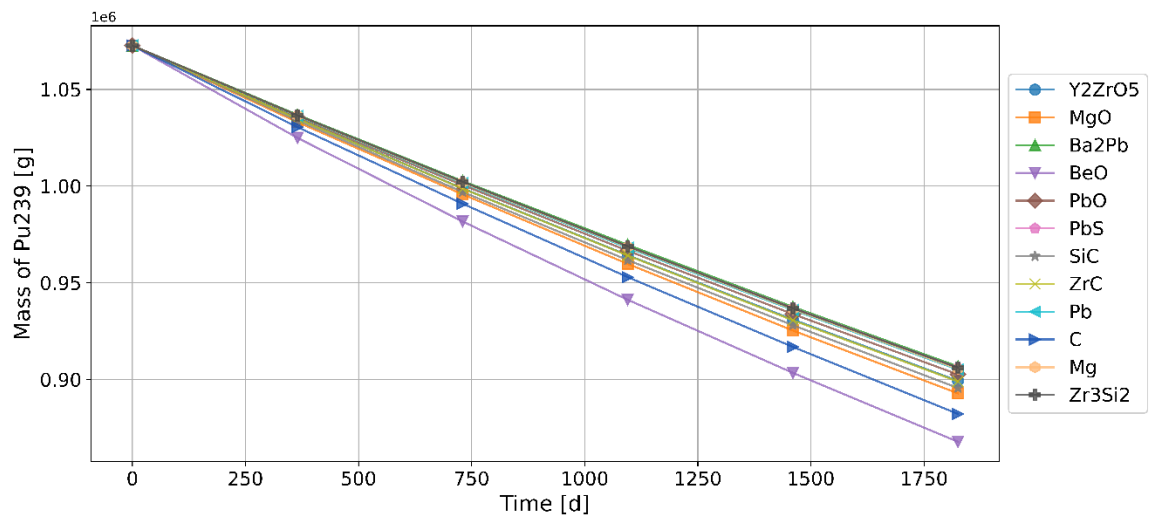


Fig. 4.41: Variation of Pu-239 across burnup time.

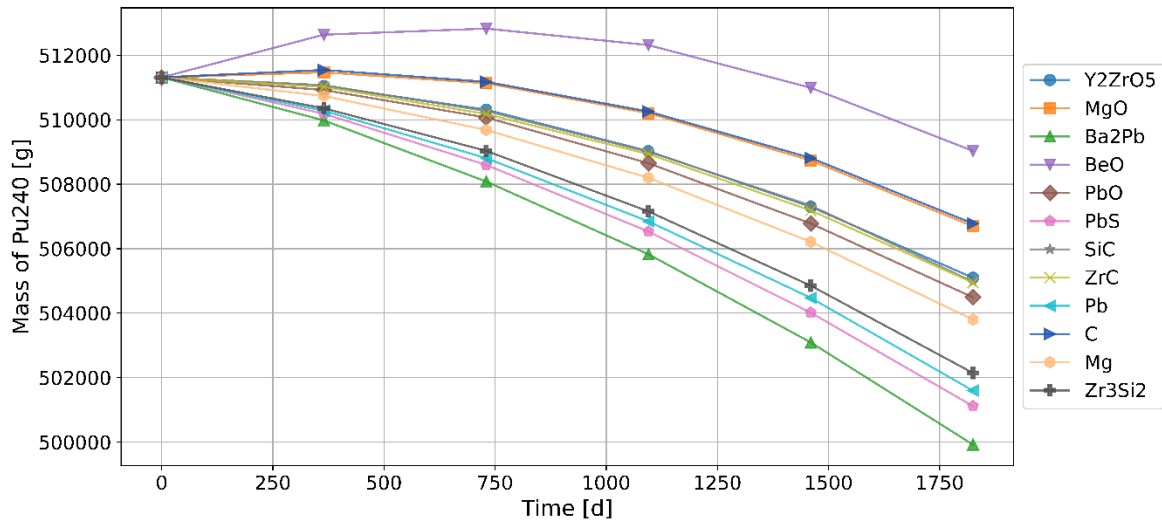


Fig. 4.42: Variation of Pu-240 across burnup time.

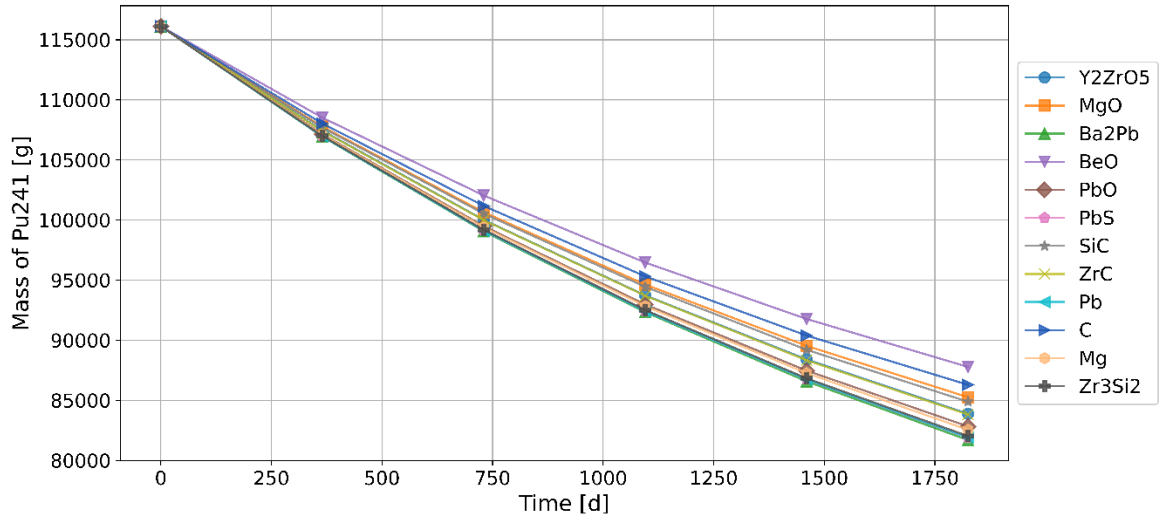


Fig. 4.43: Variation of Pu-241 across burnup time.

In the selected LFR model, the majority of the fuel consists of depleted uranium, with U-238 depletion primarily driven by fast fission and its conversion into other isotopes as a fertile material. Fig. 4.40 illustrates that BeO and Graphite exhibit a lower depletion rate for U-238 compared to other reflector materials, suggesting that neutron thermalization enhances the preservation of fertile material. In contrast, other reflectors promote a faster transmutation of U-238, highlighting their influence on the neutron spectrum and isotopic dynamics. Conversely, Pu-239, a fissile isotope critical to sustaining the chain reaction, exhibits the opposite trend. Comprising approximately 56% of the plutonium in the fuel, Pu-239 is depleted through fast fission, thermal fission (particularly near the reflectors),

and neutron capture ( $n,\gamma$ ) reactions forming Pu-240. Although a small fraction of U-238 is converted to Pu-239, Fig. 4.41 indicates that the burning rate significantly exceeds the breeding rate. Notably, BeO and Graphite exhibit a higher depletion rate compared to other reflectors, reflecting their influence on enhancing fission processes.

Initially, Pu-240 constitutes about 27% of the plutonium in the fuel, and its concentration trend is significantly influenced by the choice of reflector, more so than other isotopes analyzed. Fig. 4.42 reveals that BeO initially shows a slight increase in Pu-240, followed by a decrease, resulting in minimal overall variation after burnup. Similarly, Graphite and MgO exhibit very limited depletion of Pu-240, indicating preservation of this isotope. In contrast, Ba<sub>2</sub>Pb demonstrates the fastest depletion of Pu-240. Pu-241, another fissile isotope, is produced through the ( $n,\gamma$ ) reaction of Pu-240. Fig. 4.43 reveals a steady decrease in Pu-241 concentration across all reflectors, with BeO and Graphite exhibiting the lowest burning rates contrasting with the behavior of Pu-239 (Fig. 4.41), where these reflectors showed a higher depletion rate.

#### 4.2.7.2 Minor Actinides

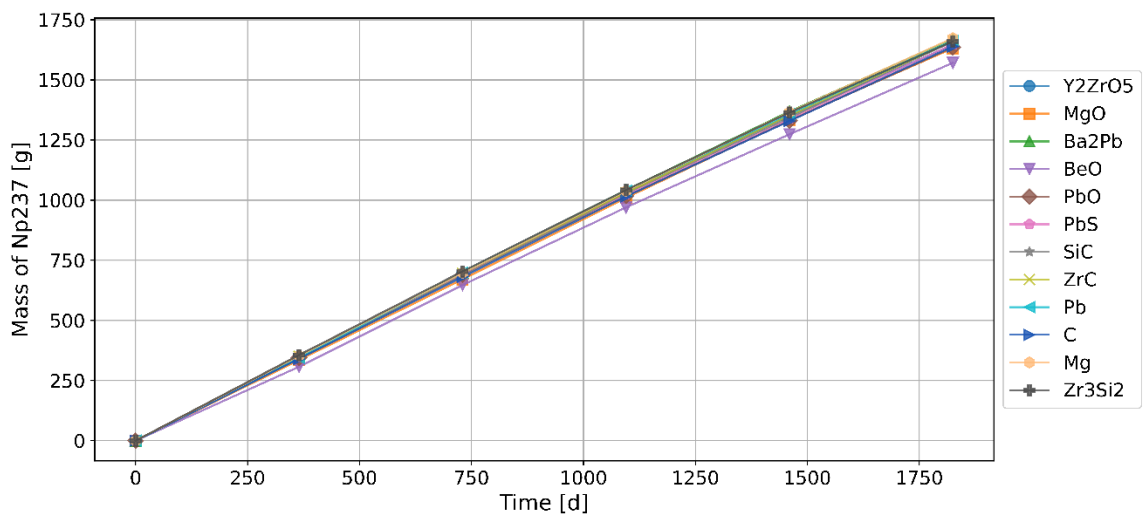


Fig. 4.44: Variation of Np-237 across burnup time.

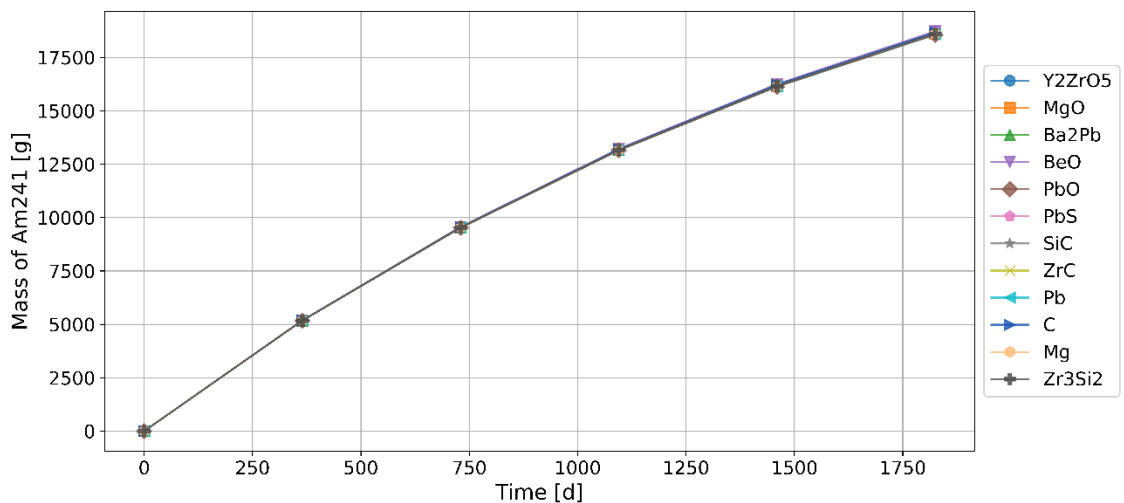


Fig. 4.45: Variation of Am-241 across burnup time.

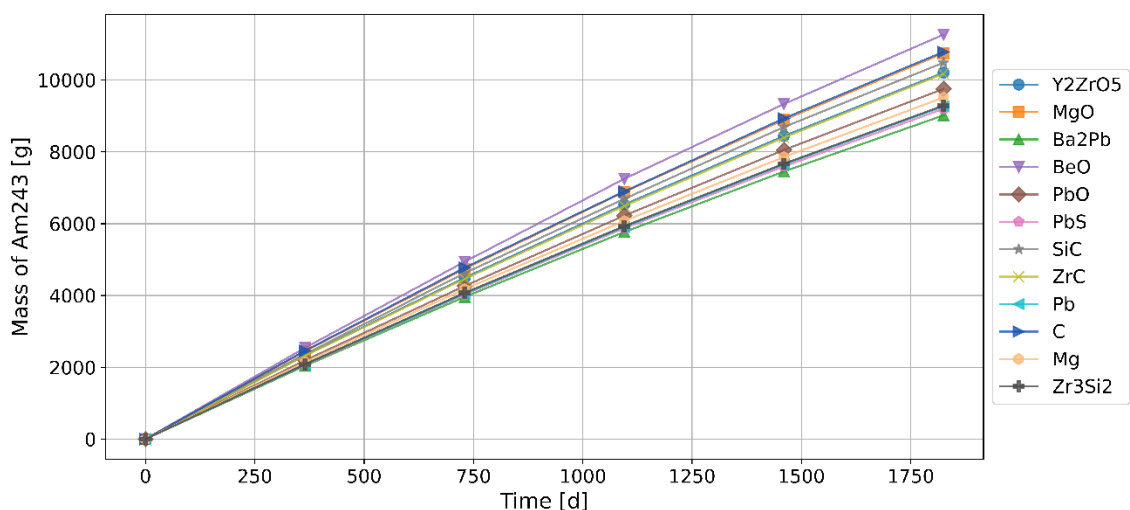


Fig. 4.46: Variation of Am-243 across burnup time.

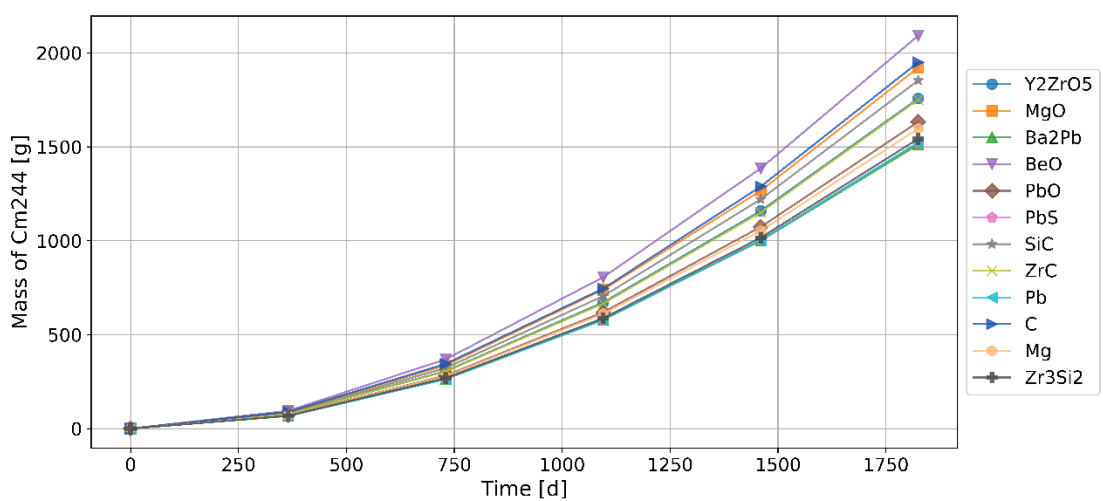


Fig. 4.47: Variation of Cm-244 across burnup time.

Fig. 4.44 to Fig. 4.47 illustrate the composition trends of minor actinides in the LFR model across the various reflector materials. Np-237, Am-241, Am-243, and Cm-244 all display increasing trends over the 1750-day period, reflecting their formation through neutron capture and decay processes. Am-241 production shows minimal variation across the reflectors, indicating consistent behavior. BeO exhibits a slightly lower increasing rate for Np-237 compared to others. In contrast, Am-243 and Cm-244 demonstrate noticeable variation, with reflectors such as BeO, MgO, Graphite and SiC showing enhanced production rates, suggesting a stronger influence on their accumulation.

### 4.3 MPRR Neutronics Analysis

After completion of the model, simulations were run, with different data, such as the effective multiplication factor ( $k_{\text{eff}}$ ), axial and radial neutron flux, power generation in each fuel assembly, burnup characteristics, reactivity coefficients, etc., from the neutronic perspective being collected as this data is tabulated then compared in the following sections.

Table 4.3: Neutronic parameters of the modeled MP RR core

Parameters	Calculated Values	Reference Values	Error (%)
$k_{\text{eff}}$	1.10693	1.107	0.0063
Average Neutron Flux (n/cm <sup>2</sup> -s)	5.8x10 <sup>14</sup>	5x10 <sup>14</sup>	17
Mean Power (MW)	0.283	0.278	1.77
Power Peaking Factor	1.197	—	—
Burnup Excess Reactivity at EOC (pcm)	1048	1039	0.86

### 4.3.1 Criticality Calculations

The effective multiplication factor ( $k_{\text{eff}}$ ) at the Beginning of Cycle (BOC) was evaluated using nuclear data library: ENDF/B-VIII.0. The table contains these data as well as the reference values taken from literature that used these specific data libraries.

Table 4.4: Effective multiplication factor (At BOC)

Calculated Value	Reference Value	Error in pcm
1.10693 (ENDF/B-VIII.0)	1.107 (ENDF/B-VII.0)	6

The findings indicate that the effective multiplication factor ( $k_{\text{eff}}$ ) is consistent with the reference value obtained from previous analyses using ENDF/B-VII.0, with the factor calculated using the ENDF/B-VIII.0 nuclear data library showing a minor deviation that is of only 6 pcm. This close agreement confirms that the simulation setup is reliable as well as supports using updated nuclear data in order to evaluate criticality in the MPRR core.

Minor  $k_{\text{eff}}$  differences may arise from variations among evaluated nuclear data files. These variations are observed when comparing reference data or modeling approaches. In this instance, the ENDF/B-VIII.0-based  $k_{\text{eff}}$  was at 1.10693, aligning well with the typical values that are reported for compact, fast-spectrum research reactor cores designed for applications involving high neutron flux. The ENDF/B-VIII.0 library's suitability in regard to accurately predicting reactor behavior within MPRR-type configurations is reinforced through such consistency. Also, the  $k_{\text{eff}}$  value calculation fits inside the range reported by similar reactor studies with deviations far below 50 pcm showing the computational model's robustness. For high-fidelity neutronic assessments, researchers must understand these small discrepancies. This understanding is important for reactor safety and performance in experimental and irradiation applications.

#### T-Test:

$$t = \frac{1.10693 - 1.107}{0.00053/\sqrt{100}} = -1.32$$

Degrees of freedom = 99, critical t-value  $\approx 1.984$ . Since  $|t| = 1.32 < 1.984$ , failed to reject  $H_0$ .

No significant difference was found between OpenMC  $k_{\text{eff}}$  value and benchmark  $k_{\text{eff}}$  value.

### 4.3.2 Neutron Flux

Fig. 4.48 visualizes the axial flux profile which is important because it has a direct impact on the reactor's heat distribution and neutron economy. As the core gets closer to the top, the neutron flux tends to drop. This phenomenon occurs due to the geometrical buckling in a reactor core.

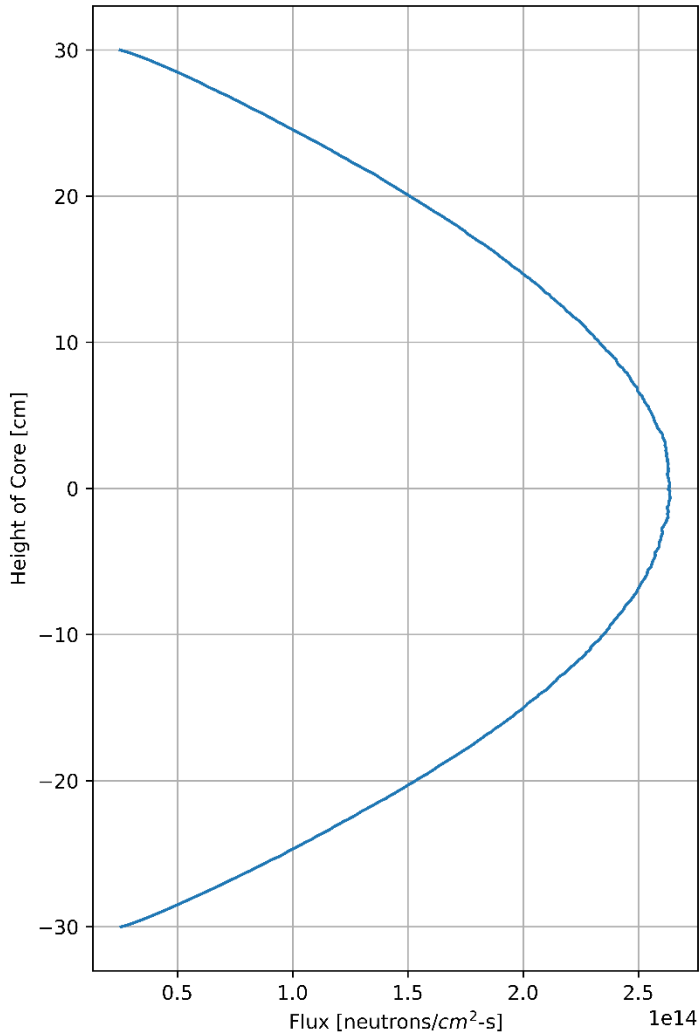


Fig. 4.48: Axial neutron flux profile.

The neutron flux varies radially from the center of the reactor core toward its outer edge, as illustrated in the radial flux distribution shown in Fig. 4.49, which represents the entire energy spectrum. Controlling the radial distribution of neutron flux is crucial for optimizing fuel utilization and coolant efficiency. Typically, the neutron flux reaches its peak near the core center and gradually decreases moving outward. The calculated average neutron flux is approximately  $4.8 \times 10^{14}$  neutrons/cm<sup>2</sup>·s. The maximum neutron flux obtained from the

simulation, normalized to practical units, is  $4.8 \times 10^{14}$  neutrons/cm<sup>2</sup>·s near the core center. This value closely matches the literature reference of  $5 \times 10^{14}$  neutrons/cm<sup>2</sup>·s, showing a small deviation of 4%.

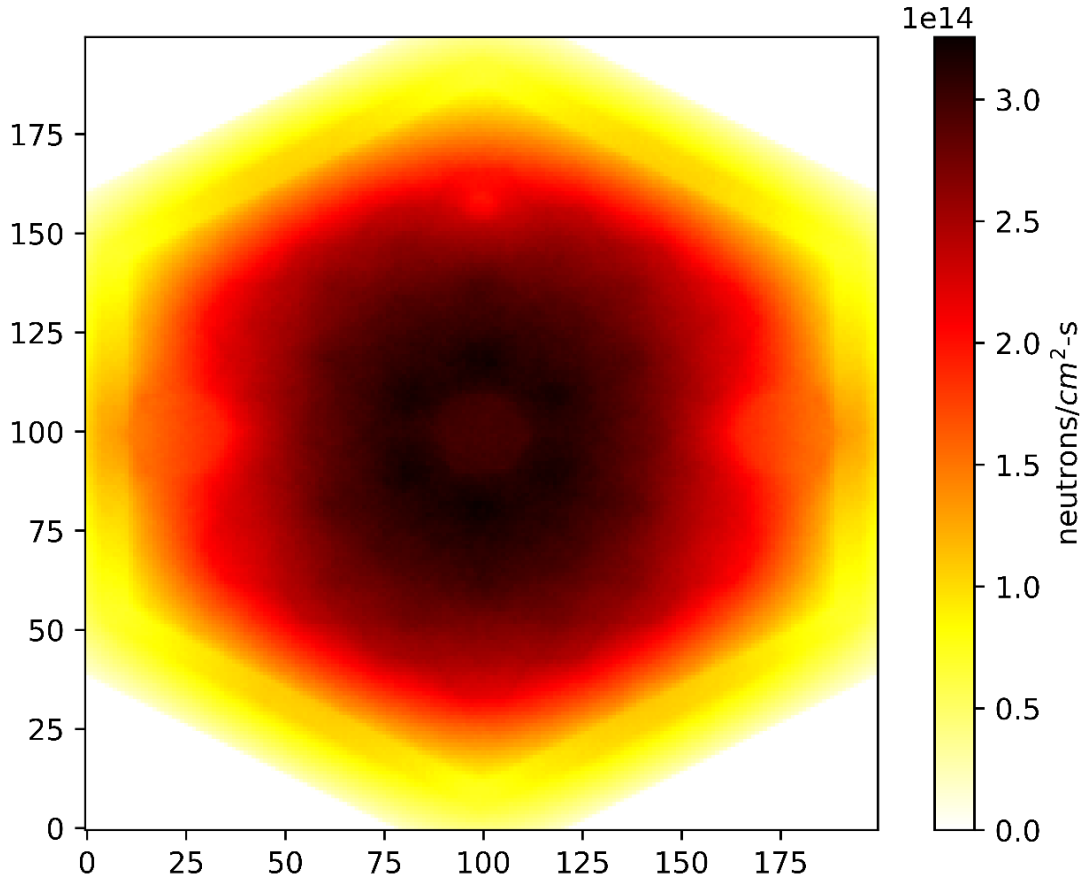


Fig. 4.49: Radial flux distribution of MPRR.

### 4.3.3 Power Distribution

The distribution of power among the fuel assemblies provides important insights into both local and overall reactor performance. Typically, a core power distribution map is presented as a 2D grid that reflects how power output varies with the position of each assembly. This allows us to identify whether power generation is uniform or if there are regions of underperformance or localized flux peaks.

Using the DistribCell feature in OpenMC, the power generated in each fuel assembly was calculated based on heating tallies. The resulting spatial distribution, illustrated in Fig. 4.49, highlights variations in power generation across the core. The highest power output, 0.339 MW, was observed near the shim rod region. This is likely due to localized neutron

moderation and absorption effects caused by the presence of the shim rods, which influence the neutron flux shape and can lead to increased power density in nearby fuel assemblies.

The calculated average power was 0.283 MW, which closely matches a previously reported value of 0.278 MW, showing a small deviation of 1.77%, indicating consistency with past results. The Power Peaking Factor (PPF), defined as the ratio of the maximum to the average power, was found to be 1.197, which reflects a reasonably balanced power distribution within the core.

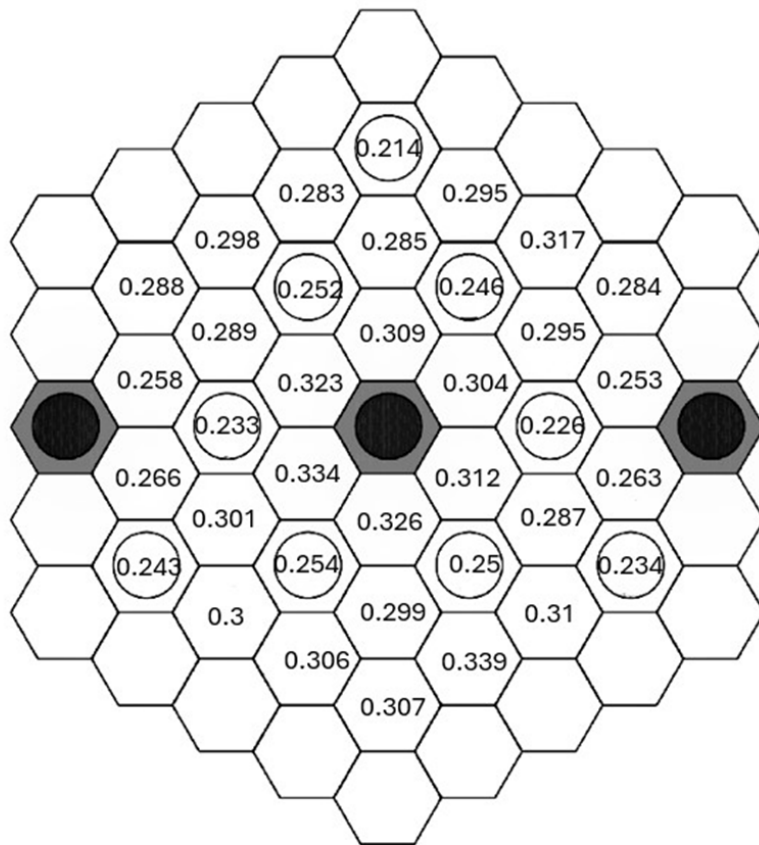


Fig. 4.50: Power (MW) for each fuel assembly.

Table 4.5: Power fraction in each assembly type

Assembly Type	Power Fraction
FA1	78.87%
ShR	14.52%
SR	4.51%
AR	2.1%

#### 4.3.4 Neutron Energy Spectrum

The neutron energy spectrum is a fundamental aspect in understanding the neutronic behavior of a research reactor, as it significantly influences reactivity, fuel utilization, and material irradiation capabilities. The Multipurpose Research Reactor (MPRR) operates as a thermal neutron reactor, utilizing light water as both the coolant and moderator. This design leads to efficient neutron moderation, resulting in a neutron spectrum that is dominated by thermal energies.

As shown in Fig. 4.51, the neutron flux is highest in the thermal energy region (below  $\sim 1$  eV), with a pronounced peak around 0.1 eV, indicating strong thermalization of neutrons. The flux then decreases through the epithermal region and remains relatively low in the fast energy range (above 100 keV). This confirms the thermal nature of the MPRR spectrum. While a small portion of fast neutrons remains due to fission and leakage effects, their contribution is minimal. This thermal spectrum is particularly suitable for applications such as neutron activation analysis, isotope production, and materials research, which rely on high thermal neutron availability.

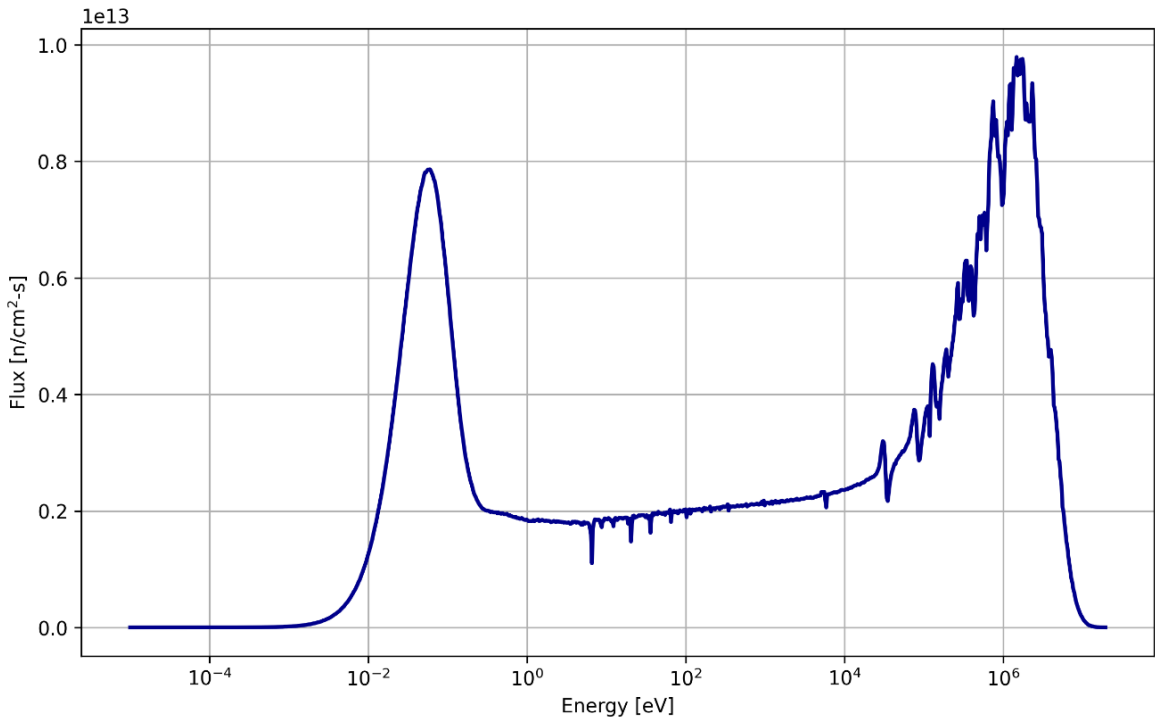


Fig. 4.51: Energy dependent neutron flux distribution spectrum.

#### 4.3.5 Fuel Burnup Results

Fig. 4.52 illustrates the depletion trend of the effective multiplication factor ( $k_{\text{eff}}$ ) for the Multipurpose Research Reactor (MPRR) over a 90-day period of operation.

At the beginning of the cycle, the reactor is highly reactive, with a  $k_{\text{eff}}$  value around 1.10, indicating a strong surplus of neutrons and excess reactivity. As the operation continues,  $k_{\text{eff}}$  steadily decreases, reaching approximately 1.003 by day 90. This decline is primarily due to the burnup of fissile fuel (such as U-235) and the accumulation of neutron-absorbing fission products like Xenon and Samarium. The initial decline is significantly sharper as an effect of these neutron poisons. The overall depletion reflects normal behavior for a thermal research reactor such as MPRR, where the reactivity margin is gradually consumed over time. The decreasing  $k_{\text{eff}}$  implies the reactor is approaching criticality ( $k_{\text{eff}} = 1$ ), after which it would need reshuffling or refueling to maintain continued operation.

This analysis is critical for core lifetime prediction, fuel cycle planning, and ensuring safe and efficient reactor performance throughout the irradiation period.

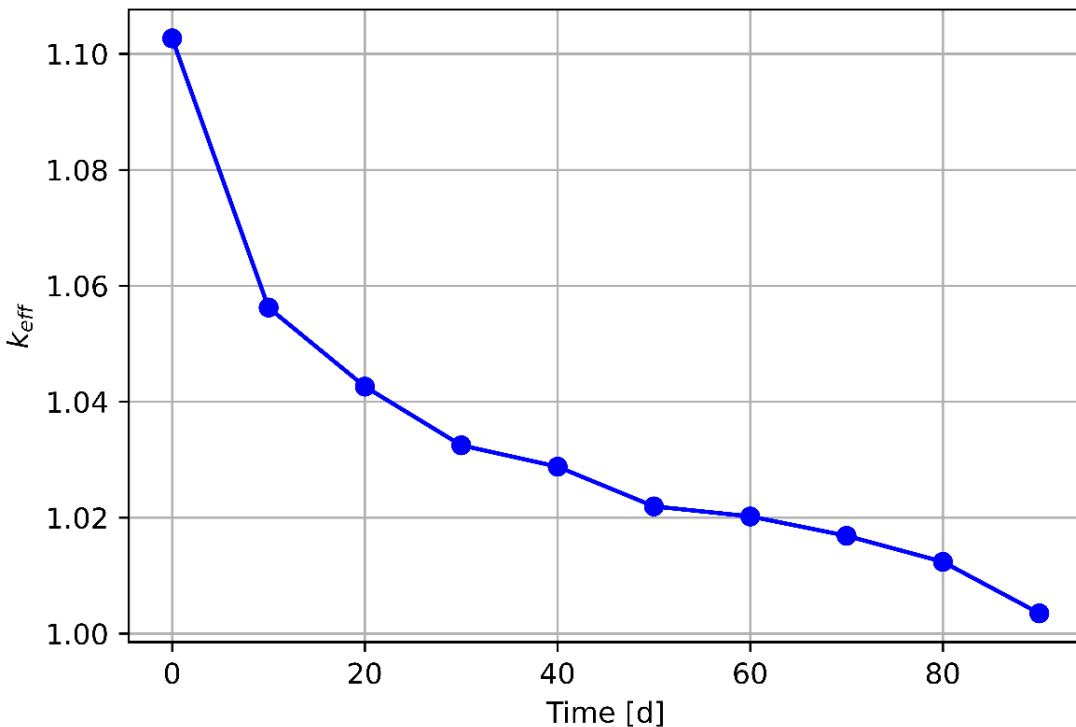


Fig. 4.52:  $k_{\text{eff}}$  as a function of burnup time.

Fig. 4.53 illustrates the nuclear fuel depletion and transmutation behavior over approximately 90 days of reactor operation in a multipurpose research reactor (MPRR). The figure shows a steady decrease in the number of U-235 atoms due to continuous fission reactions. As U-235 is the primary fissile material in the core, it undergoes neutron-induced fission when it captures thermal neutrons, releasing energy and neutrons that sustain the chain reaction:

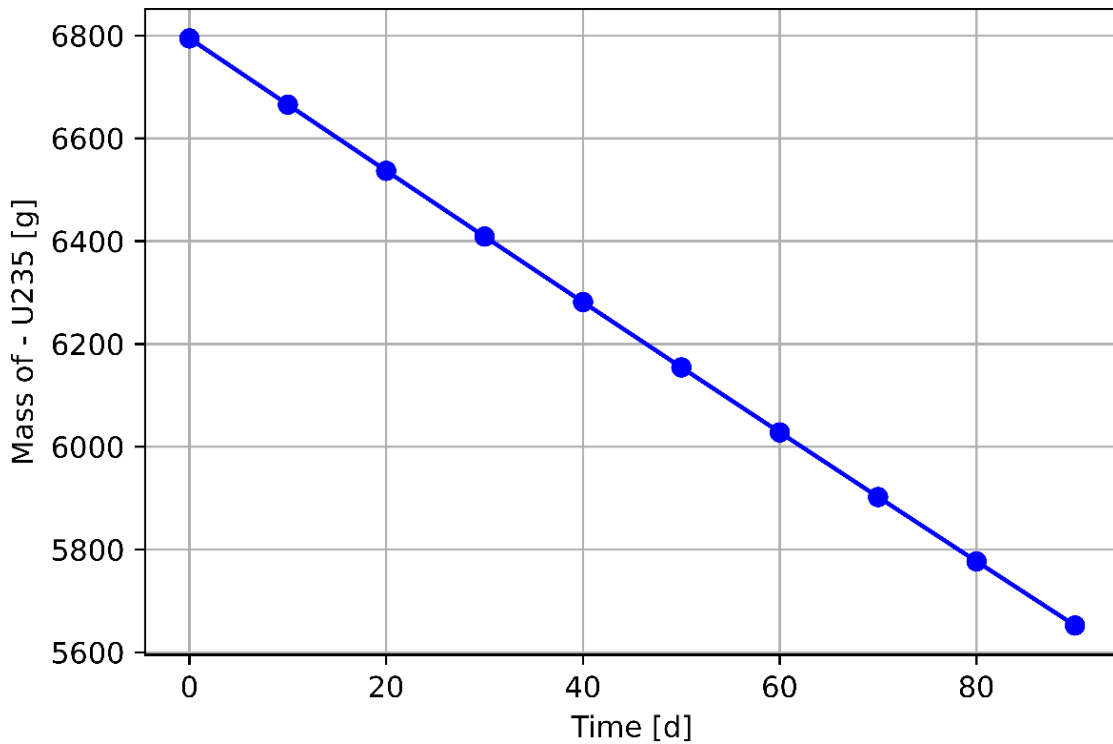


Fig. 4.53: U-235 concentration vs burnup time.

The behavior of  $^{135}\text{Xe}$  is very important for reactor control.  $^{135}\text{Xe}$  is a strong neutron absorber (a "neutron poison"). Its concentration builds up as a product of Uranium fission (through Tellurium-135 decay). The peak and subsequent decrease in  $^{135}\text{Xe}$  concentration can significantly impact the reactor's reactivity, potentially leading to operational challenges, especially during reactor startup or after power changes (a phenomenon known as Xenon Oscillations). In the beginning, the curve rises sharply. This indicates rapid production of  $^{135}\text{Xe}$ . The slope of the curve is steep and positive in this region. As time progresses, the curve continues to rise, but the rate of increase diminishes. The slope is still positive, but it decreases. This means that the production of  $^{135}\text{Xe}$  is still occurring, but it's being counteracted more and more by the processes that remove it (radioactive decay and

neutron absorption). Towards the end of the graph, the curve flattens out. The slope of the curve approaches zero. This indicates that the mass of  $^{135}\text{Xe}$  is reaching a stable value. At this point, the rate of production of  $^{135}\text{Xe}$  is nearly equal to the rate at which it is being removed. For the MPRR this equilibrium is reached after approximately 40-50 hours.

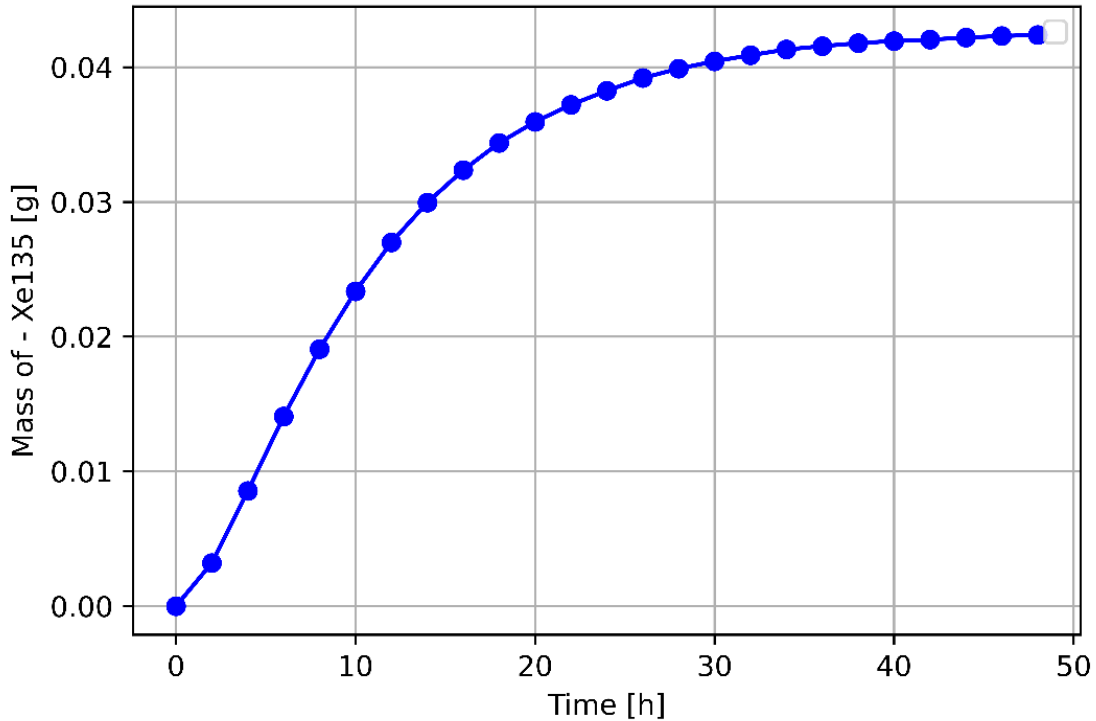
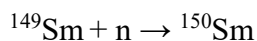


Fig. 4.54: Xe-135 concentration vs burnup time.

Fig. 4.55 depicts the buildup of Samarium-149 ( $^{149}\text{Sm}$ ), a significant neutron poison produced as a fission product. It forms through the decay of Neodymium-149 and Promethium-149.  $^{149}\text{Sm}$  accumulates quickly at first, but its growth slows as it also captures neutrons, eventually reaching an equilibrium where production and destruction rates are balanced.  $^{149}\text{Sm}$  is a strong neutron absorber and one of the fission products. It forms via:



$^{149}\text{Sm}$  absorbs neutrons (not fissile), acting as a neutron poison:



Initially,  $^{149}\text{Sm}$  accumulates rapidly due to continuous fission product decay. After  $\sim 20$  days, a saturation point is approached: the rate of production  $\approx$  rate of neutron absorption. This flattening indicates  $^{149}\text{Sm}$  equilibrium, common in long operation periods.

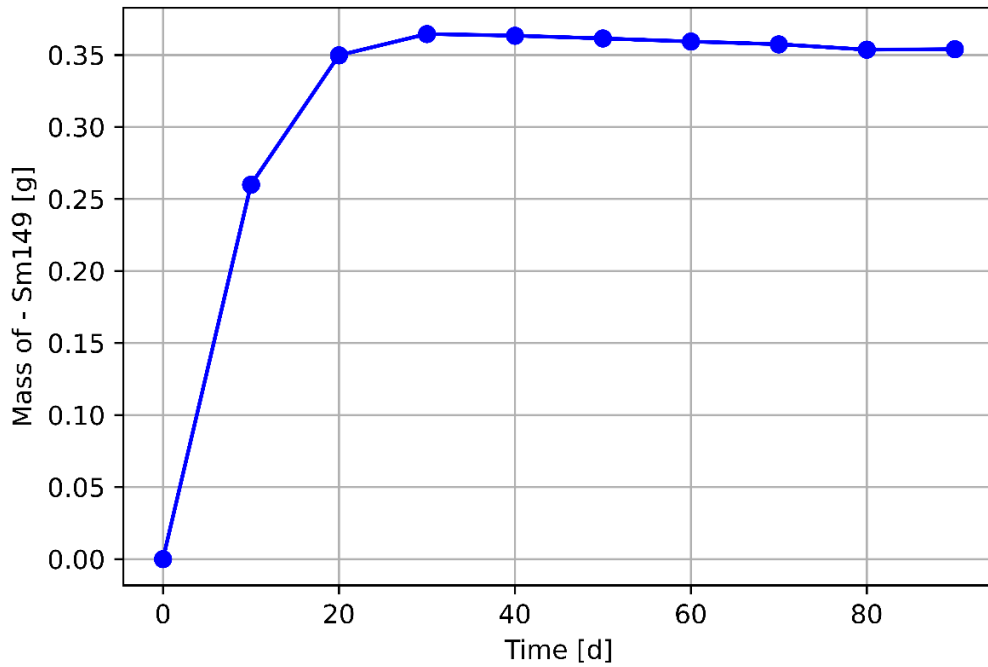
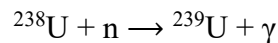


Fig. 4.55: Sm-149 concentration vs burnup time.

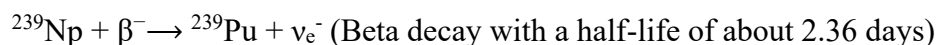
Fig. 4.56 shows a very gradual decline in the number of these  $^{238}\text{U}$  atoms over 90 days. While  $^{238}\text{U}$  itself isn't easily split (fissionable) by the slow-moving (thermal) neutrons that primarily drive the reactor, it plays a crucial role in the long-term fuel cycle. This indicates the consumption or transmutation of  $^{238}\text{U}$  within the reactor core. While  $^{238}\text{U}$  is not fissile with thermal neutrons, it can undergo neutron capture to become Plutonium-239, which is fissile.



In this reaction, a  $^{238}\text{U}$  nucleus captures a neutron and becomes Uranium-239, releasing a gamma ray ( $\gamma$ ) in the process. However,  $^{239}\text{U}$  is unstable and undergoes a series of radioactive decays:



The Uranium-239 emits a beta particle ( $\beta^-$ ) and an antineutrino ( $\nu_e^-$ ) to transform into Neptunium-239. Neptunium-239 is also unstable:



The Neptunium-239 then emits another beta particle and antineutrino, becoming Plutonium-239.

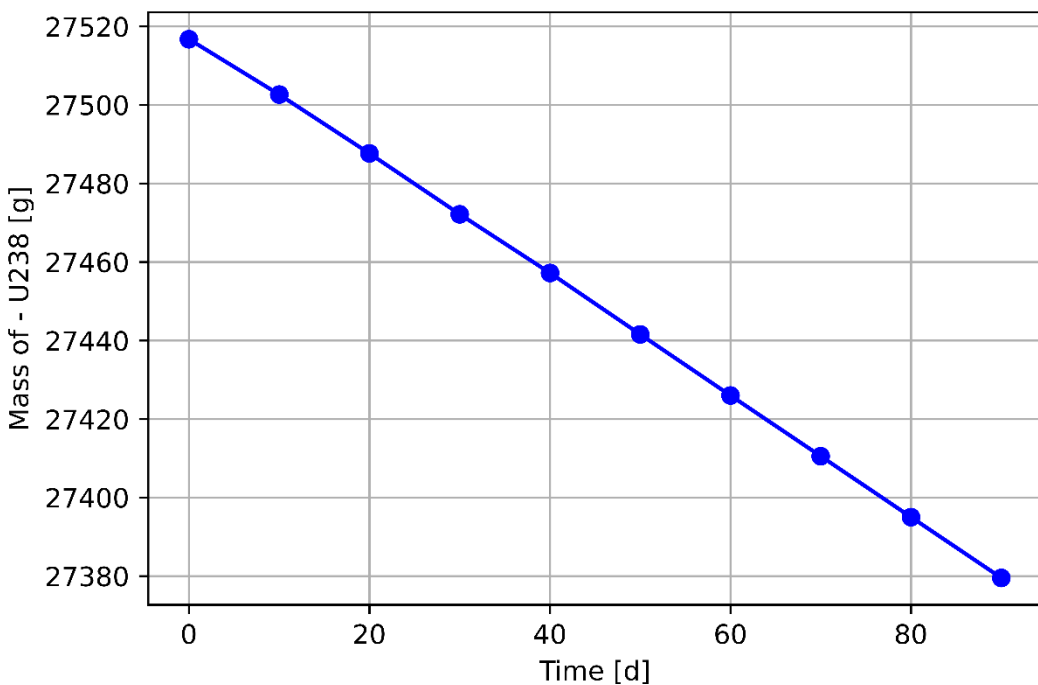
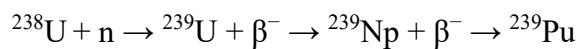


Fig. 4.56: U-238 concentration vs burnup time.

Fig. 4.57 shows the progressive increase in Plutonium-239 (Pu-239), formed via neutron capture by U-238 followed by two beta decays. As U-238 is fertile rather than fissile, it does not fission directly but breeds Pu-239, which is a fissile material and can contribute to the reactor's power generation in later stages. Pu-239 is bred from U-238 through neutron capture:



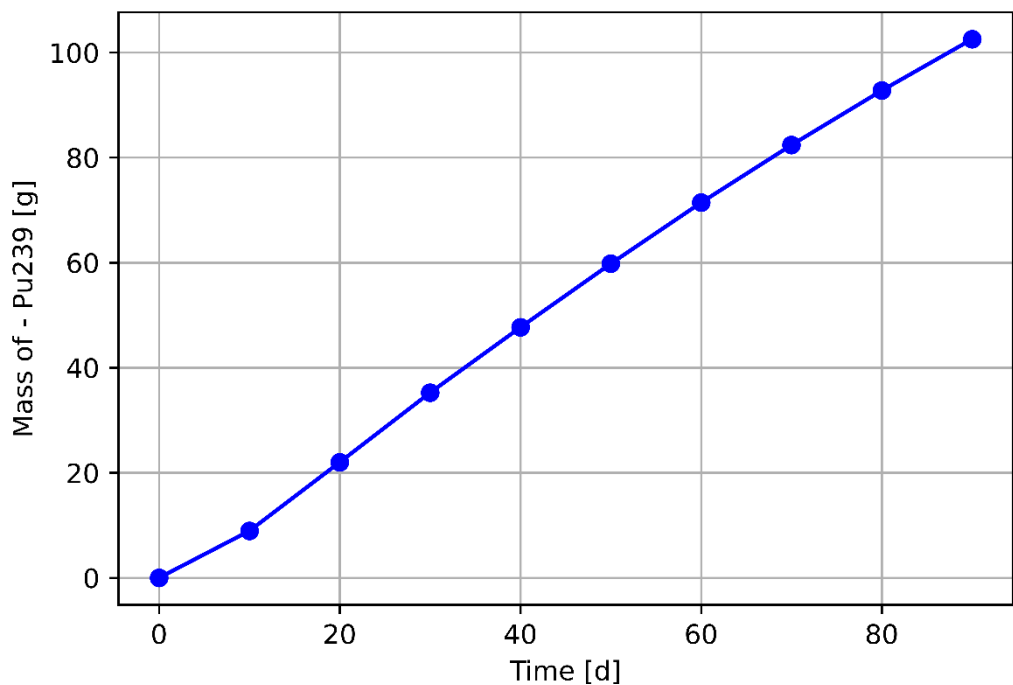


Fig. 4.57: Pu-239 concentration vs burnup time.

## CHAPTER 5

### CONCLUSION AND FUTURE PERSPECTIVES

#### 5.1 Summary of Key Findings

This study conducted a comprehensive neutronics analysis of the Advanced Lead-cooled Fast Reactor European Demonstrator (ALFRED) and a conceptual Multi-Purpose Research Reactor (MPRR) for Bangladesh, focusing on reactor physics, burnup characteristics, and material interactions using OpenMC Monte Carlo simulations. For ALFRED, the neutronics analysis (Section 4.1) revealed a  $k_{\text{eff}}$  of 1.07803 at the beginning of cycle (BOC), aligning closely with the reference value of 1.07767 (error of 0.054%), confirming the reliability of the simulation setup. The power peaking factor (PPF) was 1.276, indicating a balanced power distribution, while the control rod worth of -8650 pcm matched literature values with a 1.76% error, underscoring ALFRED's robust reactivity control. Burnup analysis over 1820 days showed a  $k_{\text{eff}}$  decline, with criticality ( $k_{\text{eff}} = 1$ ) reached at 1041 days for lead coolant and 1094 days for LBE, highlighting coolant impacts on cycle length. Isotopic depletion trends (Section 4.1.6) indicated significant Pu-241 reduction (to 0.70–0.73 of initial mass), with U-238 depleting more slowly, supporting sustainability through reduced actinide accumulation. Actinide production (Section 4.1.7) revealed higher yields in MOX2 fuel, with Am-241 2.9 times higher than MOX1, posing waste management challenges. Coolant activation (Section 4.1.8) highlighted significant Po-210 production in LBE (1 kg vs. 0.089g in lead), emphasizing radiological safety concerns.

Reflector material analysis for ALFRED (Section 4.2) identified BeO as the most effective under vacuum boundary conditions, achieving the highest  $k_{\text{eff}}$  (1.11189) and lowest leakage (18.512%), ideal for neutron retention in realistic scenarios. BeO also excelled under reflective conditions ( $k_{\text{eff}}$  1.25955, leakage 4.029%) and offered the longest cycle length (1232.69 days), though its thermalization increased peripheral fission rates (thermal fission fraction 1.89%). ZrC and Yttria-Zirconia (baseline) showed strong performance under vacuum conditions, with  $k_{\text{eff}}$  values of 1.07795 and 1.07884, and leakage rates of 19.904% and 20.178%, respectively, making ZrC, a viable alternative. Graphite and MgO also demonstrated favorable neutron economy, with cycle lengths of 1152.39 and 1142.16 days, respectively. However, Ba<sub>2</sub>Pb underperformed under vacuum conditions ( $k_{\text{eff}}$  1.06134, leakage 24.887%), despite its modest reflective performance ( $k_{\text{eff}}$  1.20846, leakage 9.578%).

For the MPRR, the neutronics analysis (Section 4.3) yielded a  $k_{\text{eff}}$  of 1.10693 at BOC using the ENDF/B-VIII.0 library, consistent with the reference value of 1.107 (error of 6 pcm), validating the model. The average neutron flux was  $5.8 \times 10^{14}$  neutrons/cm $^2$ ·s, peaking at  $4.8 \times 10^{14}$  neutrons/cm $^2$ ·s near the core center, with a 4% deviation from the reference ( $5 \times 10^{14}$  neutrons/cm $^2$ ·s), confirming its suitability for research applications. Power distribution analysis indicated an average power of 0.283 MW per assembly, with a peak of 0.339 MW near the shim rod region, resulting in a PPF of 1.197, reflecting uniform power distribution. The neutron spectrum, peaking at 0.1 eV, confirmed the MPRR's thermal reactor design, ideal for isotope production and neutron scattering. Burnup analysis over 90 days showed a  $k_{\text{eff}}$  decline to 1.003, driven by U-235 depletion and the buildup of neutron poisons like Xe-135 and Sm-149. Xe-135 reached equilibrium after 40–50 hours due to its high neutron absorption cross-section, while Sm-149 saturated after approximately 20 days, balancing production and destruction rates. U-238 exhibited a gradual decline, with neutron capture leading to increased Pu-239 production over time, contributing to long-term reactivity. The excess reactivity at the end of cycle (EOC) was 1048 pcm, aligning closely with the reference value of 1039 pcm (0.86% error). These findings collectively underscore the distinct neutronic behaviors of fast (ALFRED) and thermal (MPRR) reactors, providing insights into their operational and safety characteristics.

## 5.2 Evaluation

### 5.2.1 Evaluation Against Objectives

The primary objectives outlined in Section 1.2 were to evaluate neutronics parameters, burnup characteristics, and reflector effects for ALFRED, and to analyze neutronics and depletion for the MPRR. For ALFRED, Objective 1 (evaluating  $k_{\text{eff}}$ , flux, power peaking, and reactivity feedback) was met, with  $k_{\text{eff}}$  (1.07803), maximum neutron flux ( $2.716 \times 10^{15}$  neutrons/cm $^2$ ·s), and PPF (1.276) aligning with literature values (Table 4.2). Reactivity swing (-2530 pcm) matched the reference (-2580 pcm) within 1.94% error, confirming accurate feedback modeling. Objective 2 (burnup analysis) was achieved through a 5-year simulation, revealing isotopic depletion trends (e.g., Pu-241's significant reduction) and coolant effects (Section 4.1.6), with cycle lengths varying by coolant type (1041 days for

lead, 1094 days for LBE). Objective 3 (reflector analysis) was fulfilled by comparing 12 materials (Section 4.2), identifying BeO’s superior neutron retention under vacuum conditions and its cycle length advantage, though thermalization effects require further consideration. ZrC and Yttria-Zirconia emerged as viable alternatives, while Ba<sub>2</sub>Pb’s poor performance under vacuum conditions highlights the importance of axial leakage considerations.

For the MPRR, Objective 1 (neutronics parameters) was fully met with  $k_{\text{eff}}$  (1.10693), average flux ( $5.8 \times 10^{14}$  neutrons/cm<sup>2</sup>·s, peaking at  $4.8 \times 10^{14}$  neutrons/cm<sup>2</sup>·s), and control rod worth (-2649 pcm) calculated, showing excellent agreement with references (e.g.,  $k_{\text{eff}}$  error of 6 pcm). The power peaking factor (1.197) and thermal neutron spectrum (peak at 0.1 eV) further validate the model’s accuracy for a research reactor design. Objective 2 (burnup and depletion) was comprehensively addressed, with  $k_{\text{eff}}$  decreasing to 1.003 over 90 days due to U-235 depletion and the buildup of Xe-135 and Sm-149, which equilibrated after 40–50 hours and ~20 days, respectively. The increasing Pu-239 production from U-238 neutron capture highlights the reactor’s long-term reactivity behavior. The excess reactivity at EOC (1048 pcm) matched the reference (1039 pcm) within 0.86% error, confirming the reliability of the burnup analysis. With the completion of Section 4.3, the MPRR’s objectives are now fully met, and the results align with expectations for a thermal research reactor, supporting Bangladesh’s goals for nuclear research and isotope production.

### 5.2.2 Assessment of Research Questions and Hypothesis Test

The research questions outlined in Section 1.4.1 were addressed through the neutronics analyses. For ALFRED, key parameters ( $k_{\text{eff}}$  1.07803, flux  $2.716 \times 10^{15}$  neutrons/cm<sup>2</sup>·s) aligned with benchmarks with negligible error, answering Question 1. Burnup trends (1041-1094 days cycle length, Pu-241 reduction to 0.70-0.73) and Am-241 production clarified fuel cycle sustainability (Question 2). Reflector comparisons identified BeO’s superior  $k_{\text{eff}}$  of 1.11189 and cycle length of 1232.69 days, addressing Question 3, while LBE’s 1 kg Po-210 production highlighted safety concerns (Question 4). For MPRR, neutronics parameters ( $k_{\text{eff}}$  1.10693, flux  $5.8 \times 10^{14}$  neutrons/cm<sup>2</sup>·s) supported Question 1, burnup showed U-235 depletion, Xe-135 and Sm-149 equilibrium (Question 2), and the 0.1 eV spectrum peak confirmed research suitability (Question 3).

Hypothesis tests were done using the t-test method for ALFRED in Section 4.1.1 and for MPRR in Section 4.3.1 for their respective  $k_{\text{eff}}$  values. The null hypothesis was not rejected, thus indicating no significant statistical difference between OpenMC  $k_{\text{eff}}$  results (1.07803 for ALFRED, 1.10693 for MPRR) and benchmark values (1.07767 for ALFRED, 1.107 for MPRR).

### 5.3 Implications for Reactor Design and Safety

The findings have significant implications for the design and safety of both ALFRED and MPRR. For ALFRED, reflector selection critically impacts neutron economy and cycle length. BeO's low leakage (18.512%) under vacuum conditions enhances criticality, making it a strong candidate for operational scenarios, while its extended cycle length (1232.69 days) improves fuel utilization. However, its high thermal fission fraction (1.89%) and thermalization at the periphery (Section 4.2.3) could lead to power peaking concerns, necessitating careful core design. ZrC with leakage rate of 19.904% under vacuum condition, offer balanced alternative for neutron retention. In contrast, Ba<sub>2</sub>Pb's high leakage (24.887%) and short cycle length (821.23 days) may increase refueling frequency, making it less suitable. The significant Po-210 production in LBE coolant (1 kg, contributing 0.15 MW decay heat) underscores the need for advanced filtration systems to mitigate radiological risks, as noted in Section 4.1.8. Actinide production (Section 4.1.7), particularly Am-241's 2.9-fold increase in MOX2, highlights waste management challenges, though slower U-238 depletion (Section 4.2.7.1) supports sustainability goals by reducing long-lived actinide accumulation.

For the MPRR, the thermal spectrum with a peak flux at 0.1 eV (Section 4.3.4) is well-suited for isotope production and neutron scattering, aligning with Bangladesh's goals for medical and research applications. The uniform power distribution (PPF 1.197) ensures efficient heat removal, enhancing safety for a 10 MW reactor. The control rod worth of -2649 pcm provides sufficient shutdown margins, ensuring reactivity control during operation. However, the burnup analysis (Section 4.3.5) indicates that Xe-135 and Sm-149 buildup significantly impacts reactivity, particularly during startup or power changes, necessitating careful monitoring to prevent oscillations. The gradual Pu-239 production from U-238 suggests potential for extended operation but requires attention to long-term fuel management. The use of VVR-KN fuel supports non-proliferation standards, but its

hexagonal geometry requires precise modeling for accurate flux predictions, as noted in Section 2.3.3. These insights contribute to safer and more efficient reactor designs, addressing Gen-IV goals for ALFRED and Bangladesh’s nuclear research ambitions for MPRR.

#### 5.4 Recommendations for Future Research

Several avenues for future research emerge from this study. For ALFRED, experimental validation of OpenMC simulations against benchmark data (as planned in Section 1.3.3) is essential to confirm reflector performance, particularly for BeO and ZrC. Transient analyses, such as Unprotected Loss of Flow (ULOF) and Unprotected Transient OverPower (UTOP), should be explored to assess dynamic behavior, building on the steady-state results in Section 4.1. The significant Po-210 production in LBE (Section 4.1.8) warrants further investigation into filtration systems, potentially integrating computational and experimental approaches to quantify cover gas release risks. Additionally, thermal-hydraulic coupling, excluded in this study (Section 1.4), should be incorporated to evaluate temperature feedbacks on neutronics, especially for reflectors like BeO that induce thermalization.

For the MPRR, the completed neutronics analysis (Section 4.3) provides a strong foundation, but further studies are recommended to enhance its design. Detailed investigations into Xe-135 and Sm-149 buildup effects on reactivity control, particularly during transient scenarios like startup or shutdown, are necessary to optimize operational strategies. Validation using multiple codes (e.g., Serpent alongside OpenMC) would enhance model reliability, addressing the research gap noted in Section 2.3.3. Scaling the MPRR design to 10–20 MW, as proposed by Bangladesh, requires further neutronics and thermal-hydraulic studies to ensure safety and compliance with international standards, particularly focusing on flux distribution ( $5.8 \times 10^{14}$  neutrons/cm<sup>2</sup>·s) and power peaking (PPF 1.197) at higher power levels. Experimental validation of the VVR-KN fuel’s long-term burnup behavior, including Pu-239 production trends, is critical for ensuring fuel integrity and safety over extended cycles. Finally, material degradation effects (e.g., radiation damage in reflectors or fuel assemblies), excluded in this study (Section 1.4), should be investigated for both reactors to assess long-term operational integrity.

## **5.5 Final Remarks**

This thesis provides a foundational neutronics analysis of ALFRED and a conceptual MPRR, contributing valuable insights into fast and thermal reactor systems. The study highlights the trade-offs in reflector selection for ALFRED and confirms the MP RR's suitability for Bangladesh's nuclear research goals, aligning with Gen-IV sustainability objectives and global non-proliferation standards. These findings pave the way for future design optimizations and safety enhancements in nuclear engineering.

## REFERENCES

- Alemberti, A. and Mansani, L., 2013. The Advanced Lead Fast Reactor European Demonstrator (ALFRED). In: Proceedings of the International Conference on NURETH 15, Pisa, Italy, 12–17 May.
- Arinkin, F.M., Shaimerdenov, A.A., Gizatulin, S.K., Dyusambaev, D.S., Koltchnik, S.N., Chakrov, P.V. and Chekushina, L.V., 2017. Core conversion of VVR-K research reactors. *Atomic Energy*, 123(1), pp.17–24. Available at: <https://doi.org/10.1007/s10512-017-0294-0>.
- Blanchet, D. and Fontaine, B., 2017. Reflector and protections in a sodium-cooled fast reactor: modelling and optimization. *EPJ Web of Conferences*, 153, 05006. Available at: <https://doi.org/10.1051/epjconf/201715305006>.
- Brown, D.A., Chadwick, M.B., Capote, R., Kahler, A.C., Trkov, A., Herman, M.W., Sonzogni, A.A., Danon, Y., Carlson, A.D., Dunn, M., Smith, D.L., Hale, G.M., Arbanas, G., Arcilla, R., Bates, C.R., Beck, B., Becker, B., Brown, F., Casperson, R.J., Conlin, J., Cullen, D.E., Descalle, M.-A., Firestone, R., Gaines, T., Guber, K.H., Hawari, A.I., Holmes, J., Johnson, T.D., Kawano, T., Kiedrowski, B.C., Koning, A.J., Kopecky, S., Leal, L., Lestone, J.P., Lubitz, C., Márquez Damián, J.I., Mattoon, C.M., McCutchan, E.A., Mughabghab, S., Navratil, P., Neudecker, D., Nobre, G.P.A., Noguere, G., Paris, M., Pigni, M.T., Plompen, A.J., Pritychenko, B., Pronyaev, V.G., Roubtsov, D., Rochman, D., Romano, P., Schillebeeckx, P., Simakov, S., Sin, M., Sirakov, I., Sleaford, B., Sobes, V., Soukhovitskii, E.S., Stetcu, I., Talou, P., Thompson, I., van der Marck, S., Welser-Sherrill, L., Wiarda, D., White, M., Wormald, J.L., Wright, R.Q., Zerkle, M., Žerovník, G. and Zhu, Y., 2018. ENDF/B-VIII.0: The 8th Major Release of the Nuclear Reaction Data Library with CIELO-project Cross Sections, New Standards and Thermal Scattering Data. *Nuclear Data Sheets*, 148, pp.1-142. Available at: <https://doi.org/10.1016/j.nds.2018.02.001>. Cacuci, D.G. (ed.), 2010. *Handbook of nuclear engineering*. New York, NY: Springer. Available at: <https://doi.org/10.1007/978-0-387-98149-9>.
- Ciurluini, C., Narcisi, V., Giannetti, F., Cretara, L. and Caruso, G., 2020. Preliminary neutron kinetic – thermal hydraulic coupled analysis of the ALFRED reactor using PHISICS/RELAP5-3D. *Journal of Physics: Conference Series*, 1599(1), 012023. Available at: <https://doi.org/10.1088/1742-6596/1599/1/012023>.
- Di Lecce, F., Aufiero, M., Lorenzi, S., Saracco, P. and Alemberti, A., 2020. Coarse-mesh thermal-hydraulics and neutronics coupling for the ALFRED reactor. *The European Physical Journal Plus*, 135(2), p.221. Available at: <https://doi.org/10.1140/epjp/s13360-020-00228-8>.
- El-Alem, M. and Abdel-Latif, A., 2024. The MOX fuel performance analysis of ALFRED core using MCNPX transport code. *Fayoum University Journal of Engineering*, 7(2), pp.272–277. Available at: <https://doi.org/10.21608/fuje.2024.344952>.

- Framatome, 2023. Framatome completes first fuel element for the U.S. TRIGA research reactors. [Press release]. 7 March. Available at: <https://www.framatome.com/medias/download/?id=15082&n=framatome-completes-first-fuel-element-for-the-us-triga-research-reactors>.
- Ganjaroodi, S.Z. and Zarifi, E., 2023. Neutronic investigation of ALFRED lead-cooled fast reactor core using Monte Carlo modeling. *Atomic Energy*, 134(3), pp.264–274. Available at: <https://doi.org/10.1007/s10512-024-01054-2>.
- Generation IV International Forum, 2014. Technology roadmap update for Generation IV nuclear energy systems. [Online]. Available at: [https://www.gen-4.org/gif/jcms/c\\_9260/public](https://www.gen-4.org/gif/jcms/c_9260/public) [Accessed 18 May 2025].
- Grasso, G., Petrovich, C., Mattioli, D., Artioli, C., Sciora, P., Gugiu, D., Bandini, G., Bubelis, E. and Mikityuk, K., 2014. The core design of ALFRED, a demonstrator for the European lead-cooled reactors. *Nuclear Engineering and Design*, 278, pp.287–301. Available at: <https://doi.org/10.1016/j.nucengdes.2014.07.032>.
- Guo, H., Jin, X., Feng, K. and Gu, H., 2021. Alternative absorber materials for control rods in ALFRED. In: International Conference on Nuclear Engineering, Volume 1: Operating Plant Challenges, Successes, and Lessons Learned; Nuclear Plant Engineering; Advanced Reactors and Fusion; Small Modular and Micro-Reactors Technologies and Applications, V001T03A001. Available at: <https://doi.org/10.1115/ICONE28-61123>.
- Hanan, N.A. and Garner, P.L., 2015. Neutronic, steady-state, and transient analyses for the Kazakhstan VVR-K reactor with LEU fuel: ANL independent verification results. Available at: <https://doi.org/10.2172/1214274>.
- Hartanto, D. and Kim, Y., 2015. Alternative reflectors for a compact sodium-cooled breed-and-burn fast reactor. *Annals of Nuclear Energy*, 76, pp.113–124. Available at: <https://doi.org/10.1016/j.anucene.2014.09.048>.
- Hartanto, D., Alhamad, S., Mahmoud, K., Kurdi, N. and Zubair, M., 2020. Neutronics design study of an advanced lead-cooled modular nuclear reactor (ALMANAR). *International Journal of Nuclear Energy Science and Technology*, 14(1), pp.1–14.
- Hong, B.T., Mai Vu, T. and Hartanto, D., 2023. Preliminary study on alternative reflectors for LOTUS reactor. *VNU Journal of Science: Mathematics - Physics*, 39(2). Available at: <https://doi.org/10.25073/2588-1124/vnumap.4791>.
- Ibrahim, M., Ibrahim, A., Aziz, M., Saudi, H.A. and Hassaan, M., 2021. Comparative neutronic study for heterogeneous and homogeneous fuel assembly in a lead-cooled fast reactor. *IOP Conference Series: Materials Science and Engineering*, 1171, 012009. Available at: <https://doi.org/10.1088/1757-899X/1171/1/012009>.
- International Atomic Energy Agency, Research reactor fuel cycle. [Online]. Available at: <https://www.iaea.org/topics/research-reactor-fuel-cycle> [Accessed 19 May 2025].
- International Atomic Energy Agency, 2022. Research reactors: purpose and future (IAEA Technical Report Series No. 982). Vienna: International Atomic Energy Agency.

- International Atomic Energy Agency, 2023. Application of the concept of exemption (IAEA Safety Standards Series No. GSG-17). Vienna: International Atomic Energy Agency. Available at: <https://www.iaea.org/publications/15477/application-of-the-concept-of-exemption>.
- Islam, S. and Ahmed, M.T., 2025. Alternative core configurations analysis to improve the neutronics performance of modular gas cooled fast reactor. *Annals of Nuclear Energy*, 211, 110951. Available at: <https://doi.org/10.1016/j.anucene.2024.110951>.
- Lewis, E.E., 2008. Fundamentals of nuclear reactor physics. Boston, MA: Academic Press. Available at: <https://doi.org/10.1016/B978-0-12-370631-7.X0001-0>.
- Lodi, F., Grasso, G., Cammi, A., Lorenzi, S., Petrovich, C., Mattioli, D. and Sumini, M., 2015. Characterization of the new ALFRED core configuration. Report number: ADPFIISS-LP2-085 Rev. 0.
- Luzzi, L., Cammi, A., Di Marcello, V., Lorenzi, S., Pizzocri, D. and Van Uffelen, P., 2014. Application of the TRANSURANUS code for the fuel pin design process of the ALFRED reactor. *Nuclear Engineering and Design*, 277, pp.173–187. Available at: <https://doi.org/10.1016/j.nucengdes.2014.06.032>.
- Macdonald, R. and Driscoll, M.J., 2010. Magnesium oxide: an improved reflector for blanket-free fast reactors. In: *Transactions of the American Nuclear Society*, 102, pp.488–489.
- Mao, L., Dang, T., Pan, L., Zeng, Q. and Bai, Y., 2014. Preliminary analysis of polonium-210 contamination for China LEAd-based Research Reactor. *Progress in Nuclear Energy*, 70, pp.39–42. Available at: <https://doi.org/10.1016/j.pnucene.2013.07.009>.
- Nguyen, N.D., Huynh, T.N., Le, V.V., Doan, H.D.V., Seo, C., Park, C. and Kim, H.S., 2014. Conceptual nuclear design of a 20 MW multipurpose research reactor. *Nuclear Science and Technology*, 4(1), pp.26–35. Available at: <https://doi.org/10.53747/jnst.v4i1.210>.
- Nguyen, N., Nguyen, K., Huynh, T., Vo, D. and Tran, H., 2020. Conceptual design of a 10 MW multipurpose research reactor using VVR-KN fuel. *Science and Technology of Nuclear Installations*, 2020, 7972827. Available at: <https://doi.org/10.1155/2020/7972827>.
- Niloy, M.H.H., Ahmed, M.T. and Farha, F.I., 2025. A neutronic comparative study of reflectors in radially and axially heterogeneous cores for the ABR-1000 sodium cooled fast reactor. *Annals of Nuclear Energy*, 211, 111019. Available at: <https://doi.org/10.1016/j.anucene.2024.111019>.
- Osipovich, S.V., Kuatbekov, R.P., Lukichov, V.A., Sokolov, S.A., Tretiyakov, I.T. and Trushkin, V.I., 2012. A new generation of research reactors fuelled with LEU. In: International Atomic Energy Agency, Division of Physical and Chemical Sciences and Division of Nuclear Fuel Cycle and Waste Technology, Vienna, Austria. Available at: <https://www.osti.gov/etdeweb/biblio/22059039>.

Plompen, A. J. M., Cabellos, O., De Saint Jean, C., Fleming, M., Algora, A., Angelone, M., Archier, P., Bauge, E., Bersillon, O., Blokhin, A., Cantargi, F., Chebboubi, A., Diez, C., Duarte, H., Dupont, E., Dyrda, J., Erasmus, B., Fiorito, L., Fischer, U., Flammini, D., Foligno, D., Gilbert, M. R., Granada, J. R., Haeck, W., Hambsch, F.-J., Helgesson, P., Hilaire, S., Hill, I., Hursin, M., Ichou, R., Jacqmin, R., Jansky, B., Jouanne, C., Kellett, M. A., Kim, D. H., Kim, H. I., Kodeli, I., Koning, A. J., Konobeyev, A. Yu., Kopecky, S., Kos, B., Krásá, A., Leal, L. C., Leclaire, N., Leconte, P., Lee, Y. O., Leeb, H., Litaize, O., Majerle, M., Márquez Damián, J. I., Michel-Sendis, F., Mills, R. W., Morillon, B., Noguère, G., Pecchia, M., Pelloni, S., Pereslavtsev, P., Perry, R. J., Rochman, D., Röhrmoser, A., Romain, P., Romojaro, P., Roubtsov, D., Sauvan, P., Schillebeeckx, P., Schmidt, K. H., Serot, O., Simakov, S., Sirakov, I., Sjöstrand, H., Stankovskiy, A., Sublet, J. C., Tamagno, P., Trkov, A., van der Marck, S., Álvarez-Velarde, F., Villari, R., Ware, T. C., Yokoyama, K. and Žerovnik, G., 2020. The joint evaluated fission and fusion nuclear data library, JEFF-3.3. The European Physical Journal A, 56(7), p.181. Available at: <https://doi.org/10.1140/epja/s10050-020-00141-9>.

Pónya, P., Ding, C., Czifrus, S. and Shwageraus, E., 2024. Evaluation of reflector design of ALLEGRO refractory core. Annals of Nuclear Energy, 206, 110602. Available at: <https://doi.org/10.1016/j.anucene.2024.110602>.

Raflis, H., Muhammad, I., Su'ud, Z., Waris, A. and Irwanto, D., 2021. Reflector materials selection for core design of modular gas-cooled fast reactor using OpenMC code. International Journal of Energy Research, 45(8), pp.12071–12085. Available at: <https://doi.org/10.1002/er.6042>.

Romano, P.K., Horelik, N.E., Herman, B.R., Nelson, A.G., Forget, B. and Smith, K., 2015. OpenMC: a state-of-the-art Monte Carlo code for research and development. Annals of Nuclear Energy, 82, pp.90–97. Available at: <https://doi.org/10.1016/j.anucene.2014.07.048>.

Sobolev, V., Malambu, E. and Aït Abderrahim, H., 2009. Design of a fuel element for a lead-cooled fast reactor. Journal of Nuclear Materials, 385(2), pp.392–399. Available at: <https://doi.org/10.1016/j.jnucmat.2008.12.027>.

Teruel, F.E. and Rizwan-uddin, 2009. An innovative research reactor design. Nuclear Engineering and Design, 239(2), pp.395–407. Available at: <https://doi.org/10.1016/j.nucengdes.2008.10.025>.

Tuček, K., Carlsson, J. and Wider, H., 2006. Comparison of sodium and lead-cooled fast reactors regarding reactor physics aspects, severe safety and economical issues. Nuclear Engineering and Design, 236(14), pp.1589–1598. Available at: <https://doi.org/10.1016/j.nucengdes.2006.04.019>.

Yu, K., 2003. Neutronic evaluation of GCFR core diluents and reflectors. Doctoral dissertation, Massachusetts Institute of Technology.

Zavala, G.H., Gheeraert, T., Sánchez-Espinoza, V.H., Almachi, J.C. and Imke, U., 2025. Coupled serpent/subchanflow analysis with unstructured mesh interfaces for a hexagonal, plate-type VVR-KN fuel assembly. Frontiers in Nuclear Engineering, 4, 1570855. Available at: <https://doi.org/10.3389/fnuen.2025.1570855>.

- Zhang, J., 2014. Lead-bismuth eutectic (LBE): a coolant candidate for Gen. IV advanced nuclear reactor concepts. *Advanced Engineering Materials*, 16(4), pp.349–356. Available at: <https://doi.org/10.1002/adem.201300296>.
- Zulquarnain, M., Haque, M., Salam, M., Islam, Saha, P., Sarder, M., Haque, A., Soner, M., Uddin, M., Rahman, M., Kamal, I., Islam, M. and Hossain, S., 2009. Experience with the operation, maintenance and utilisation of the 3 MW TRIGA Mark-II research reactor of Bangladesh. *International Journal of Nuclear Energy Science and Technology*, 4(4), pp.299–312. Available at: <https://doi.org/10.1504/ijnest.2009.028591>.